THE DISTRIBUTION, CIRCULATION AND VARIABILITY OF SUBANTARCTIC MODE WATER

Laura Herraiz-Borreguero
BSc., GradCert. MarSc.

Submitted in fulfilment of the requirements for the Degree of Doctor of Philosophy in Quantitative Marine Science (A joint CSIRO and UTAS PhD program in quantitative marine science)
at University of Tasmania.

School of Mathematics and Physics, University of Tasmania

NOVEMBER 2010

Statement of Declaration

I declare that this thesis contains no material which has been accepted for a degree or diploma by the University or any other institution, except by way of background information and duly acknowledged in the thesis, and to the best of my knowledge and belief no material previously published or written by another person except where due acknowledgement is made in the text of the thesis, nor does the thesis contain any material that infringes copyright.

This thesis may be made available for loan and limited copying in accordance with the *Copyright Act of 1968*

Laura Herraiz–Borreguero

Abstract

The temporal and spatial variability of Subantarctic Mode Water (SAMW) is investigated using a compilation of several observational data sets: hydrography, XBTs, Argo profiles, satellite altimetry, and a climatology. The subduction and export of SAMW as part of the overturning circulation play an important role in global heat, freshwater, carbon and nutrient budgets. Determining the formation, circulation, and variability of SAMW is therefore an important step towards understanding the Southern Ocean's role in climate variability and change.

The spatial distribution of SAMW properties and export paths is investigated. SAMW is identified by a dynamical tracer: a minimum in potential vorticity. SAMW consists of several modes with distinct properties rather than a continuous water mass with properties that gradually evolve towards the eastern region of the Southern Ocean as previously believed. (Modified) Montgomery streamlines on the density surfaces corresponding with potential vorticity (PV) minima are used to determine the circulation paths of SAMW. The different SAMW modes are injected into the ocean interior at "hot spots" north of the Subantarctic Front (SAF), and then follow narrow export pathways into the subtropical gyres.

We have also investigated the temporal variability of SAMW in the formation region, south of Australia. SAMW properties show high intra– and inter–annual variability, but no evidence of a trend over the 17–yr mean temperature record studied (1991-2007). Abrupt changes in temperature and salinity at the SAMW core are related to cross–frontal advection of cool and fresh surface water through eddies and meanders from the SAF,

and warm and salty water originating from the East Australian Current in the north. In addition, the SAMW pool on a single section often consists of two or more modes with distinct temperature, salinity and vertical homogeneity characteristics, but similar density.

The main features of the regional circulation and the physical drivers of the east/west contrast in biomass concentration in the Subantarctic Zone (SAZ) south of Tasmania have been identified. Enhanced input of subtropical water high in micronutrients (such as iron) in the east likely supports the higher surface biomass observed there. The physical processes shown to be responsible for maintaining the east/west contrast south of Tasmania (e.g., regional circulation, eddies and subsurface salinity intrusions) are likely to drive variability in physical and biogeochemical properties of SAMW, Antarctic Intermediate Water and the SAZ elsewhere in the Southern Ocean.

These results have revealed the spatial and temporal variability of SAMW in greater detail than was possible due to lack of data. Different modes of SAMW are formed in each ocean basin. Ventilation "windows" revealed by the PV distribution show hot spots where SAMW subducts. The export of warmer, saltier modes in these "hot spots" contributes to the circumpolar evolution of mode water properties towards cooler, fresher and denser modes in the east. We also found that mesoscale features strongly influence SAMW variability south of Tasmania, and are likely to be important in setting SAMW properties in other regions with high eddy kinetic energy.

Contents

List of Figures

List of Acronyms

AABW	Antarctic Bottom Water
AAIW	Antarctic Intermediate Water
ACC	Antarctic Circumpolar Current
BMC	Brazil–Malvinas Confluence
CARS	CSIRO Atlas of Regional Seas
CTD	Conductivity Temperature Depth
EAC	East Australian Current
EKE	Eddy Kinetic Energy
JPA–25	Japanese 25-year Reanalysis
LUC	Leeuwin Undercurrent
ML	Mixed Layer
NCAR	National Center for Atmospheric Research
NCEP	National Centers for Environmental Prediction
P11	WOCE Section P11 South
PF	Polar Front
PV	Potential Vorticity
PVmL	Potential Vorticity minimum Layer
SAF	Subantarctic Front
SAM	Southern Annular Mode
SAMW	Subantarctic Mode Water
SAZ	Subantarctic Zone
SICW	South Indian Central Water
SR3	WOCE Repeat Section 3
STF	Subtropical Front
SSH	Sea Surface Height
STMW	Subtropical Mode Water
WOCE	World Ocean Circulation Experiment
XBT	Expendable Bathythermograph
ZC	Zeehan Current

Acknowledgements

The complexion of this thesis would not have been possible without the help of many people. In particular, I would like to acknowledge the professional and personal support and guidance, resources and inspirational dedication of my supervisors Stephen R. Rintoul and Richard Coleman. Steve always had his door opened, and received my crazy ideas with a smile. Discussion with him were always very positive and highly enjoyable. Richard was a model to follow, for his constant support and dedication to science.

I would also like to thank, in no particular order, Catia Domingues (CSIRO), Bernadette Sloyan (CSIRO), Susan Wijffels (CSIRO), Peter Campbell (IT-CSIRO) for fantastic computer support, Trevor McDougall (CSIRO), Serguei Sokolov (CSIRO), Louise Bell (CSIRO), Simon Wotherspoon (UTAS), The Society of Sub-professional Oceanographers (SoSO), and last, but not least, Jean-Baptiste Sallée for useful discussion. I would also like to thank my friends and colleges, Ben Galton-Fenzi and Wenneke Ten Hout; Andrew Bowie, Anne Elise Nieblas, and Tessa Vance.

To Joel Pedro, for helping me getting out of bed and making sure I did enough exercise and ate properly in the final stages of the thesis. He showed me to look beyond my results. His passion for science and the interest about the troubles we, as a society, are facing is an inspiration for me.

This research was supported by a scholarship jointly provided by the Commonwealth Science and Industry Research organization and the University of Tasmania as part of the Quantitative Marine Science PhD program.

El apoyo que he recibido de mis hermanos, Agustín y María, y de mi tía, Nati, ha sido fundamental. Su continuo apoyo y cariño me ha ayudado a soportar tanto tiempo lejos de la familia en un momento delicado de nuestras vidas. Ya voy para casa prontito y nos vamos de fiestaaaaaaaa, y nos comemos todo el turrón que me he perdido en 4 añitos, pufff

The courage and support I received from my family have been the energy that kept me going until now. In special, I would like to thank my sister María who has been my pillar since my parents passed away on my first year of PhD. She guided me back to the real world. Almost everyday, she has been arriving at least 15 minutes earlier to her office to have a chat with me. This strong communication has meant a lot to me. She is my role model and as a younger sister, she will always be my role model :-) Muchas gracias cosita !!!!!.

My parents always taught me how important education is, and do the best I can in anything I do. Both my parents encouraged and supported me even when it meant I would be so far from them. I am very proud of them, for their love, respect, and support toward me.

This work is entirely dedicated to them.

A mis padres, Agustín and Pilar, con todo mi amor y cariño

Chapter 1 Introduction

Contrary to the other oceans, the Southern Ocean exerts a strong influence over the global ocean circulation and climate. The Southern Ocean occupies 22% of the surface of the global ocean and its unique structure allows a strong eastward flow, the Antarctic Circumpolar Current (ACC) to exist. The ACC circles the Antarctic continent isolating the cold and fresh Antarctic Waters from the warm and salty subtropical waters. It connects 3 of the main oceans: the South Atlantic, South Indian and South Pacific Ocean, making the ACC the largest current of the world's ocean currents, covering a distance of 21,000 km and a mean transport of 134 $\pm$ 13 Sv of water through Drake Passage (*Rintoul et al.*, 2001).

One of the main obstacles in Southern Ocean studies has been the lack of data mainly due to the harsh environment and the difficulty in retrieving data. As a consequence, historical data are scarce and, sometimes, not very reliable. **Discovery cruise 15**, which comprised 19 sections, was the first oceanographic circumpolar cruise in the Southern Ocean. In doing so these early scientific explorers encountered *"the notoriously stormy conditions of the Southern Ocean"* (*Deacon*, 1937). *Schott* (1933) reported that:

> *"to give a suitable account of the long winter nights with very little daylight, stopping the ship in rough weather and high seas to make scientific observations, would take more space than is available here."*

The next major series of cruises in the Southern Ocean were the USNS Eltanin Cruises conducted in the 1960s and 1970s. This was followed by the World Ocean Circulation

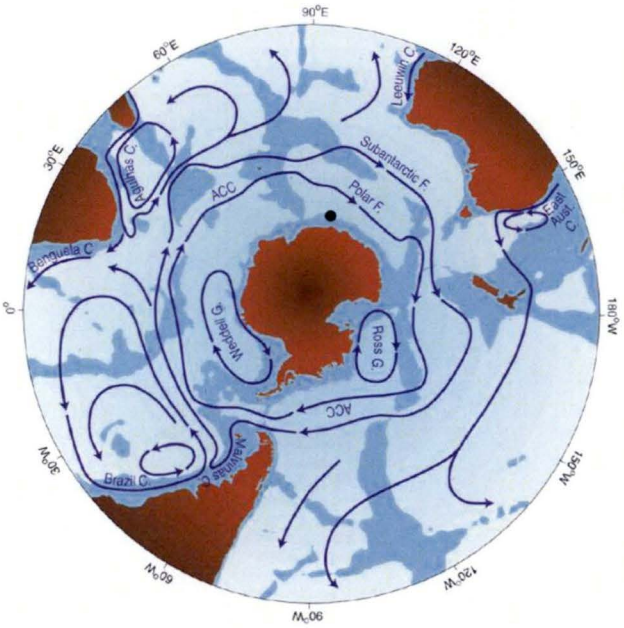

Figure 1.1: A simplified view of the Southern Ocean currents. The two major fronts of the ACC are shown, the Subantarctic Front and the Polar Front. Depths shallower than 3500 m are shaded. From *Rintoul et al.*, 2001.

Experiment (WOCE) cruises in the 1990s which involved a series of high resolution cruises spanning the entire globe. Another step forward was taken with the launch of the Argo program. Argo was born from the necessity to improve the knowledge of the oceans and their role in the global climate, as well as to improve the number of observations from the ocean, both in time and space. The program deploys autonomous profiling floats, measuring temperature and salinity profiles from the surface to depths of up to 2000 metres. Nowadays, Argo, with $\sim$ 3000 floats, covers most of the world's oceans for several years since the beginning of the 21^{st} century. Argo provides data covering vast areas of the Southern Ocean for the first time. Data are made freely available by the International Argo Project[1] and the national programs that contribute to it.

The ACC is a deep–reaching current formed of several jets. A schematic view of the

[1]http://www.ifremer.fr/coriolis/cdc/argo.htm and http://www.argo.ucsd.edu

ACC is shown in figure 1.1. *Deacon* (1937) first described the upward slope of physical properties across the ACC in a series of steps or fronts. *Orsi et al.* (1995) and *Belkin and Gordon* (1996) used hydrographic sections across the ACC to describe its circumpolar structure and properties. The northern boundary of the ACC is represented by the Subtropical Front (STF) (denoted Subtropical Convergence by *Deacon* (1982))(*Orsi et al.*, 1995). The STF is a narrow transition between relatively warm and salty surface subtropical waters and cold and fresh Subantarctic waters. It is the only front that is interrupted by the South American continent and does not flow through Drake Passage. Following the definitions of *Orsi et al.* (1995), the ACC is formed by three main deep–reaching fronts uninterrupted by land around Antarctica, from north to south: the Subantarctic Front (SAF), the Polar Front (PF), and the southern ACC Front (SF). They account for most of the ACC transport. The SAF is the northernmost and strongest jet of the ACC south of Australia (*Sokolov and Rintoul*, 2002). The southern boundary of the ACC coincides with the poleward limit of the Upper Circumpolar Deep Water (UCDW) regime.

The fact that the fronts are associated with strong horizontal gradients of water masses makes it possible to identify them through specific isotherms at a certain depth. For example, the northern branch of the SAF is found where the horizontal gradient of potential temperature (θ) is maximum at 400 dbars in a θ range of [6 – 8]°C; and, the PF is often associated with a θ–minimum layer of 2.0°C and a θ–maximum layer of 2.2°C (*Sokolov and Rintoul*, 2002). The identification of the fronts by hydrography was improved with the arrival of remote sensing techniques and improvements in modeling (*Gille*, 1994; *Hughes and Ash*, 2001). The combination of the different techniques just pointed out more clearly the complicated structure of the fronts already inferred from the hydrography studies (*Orsi et al*, 1995; *Sokolov and Rintoul*, 2002). However there is still disagreement on how many different branches there are per front and their locations. Although the fronts are clearly differentiated at Drake Passage, this is not the case for

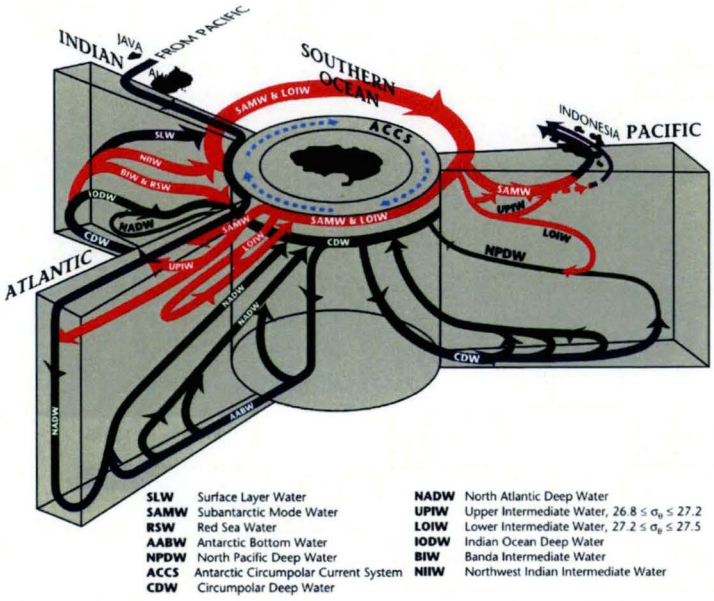

Figure 1.2: A schematic view of the global overturning circulation, from *Schmitz* (1996). The ACC is the red wide arrow that circles Antarctica. The surface layer circulations are in purple, intermediate and SAMW are in red, deep in green, and near bottom in blue. The circulation in the deep ocean is connected to the upper ocean primarily by water mass transformation in the Southern Ocean.

some parts of the Southern Ocean where the fronts seem to split in several branches or merge between one another. An example of this is the SAF and PF which are formed by two or more branches which merge or diverge along the circumpolar path (*Sokolov and Rintoul*, 2002; 2007).

The ACC provides the primary pathway for exchange of water masses between the ocean basins and allows a global overturning circulation to exist. Figure 1.2 shows a schematic view of the global ocean circulation, from a Southern Ocean perspective. The shoaling of a wide range of isopycnals across the Southern Ocean towards Antarctica brings deep and intermediate waters close to the surface. Here, the outcropped waters exchange heat, freshwater and momentum with the atmosphere and ice, leading to the physical and

chemical transformation of water properties across densities to create lighter mode and intermediate waters — Subantarctic Mode Water (SAMW) and Antarctic Intermediate Water (AAIW)— as well as bottom water, Antarctic Bottom Water (AABW). Water mass transformations in the outcrop regions link the upper and lower limbs of the overturning circulation (*Sloyan and Rintoul*, 2001). The water masses exported from the Southern Ocean as part of the overturning circulation are responsible for ventilating intermediate waters in other regions, and influence regional climate. Thus, the ACC plays a major role in regulating the global transport of heat, fresh water and other properties that affect climate (*Gordon*, 2001; *Bryden and Imawaki*, 2001).

"Mode Water" is the name given to a surface layer of uniform properties gradient formed by deep convection during late winter conditions and which sinks along isopycnal surfaces. Mode waters are characterized by the homogeneity of their properties such as temperature, salinity and density, in the vertical (with thickness of up to 600 – 700 m) as well as in the horizontal. Their characteristics tend to be retained for great distances as they move around the ocean basins away from their formation zone and are excellent tracers for climate change studies since they retain a record of surface conditions at the time of their formation (*Hanawa and Talley*, 2001). The low potential vorticity signal of the mode waters provides an excellent physical tracer of subtropical ventilation, as useful as chemical tracers of ventilation (*Sarmiento et al.* ,1982; *Talley*, 1988; *Joyce et al.*, 1998; *Scheneider et al.*, 1999).

McCartney (1977, 1982) identified and mapped the properties of a thick near–surface layer that reached a thickness of more than 600m on the equatorward side of the SAF, and named it SAMW. SAMW is characterized by: 1) being a pycnostad: thick layer of uniform density (potential density range, [26.8 – 26.95] kgm^{-3}) and, thus, a layer of very low potential vorticity; 2) high oxygen concentration (*McCartney*, 1977); and, 3) vertical extent from the sea surface to 450 – 700 dbar, from 45°S (STF mean position) to 50°S – 53°S (SAF mean position) (*Sokolov and Rintoul*, 2002). Figure 1.3 shows the vertical

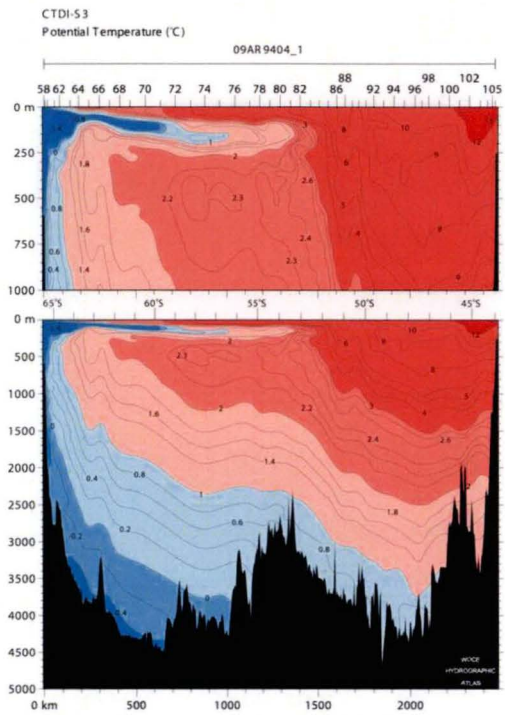

(a)

Figure 1.3: a) Potential temperature; b) Neutral density (kgm^{-3}).; and, c) Oxygen concentration ($\mu mol/kg$). SAMW is found between 45°S and 49°S, and between 100 and 700 m, approximately; with a potential temperature range of 8°C – 9.5°C and a neutral density of 26.9 to 27 $kg.m^{-3}$.

section for potential temperature (a), neutral density (b) and oxygen concentration (c) corresponding to WOCE SR3 in which SAMW is found between approximately 45°S and 50°S.

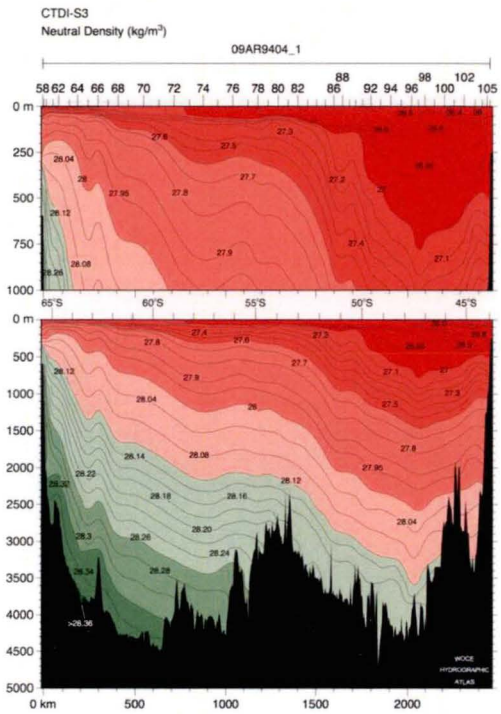

(b)

Figure 1.3: continued: Neutral density (kgm^{-3})

SAMW properties vary in relation to the southward spiraling of the SAF around Antarctica: while the warmest SAMW (15°C) is found where the SAF is furthest north, in the western Atlantic, the coldest mode water (4°C – 5°C) occurs just west of Drake Passage (*Hanawa and Talley*, 2001). It is not clear yet how continuous the SAMW is around the whole SAF although different varieties of SAMW have been found in every basin around Antarctica. Even less attention has been paid to the export of SAMW/AAIW away from their formation zone or what other water masses supply SAMW/AAIW and where and how this occurs. *Talley* (1999) mapped an updated mode water distribution including the same features as *McCartney* (1982) (figure 1.4). The variability of SAMW properties is driven by several mechanisms. Air–sea fluxes of heat and freshwater in the SAZ were first suggested to drive changes in the SAMW properties by *McCartney* (1977;

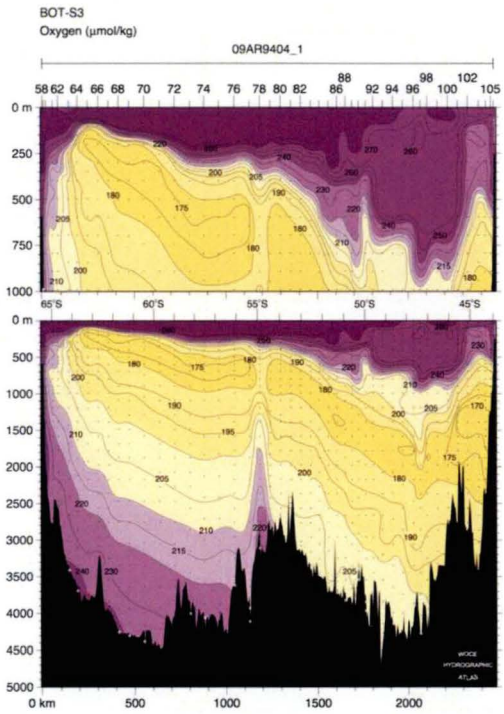

(c)

Figure 1.3: continued: Oxygen ($\mu mol/kg$)

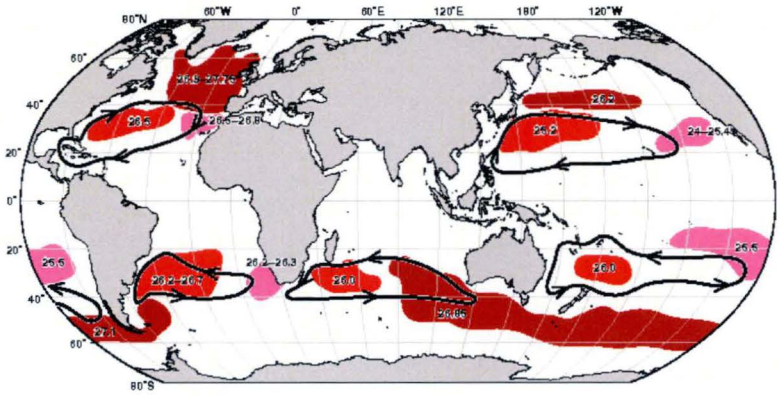

Figure 1.4: Location of upper ocean mode waters. Subtropical Mode Waters (around 18°C) of each subtropical gyre (red). Lower density subtropical type mode waters of the eastern region of each subtropical gyre (pink). Subpolar Mode Water of the North Atlantic, Subantarctic Mode Water north of the Subantarctic Front (only the region of deepest mixed layers is shown), North Pacific Central Mode Water (brown). Schematics of the gyre circulations are indicated with black arrows (Updated figure from *Talley* (1999), in *Hanawa and Talley*, 2001).

1982). Later authors concluded that air–sea fluxes alone are not sufficient and northward Ekman transport across the Southern Ocean fronts was also suggested to contribute to SAMW formation and hence, its variability (*Speer et al.*, 2000; *Sloyan and Rintoul*, 2001; *Rintoul and England*, 2002). Eddy heat diffusion has recently been shown to modify the action of Ekman and air–sea fluxes causing local heating/cooling of the SAMW (*Sallèe et al.*, 2008). However, the relative importance of one mechanism over the others is still under debate.

AAIW is the low–salinity intermediate–depth layer of the southern hemisphere. It

represents one of the principal contributors to the upper, northward branch of the global thermohaline circulation (*Rintoul*, 1991). Two formation regions of AAIW are found on the eastern corner of the South Pacific Ocean and off the Argentinian coast in the South Atlantic. South of Australia, AAIW properties correspond to a wide range of density with different ventilation ages reflecting different formation locations, formation mechanisms, and circulation histories (*Rintoul and Bullister*, 1999). Depending on the author, AAIW spread is thought to be driven by either wind, buoyancy loss, or mixing along isopycnal surfaces. *McCartney* (1977) linked the coldest and densest SAMW as a precursor of the AAIW on the western side of Drake Passage. Recent studies claim Antarctic Surface Water to be the main driver of the variability of AAIW in the southeast Pacific Ocean (*Santoso and England*, 2004; *Naveira–Garabato et al.*, 2009).

When SAMW/AAIW sink from the sea surface, they carry oxygen, dissolved carbon dioxide and other tracers to the ocean interior. About 40% of the total ocean anthropogenic carbon sink/storage occurs in the Subantarctic Zone (SAZ), the region delimited by the STF and the SAF. As a result, the SAZ is the largest zonally–integrated ocean store of anthropogenic carbon dioxide (*Sabine et al.*, 2004). The SAMW and AAIW are relatively fresh, and their export to lower latitudes closes the hydrological cycle by returning the excess precipitation falling at high latitudes. The upwelling of nutrient–rich water and their transport through SAMW and AAIW export from the Southern Ocean are claimed to be responsible for up to 75% of the nutrient input in the subtropics (*Sarmiento et al.*, 2004). For each of these reasons — the overturning circulation, carbon storage, the hydrological cycle, and nutrient export — the SAMW and AAIW are critical components of the Earth's climate system.

The variability and changes of the Southern Ocean likely has strong implications for the regional climate of other regions due to its dominant role in the heat and freshwater cycles. Moreover, as the transformation into intermediate waters and bottom waters occurs at the surface, changes in the Southern Ocean dynamics and properties are transported into the

ocean interior. Also, SAMW and AAIW are renewed on decadal timescales keeping the imprints of the atmospheric conditions at the time of their formation. This property makes Mode Waters a great tool to look at when seeking evidence of past changes in atmospheric–oceanic forcing. Recent studies using modern and historical data have begun to document changes in the Southern Ocean, with the largest warming found in the northern side of the ACC where the subduction of Southern Ocean waters occurs (*Gille*, 2002) (figure 1.5).

Cooling and freshening of SAMW and AAIW on neutral density surfaces were observed in the interior of the Pacific and Indian Ocean possibly due to surface warming and freshening in the formation zones (*Bindoff and Church*, 1992; *Johnson and Orsi*, 1997; *Wong et al.*, 1999; *Bindoff and McDougall*, 2000; *Banks and Bindoff*, 2003) (figure 1.5). *Bryden et al.* (2003) reported a recovery of the salinity values in SAMW back to the 1960s values, counteracting the observed freshening. Recent analysis of SAMW and AAIW variability in Drake Passage highlighted the high intra–annual variability in their physical properties (*Naveira–Garabato et al.*, 2009). While AAIW suffered a net freshening since the 1970s, SAMW experienced warming (cooling) and increased salinity (freshening) during the 70s (between the 1990s and 2005). These observed interdecadal variability changes found in SAMW and AAIW in Drake Passage are ascribed to fluctuations on the major modes of hemispheric variability (Southern Annular Mode, El Niño Southern Oscillation and Interdecadal Pacific Oscillation) (*Naveira–Garabato et al.*, 2009). The lack of data in the formation areas in the Southern Ocean make it difficult to detect and interpret changes observed in areas far from the subduction areas in the Southern Ocean.

Despite the importance of SAMW (and AAIW), very little is known about their spatial and temporal variability, or even, the mechanisms by which they are formed. The increased interest in the role of the Southern Ocean in climate change, in addition to the new oceanographic instrument development, such as profiling Argo floats and the deployment of ships, makes SAMW variability more feasible to look at in detail. Variations in its

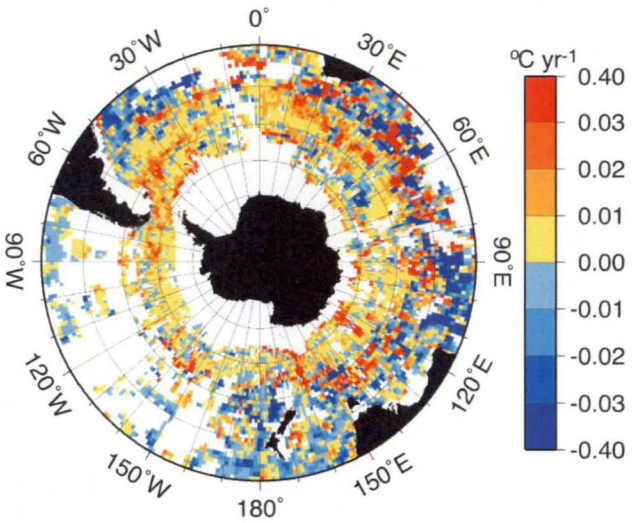

Figure 1.5: Temperature trends ($°Cyr^{-1}$) at 900 m depth using data collected from the 1930s to 2000, including shipboard profile and Autonomous Lagrangian Current Explorer float data. The largest warming occurs in subantarctic regions, and a slight cooling occurs to the north. From Gille (2002).

properties, distribution and circulation are manifestations of variations in winter–time air–sea interaction and eddy activity in the formation area. By understanding the formation and variability of the SAMW, this thesis will provide a tool to infer how the likely changes in the Southern Ocean overturning under climate warming is likely to influence SAMW properties. It will also yield insight into how the Mode Water variability is transferred to the ocean interior affecting regions far away from the source of SAMW. This research will also help to evaluate how well ocean circulation models reproduce the formation and variability of SAMW.

The thesis will be presented as follows. The new spatial distribution and circulation patterns of the SAMW are described for the three oceanic basins of the southern hemisphere in Chapter 2. Chapter 3 centers on the characterization of the magnitude and cause of SAMW temporal variability south of Australia (this chapter is published in press in Journal of geophysical research–Oceans). Chapter 4 gives a complete review of

the regional circulation south of Tasmania and its impact on the surface phytoplankton biomass and on the upper ocean variability, including SAMW and AAIW (this chapter has been accepted by Deep-Sea Research). The final summary and conclusions of this research are presented in Chapter 5.

Chapter 2 Subantarctic Mode Water spatial variability

2.1 Introduction

SAMW was first identified and mapped as a uniform layer extending from near the surface to depths of more than 600 metres on the equatorward side of the SAF (*McCartney*, 1977, 1982). *McCartney* (1977) used the notion of "Subantarctic" due to the proximity to the Subantarctic Zone along the ACC extension. He also introduced the idea that SAMW properties vary in relation to the southward spiralling of the Subantarctic Front, becoming denser and cooler from the southwest Atlantic Ocean, where it is warmer (~15°C), to the southeast Pacific Ocean, where it is the coldest and densest (4 °C – 5°C) (figure 2.1, from *McCartney*, 1977). These changes in the SAMW properties imply that the transformation of less dense SAMW into denser SAMW is a gradual, continuous process, which *McCartney* (1977) suggests is the result of air–sea fluxes. However, the continuity of the SAMW along the Subantarctic Zone is not clear yet.

Two SAMW varieties are found in the southwestern Atlantic Ocean. The cold and fresh SAMW (first variety) that crosses Drake Passage from the southeastern Pacific Ocean is the densest of the two varieties. In its northward flow following the Falkland Current, west of 60 °W, it encounters lighter waters and progressively sinks to occupy 800 – 1000 m depths (*McCartney*, 1977). The high spatial variability of the SAF, mainly due to effects of bathymetry on the flow and the confluence of the Brazil and Falkland Currents, make the southwest Atlantic one of the regions with highest eddy kinetic energy of the world ocean (*De Miranda et al.*, 1999). As a result, several definitions and locations of the

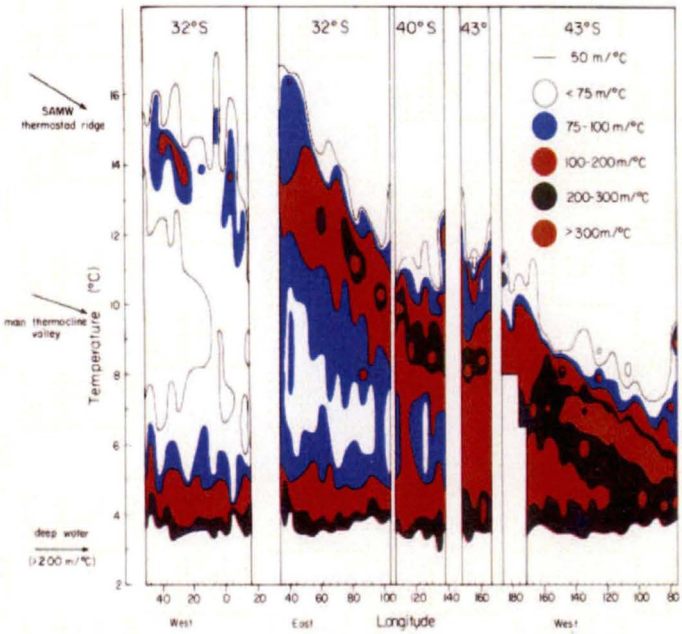

Figure 2.1: SAMW thermostad strength as a function of temperature and longitude. The SAMW thermostad runs from the 14 °C –15 °C in the western Atlantic through 8 °C – 9°C (South of Australia,120°E) and ending at 5°C in the eastern Pacific (McCartney, 1977)

warm SAMW (second variety) and Subtropical Mode Water have been given due partly to their close proximity in this region (e.g., *McCartney*, 1977, 1982; *Tsuchiya et al.*, 1994; *Provost et al.*, 1995; *Mèmery et al.*, 2000). The relatively warmer and saltier SAMW variety is found at the surface, in the Brazil–Malvinas Confluence. The Subtropical Mode Water can be split into two variants separated by the eastward extensions of the Brazil Current Front at approximately 42 °W (*Roden*, 1986; *Tsuchiya et al.*, 1994) and they are highly constrained to the region west of 25 °W and south of 20 °S.

Two varieties of Subantarctic Mode Water are found in the south Indian Ocean. The western side of the Indian Ocean holds the lighter and lower volume of the two varieties (*McCartney*, 1982; *Hanawa and Talley*, 2001). The Kerguelen Plateau (70 °E – 80 °E) represents the boundary between the two varieties, with significantly higher oxygen saturation in the mixed layer on the eastern side of the Plateau (*Talley*, 1999). *McCarthy and Talley* (1999) found a layer of potential vorticity minimum centered at 90 °E – 40 °S which is a signature of deep mixed layers formed by convection, subducted and advected toward the subtropics in agreement with *McCartney*'s work (1982). The combination of several conditions (e.g., convergence of two deep–reaching fronts with an energetic eddy field resulting from flow interactions with bathymetry, strong cooling due to the eddy diffusion term, Ekman heat transport and circumpolar maximum in mean wind field) downstream of the Kerguelen Plateau make this region the most efficient source of SAMW in the Indian Ocean (*Sallèe et al.*, 2006).

As in the Indian Ocean, the properties and circulation of SAMW in the south Pacific differ from west to east. SAMW is relatively cooler and fresher in the Subantarctic Zone east of New Zealand compared to the SAMW west of New Zealand. The deflection of the northern branch of the SAF (SAF–n) as it encounters the Campbell Plateau, and eddy heat diffusion act to restratify the deep mixed layer associated with SAMW, east of New Zealand (*Sallèe et al.*, 2008). This can explain the discontinuity of deep mixed layers south and southeast of New Zealand. The meridional extent of the lightest Pacific

SAMW is restricted to the south west Pacific and up to 35 °S (*McCartney and Baringer*, 1993; *Sokolov and Rintoul*, 2000). The southeastern Pacific SAMW is the densest of the Pacific SAMWs and has a close relationship with Antarctic Intermediate Water (AAIW). This dense SAMW shows two export paths from the Subantarctic Zone: through Drake Passage into the Atlantic Ocean, and into the subtropical gyre of the south Pacific Ocean (*McCartney*, 1977; 1982).

The close relationship between SAMW and AAIW in the south eastern Pacific is still under debate. Early studies claim SAMW is the precursor of AAIW, an intermediate water mass coincident with a salinity minimum (e.g., *McCartney*, 1977; *Talley*, 1996; *Hanawa and Talley*, 2001). On the other hand, the independence of AAIW inter–annual variability was discussed recently and claimed to be primarily driven by Antarctic Surface Water (*Naveira–Garabato et al.*, 2009).

Potential vorticity (PV) plays an important role in large–scale oceanography, acting both passively as a tracer and dynamically to direct the flow. Potential vorticity is given by :

$$PV = \frac{(f+\xi)}{\rho} \cdot \frac{\partial \rho}{\partial z} \tag{2.1}$$

where f is the planetary vorticity, ξ is the relative vorticity, $(v_x - u_y)$, and $(\frac{1}{\rho})\frac{\partial \rho}{\partial z}$ is the stretching term. The relative vorticity is negligible in comparison to the other two terms in large–scale studies, where the Rossby number is small, except in strong boundary currents. And so, we will refer to potential vorticity as the quantity

$$PV = \frac{f}{\rho}\frac{\partial \rho}{\partial z} \tag{2.2}$$

The main property characterizing *Mode Waters* is their homogeneity, that is, a minimum in vertical gradients of, typically, temperature, salinity, density and oxygen. These properties can be traced to reveal the spreading paths of mode waters after they leave the surface,

as the characteristic properties are retained for great distances. In terms of potential vorticity, mode waters stand out from the surrounding water masses as a potential vorticity minimum layer (minimum in hydrostatic stability). Potential vorticity is conservative (away from source and mixing regions) and hence, an excellent tracer for mode water (*McCartney*, 1982). The goal of this chapter is to give a detailed description of the spatial variability of SAMW in the Southern Ocean and its path equatorward. We identify regions where SAMW is formed and where it subducts, and the properties in each oceanic basin. We also describe the circulation paths that SAMW follows away from the formation regions in the Subantarctic Zone. Following *McCartney* (1982), potential vorticity is used as a tracer to identify SAMW in the Subantarctic Zone, and describe the circulation paths. The Argo float program[1] provides an extensive data set of the ocean, especially of the Southern Ocean and the south Pacific Ocean where vast areas have been poorly sampled. The Argo data is complemented by the representation of the SAMW from the CSIRO climatological Atlas for Regional Seas (CARS2006a)[2]. Section 2.2 introduces the vertical structure of SAMW as seen in CARS2006a. The spatial variability of SAMW properties on density surfaces (i.e., isopycnals) is assessed by using Argo temperature and salinity profiles in Section 2.3. A synthesis of the results from the Argo "era" (since data of the Southern Ocean are available) and previous studies are addressed in Section 2.4.

[1]http://www.ifremer.fr/coriolis/cdc/argo.htm and http://www.argo.ucsd.edu/index.html
[2]For more information, go to: http://www.marine.csiro.au/~dunn/cars2006/

2.2 Subantarctic Mode Water distribution from CARS climatology

The spatial coverage provided by Argo is excellent compared to historical data, however some regions are not well sampled and only a short time period is covered. CARS2006a has been used to complement the analysis of SAMW spatial variability. CARS2006a is an atlas of seasonal ocean water properties, covering the entire southern hemisphere and equatorial regions in which temperature, salinity, oxygen, nitrate, silicate and phosphate are mapped (*Ridgway et al.*, 2002; *Dunn and Ridgway*, 2002). It comprises mean fields and average seasonal cycles, derived from all available historical subsurface ocean property measurements mostly collected from the last 50 years (primarily research vessel instrument casts and autonomous profiling buoys.) A minimum in potential vorticity is used to identify SAMW from the CARS climatology. The annual representation of temperature and salinity was used to calculate the potential vorticity (PV). In this Section, the CARS climatology is used to describe the circumpolar distribution of SAMW.

The potential vorticity minimum pool associated with SAMW is followed across latitudinal sections, from south to north: 55 °S, 50 °S, 45 °S, 40 °S, 35 °S, and 25 °S. SAMW is found as a uniform pool of neutral density range of 27.1 to 27.2 kgm^{-3} west of Drake Passage at 55 °S (figure 2.2 e). East of Drake Passage, a denser SAMW (γ^n = 27.2 – 27.3 kgm^{-3})[1] enters the south Atlantic Ocean. Its track is rapidly lost east of 320 °E (40 °W). Further north at 50 °S, SAMW occupies most of the south Pacific Ocean, extending from west of New Zealand ($\sim$ 180 °E) to South America (figure 2.2, b – e). Note that two SAMW pools are seen at this latitude and can be traced up to 25 °S. These two pools appear as two independent features at all latitudes.

A common feature seen in the SAMW pool is the "stacking" of modes of different density in most latitudinal sections. In the Indian sector, three main γ^nranges form the SAMW pool:

[1] $\gamma^n$is the neutral density variable of *Jackett and McDougall* (1997)

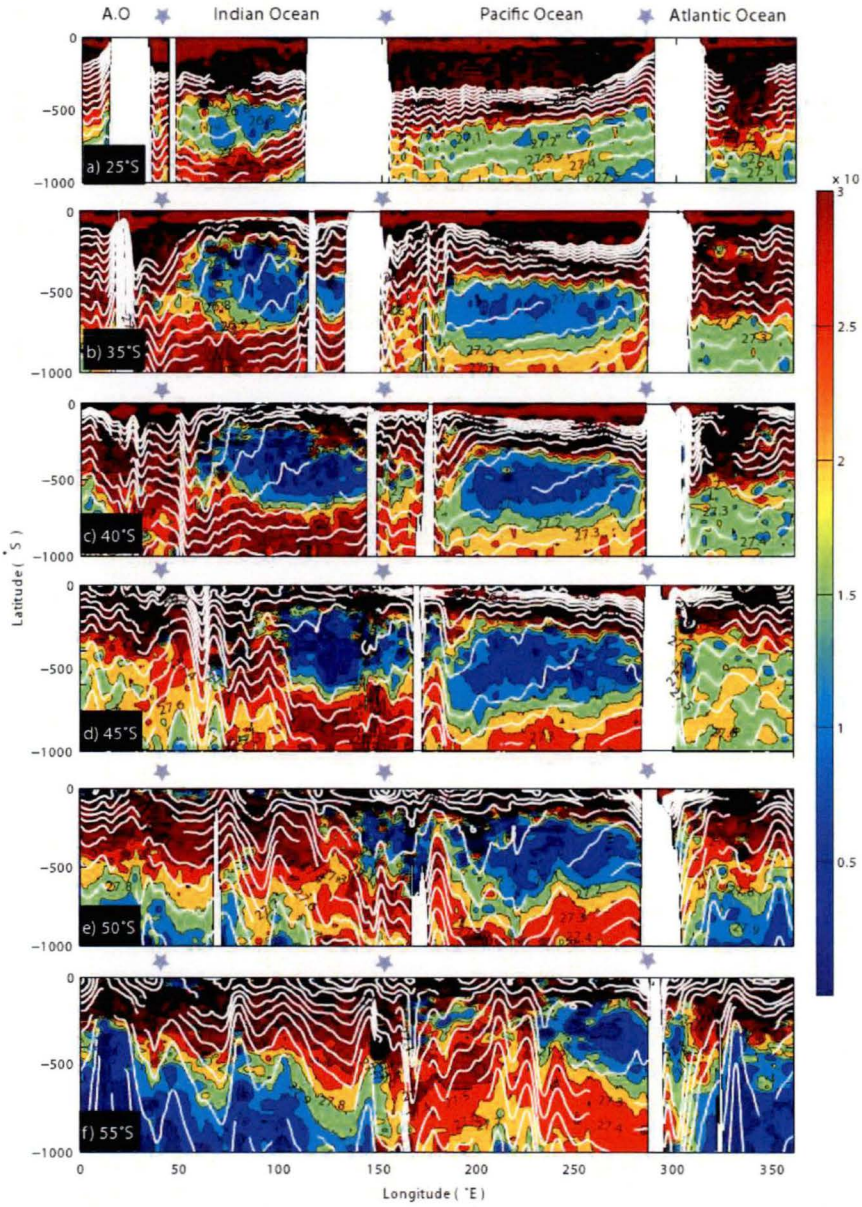

Figure 2.2: Annual mean of potential vorticity (PV) as a function of depth and longitude (°E) at 55°S (f), 50°S (e), 45°S (d), 40°S (c), 35°S (b), and 25°S (a). Data taken from CARS Climatological Atlas for Regional Seas (CARS2006a). White lines depict neutral density isopycnals. Grey stars in the x-axes show the extent of the Atlantic, Indian and Pacific Oceans.

- $26.7 \leq \gamma^n \leq 26.8$ (at 40 °S, figure 2.2 c)
- $26.8 \leq \gamma^n \leq 26.9$ (from 40 °S to 25 °S, figure 2.2 a – c)
- $26.9 \leq \gamma^n \leq 27$ (from 50 °S to 25 °S, figure 2.2 a – f)

In the south Pacific, SAMW is formed by denser modes:

- $27 \leq \gamma^n \leq 27.1$ (from 50 °S to 35 °S, figure 2.2 b – e)
- $27.1 \leq \gamma^n \leq 27.2$ (from 50 °S to 35 °S, figure 2.2 b – e)
- $27.2 \leq \gamma^n \leq 27.3$ (at 55 °S, figure 2.2 f)

In each basin, lighter modes are restricted to the south west. Denser modes, originating in the south east, travel further north, especially in the Indian Ocean.

2.3 Subantarctic Mode Water from Argo observations

Since 2000, the ocean has been populated with temperature/salinity profiling floats, known as Argo. Argo floats are deployed in ice–free oceans, profiling temperature/salinity in the upper ocean to depths up to 2000 metres. The autonomous floats use a battery as its power and are programmed to drift at a certain depth, the "parking depth", where they are stabilized by being neutrally buoyant. Approximately every 10 days, they pump fluid into an external bladder and start profiling temperature /salinity as they ascend to the surface. Once at the surface, the recorded data are transmitted to a satellite which sends the data to the processing station. To ensure error free data transmission, floats stay at the surface for about 6 to 12 hours before returning to their "parking depth". Their mean life–time is about 5 years, although some floats have surpassed 7 years. The extensive spatial

coverage that Argo provides allows, for the first time, the opportunity to study SAMW in areas where data have been very poor or nonexistent.

The geostrophic circulation transporting SAMW from the formation regions is analyzed on neutral density surfaces using an improved Montgomery geostrophic streamfunction (*Montgomery*, 1937; *McDougall*, 1989; *Zhang and Hogg*, 1992) by using a reference point on the isopycnal surface in question (*McDougall and Klocker*, 2009; submitted to Ocean Modeling). The geostrophic streamfunction on approximately neutral surfaces is expressed as,

$$M = \frac{1}{2}(p - \hat{p})\hat{\delta}(S, \Theta, p) - \frac{1}{12}\frac{T_b^{\Theta}}{\rho}(\Theta - \hat{\Theta})(p - \hat{p})^2 - \int_0^p \hat{\delta}\, dp \tag{2.3}$$

where p represents the depth of the isopycnal surface and varies spatially, and

$$\hat{\delta} = \frac{1}{\rho(S, T, p)} - \frac{1}{\rho(\hat{S}, \hat{\Theta}, \hat{p})} \tag{2.4}$$

where $\rho(S, T, p)$ represents the *in situ* density, $\rho(\hat{S}, \hat{\Theta}, \hat{p})$ at a point on the isopycnal surface and, T_b^{Θ} is the thermobaric coefficient (note that $T_b^{\Theta}\rho^{-1} \approx 2.7\ x\ 10^{-15} K^{-1}(Pa)^{-2}m^2s^{-2}$). Here we defined $\hat{S}$, $\hat{\Theta}$ and $\hat{p}$ as the median values on the isopycnal surface. We have based our analysis on neutral density surfaces. Note that this is an approximation and no exact streamlines on isopycnals exist. The circulation analysed in this work corresponds to the baroclinic mode, as our profiles only reach a mean maximum depth of 2000 metres.

The properties of the SAMW in the Southern Ocean and away from the formation areas will be examined as follows. SAMW was identified as a PV minimum between [0, 1.5×10^{-9}] $m^{-1}s^{-1}$. The analysis of the PV minimum on neutral density surfaces is used to select the density surface that best represents the pycnostad layer in each oceanic basin that surrounds the Southern Ocean. The properties of SAMW on each γ^n surface will be

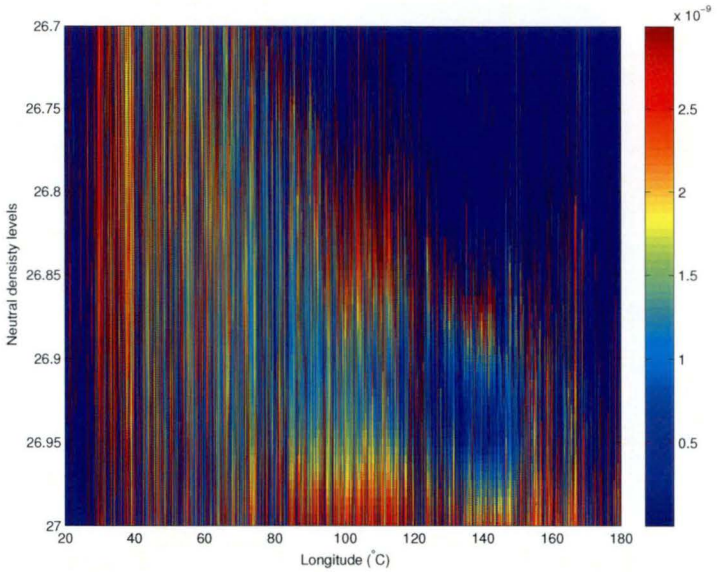

Figure 2.3: SAMW tracer, potential vorticity as a function of Longitude ($^{\circ}E$) and neutral density (γ^n) in the South Indian Ocean. This figure shows all the available profiles, sorted by longitude. The navy blue in the background just shows values out of our PV range ($[0, 3 \times 10^{-9}]\ m^{-1}s^{-1}$).

described as well as the likely export paths to the subtropics. Temperature and salinity on isopycnal surfaces will only be shown for the SAMW core PV minimum range, denoted by values of PV $\leq 1 \times 10^{-9}\ m^{-1}s^{-1}$. Note that the first 200 metres of the temperature and salinity profiles were not used in our analysis in order to reduce the seasonal signal of the mixed layer.

2.3.1 SAMW in the south Indian Ocean

The basin–wide PV along longitude at γ^n surfaces is depicted in figure 2.3. The PV minimum (PV $\leq 1.5 \times 10^{-9} m^{-1}s^{-1}$) spans a range of 26.75 – 26.97 kgm^{-3} in neutral density, extending across most of the south Indian Ocean Basin (~40°E to 170°E). The colour bar was chosen to highlight the potential vorticity minimum. A relatively light

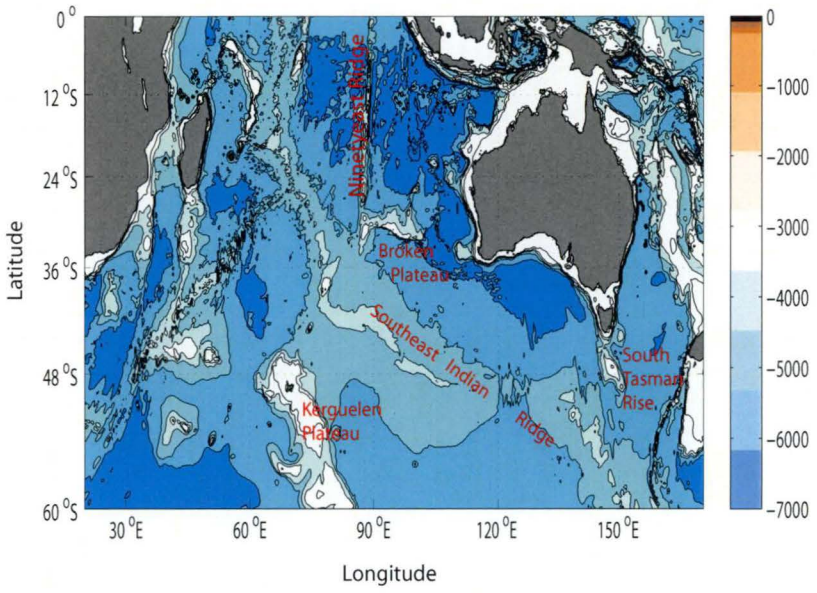

Figure 2.4: Ocean topography in the south Indian Ocean. The major topographic features have been labeled.

SAMW type with a density range of γ^n from 26.75 to 26.85 kgm^{-3} is found in the western side of the south Indian Basin, between ~70°E and 90°E. A slightly denser SAMW type, $\gamma^n \simeq$ [26.85, 26.97], is found south of Australia between 120°E and 170°E. It is also the most homogeneous SAMW with a PV minimum lower than $1 \times 10^{-9} m^{-1} s^{-1}$. SAMW properties and circulation paths are next described on two isopycnal surfaces, $\gamma^n = 26.8$ and 26.9. Figure 2.4 shows the main bathymetry in the south Indian Ocean, labeled are the topography referred in the text.

SAMW on γ^n = 26.8

SAMW spatial variability

The modified Montgomery streamlines at γ^n= 26.8 kgm^{-3} represent the subtropical gyre in the western and central side of the south Indian Ocean (figure 2.5, grey contours).

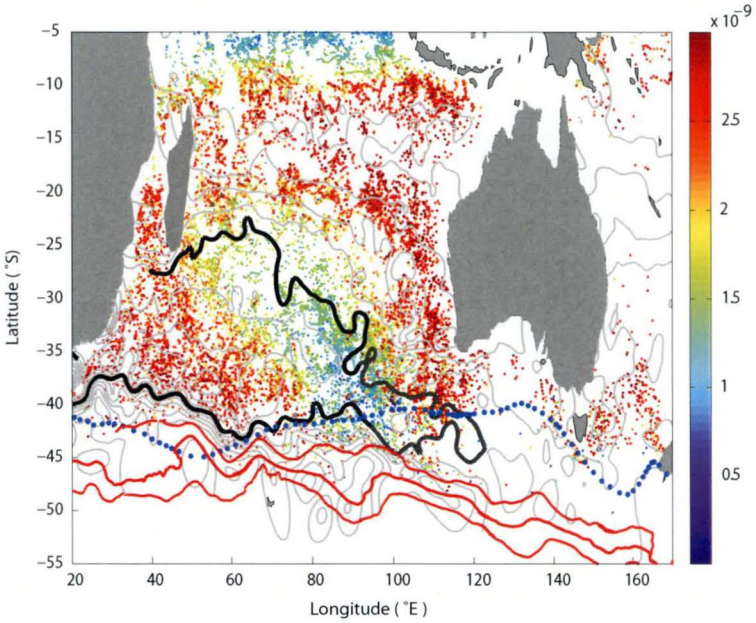

Figure 2.5: Potential vorticity on the 26.8–γ^n surface. SAMW is identified as PV $\leq$ $1.5 \times 10^{-9} m^{-1} s^{-1}$. Modified Montgomery streamlines are depicted by grey lines. The streamline, $\Psi_{26.8}$ better representing the SAMW flow is shown as a thick black line. Blue dotted and red lines depict the Subtropical Front and the Subantarctic Front, respectively. Each dot represents an Argo profile.

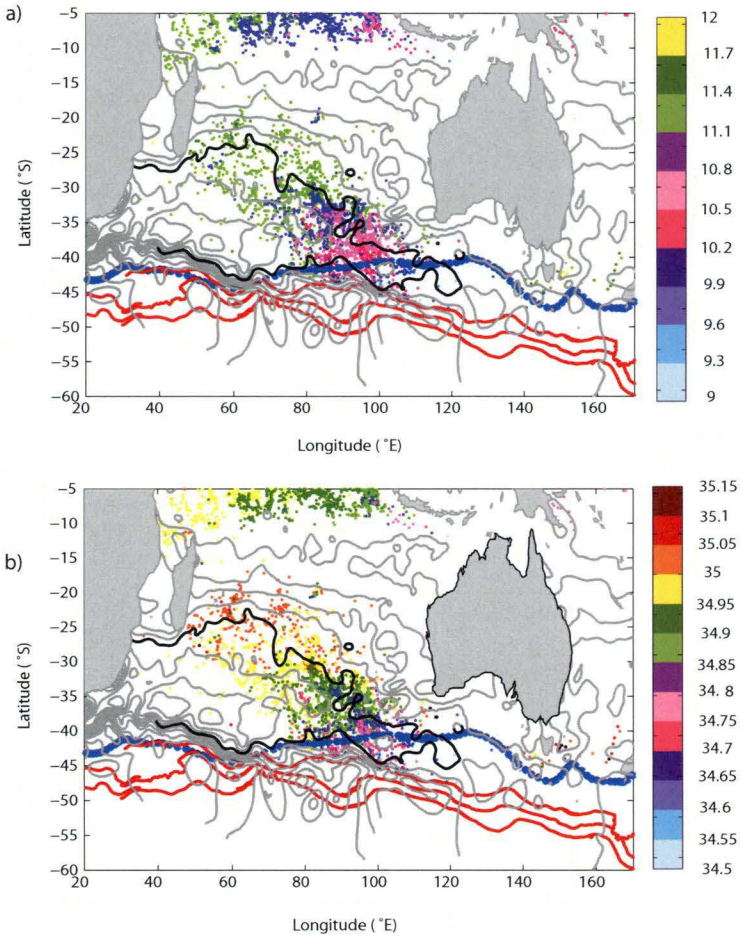

Figure 2.6: SAMW (PV $\leq 1.5 \times 10^{-9} m^{-1} s^{-1}$) temperature (a) and salinity (b) spatial variability on the 26.8–γ^n surface.Modified Montgomery streamlines are depicted by grey lines. The $\Psi_{26.8}$ streamline is shown as a thick black line. Blue dotted and red lines depict the Subtropical Front and the Subantarctic Front, respectively. Each dot represents an Argo profile.

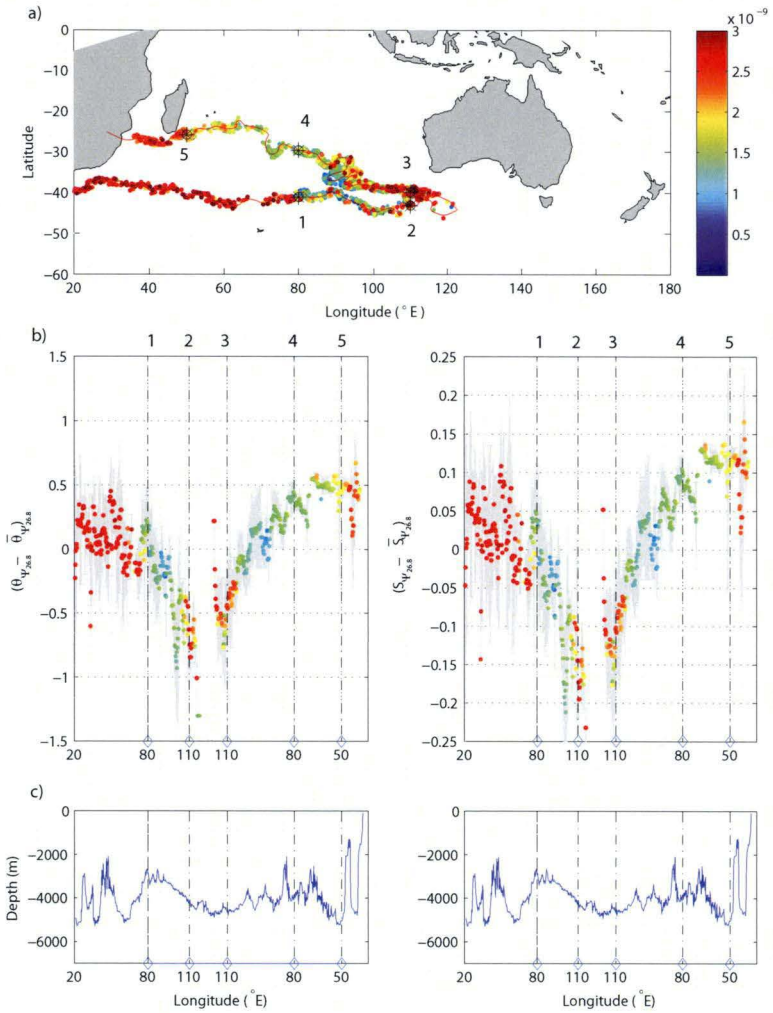

Figure 2.7: Temperature and salinity changes along $\Psi_{26.8}$. a) Colour–coded dots (according to the Potential vorticity) are Argo floats within 100 km from $\Psi_{26.8}$ (in red). Black stars where placed randomly to mark the eastward temperature and salinity anomaly changes along $\Psi_{26.8}$. b) Temperature and salinity anomaly along $\Psi_{26.8}$. Grey bars denote the standard deviation. Each dot is the mean within a 100 km radius for every position in the streamline. Vertical black dashed lines indicate the position of the black stars in (a). c) Ocean topography along $\Psi_{26.8}$

The Agulhas Return Current and the ACC are depicted as a tight group of streamlines between 20°E and 60°E, east of which the ACC is poorly represented on this density surface. The circulation is mainly described by an anticyclonic recirculation west of 110°E and between 20°S and 40°S with the easternmost turning point just west of the Southeast Indian Ridge (figure 2.4). Southwest of Australia, the streamlines suggest that the circulation is mainly northwestward although data are sparse at this density surface. Note that the PV minimum aligns well with the streamlines suggesting they do a reasonable job of representing the flow on this isopycnal. Blue dotted and red lines represent the Subtropical Front (STF) (*Orsi et al.*, 1995) and the Subantarctic Front (SAF) (*Sokolov and Rintoul*, 2007), respectively.

The 26.8–γ^n surface reveals a tongue–like distribution of the light Indian SAMW (figure 2.5, colour–coded dots). It is found in a narrow region between 80°E and 100°E, south of 30°S, surrounded in the west and south by the Southeast Indian Ridge and, in the northeast, by the Broken Plateau (figure 2.4). The lowest PV minimum (strongest SAMW pycnostad) lies just south of the STF (80°E – 100°E) and embedded inside the anticyclonic circulation turning point. The streamline enclosing the SAMW "pool", hereafter $\Psi_{26.8}$, will be used as a reference to discuss the spatial SAMW features (black contour, figures 2.5 and, 2.6). Similar nomenclature is used in the following Sections with the corresponding isopycnal subscript, $\Psi^i_{\gamma^n}$, where i is the order number of streamlines used, and $\gamma^n$is the isopycnal surface we are focused on.

The PV minimum is injected into the ocean interior at a particular location. The PV minimum spreads northwestward along $\Psi_{26.8}$ over a wider region after passing through the passage between the Southeast Indian Ridge and the Broken Plateau (~30°S, 80 °E – 90°E) (figure, 2.4), reaching as far north as 20 °S – 25°S before its signal vanishes. North of this passage, the erosion of the PV minimum is enhanced as it spreads along $\Psi_{26.8}$. The PV minimum is limited by a sharp boundary between the PV minimum and the high PV waters east of 100°E.

SAMW Temperature and Salinity

SAMW properties on γ^n= 26.8 are shown in figures 2.6. SAMW in the Subantarctic Zone has a temperature of 10 °C – 10.5°C and a salinity of 34.7 – 34.8 psu. From the SAMW formation to the northern–most extent of SAMW in the northwestern south Indian Basin, SAMW temperature and salinity increase ~1.2°C and 0.3 psu, respectively. Temperature and salinity increase up to 0.5°C (10.5 °C – 11°C) and 0.1 (34.85 – 34.95) psu, respectively, north of the STF. South of the region delimited by the Southeast Indian Ridge and the Broken Plateau, SAMW temperature and salinity remain constant along $\Psi_{26.8}$. North of it, SAMW properties change again after the passage formed by the two main bathymetric features just mentioned, entering the central south Indian Basin where temperature and salinity change very slowly at the same rate as the PV minimum until the latter has been completely eroded.

Temperature and salinity anomalies (relative to the mean properties along $\Psi_{26.8}$) are followed along the streamline and compared to the PV minimum changes (figure 2.7). A PV minimum is seen between "stations" 1 and 2 (80 °E and 110 °E, respectively) where temperature and salinity decrease rapidly associated to eddy heat diffusivity (*Sallée*, 2006). Temperature and salinity change step–wise close to the Broken Plateau (between "stations" 3 and 4), seen as the sharp shallowing of the ocean topography (figure 2.7, c). Westward of the Broken Plateau, the PV signal is progressively eroded, and temperature and salinity in the PV minimum layer increase as the African coast is approached.

SAMW on γ^n = 26.9

SAMW spatial variability

The Montgomery streamlines on the 26.9–γ^n surface show the circulation from a wide region of the south Indian Ocean (SIO) (figure 2.8). The ACC is depicted by a tight group

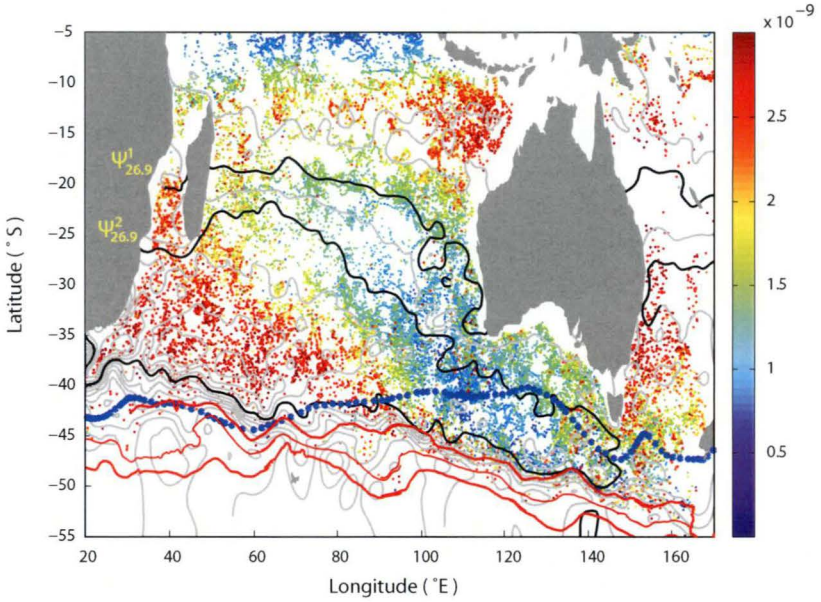

Figure 2.8: Potential Vorticity on the 26.9–γ^n surface. SAMW is identified as PV $\leq$ $1.5 \times 10^{-9} m^{-1} s^{-1}$. Modified Montgomery streamlines are depicted by grey lines. The $\Psi^1_{26.9}$ and $\Psi^2_{26.9}$ streamlines are shown as a thick black line. Blue dotted– and red lines depict the Subtropical Front and the Subantarctic Front, respectively. Each dot represents an Argo profile.

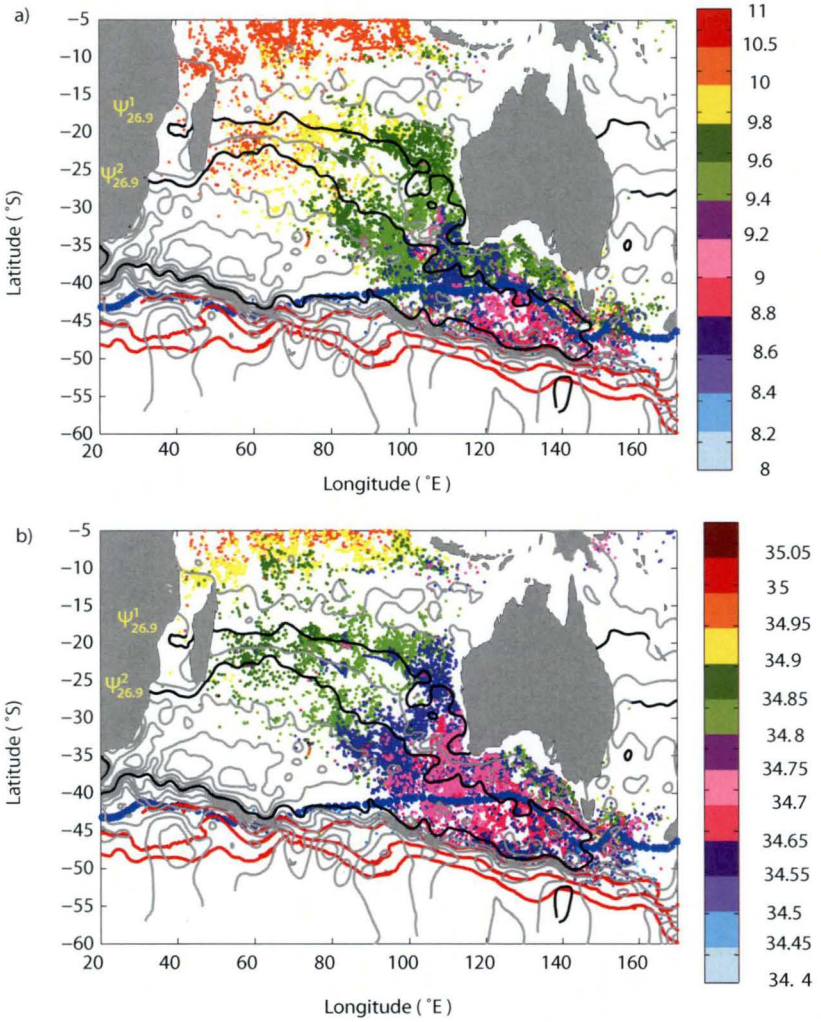

Figure 2.9: SAMW (PV $\leq 1.5 \times 10^{-9} m^{-1} s^{-1}$) temperature (a) and salinity (b) spatial variability on the 26.9–γ^n surface.Modified Montgomery streamlines are depicted by grey lines. Two streamlines have been highlighted, $\Psi^1_{26.9}$ and $\Psi^2_{26.9}$ (thick black lines). Blue dotted and red lines depict the Subtropical Front and the Subantarctic Front, respectively. Each dot represents an Argo profile.

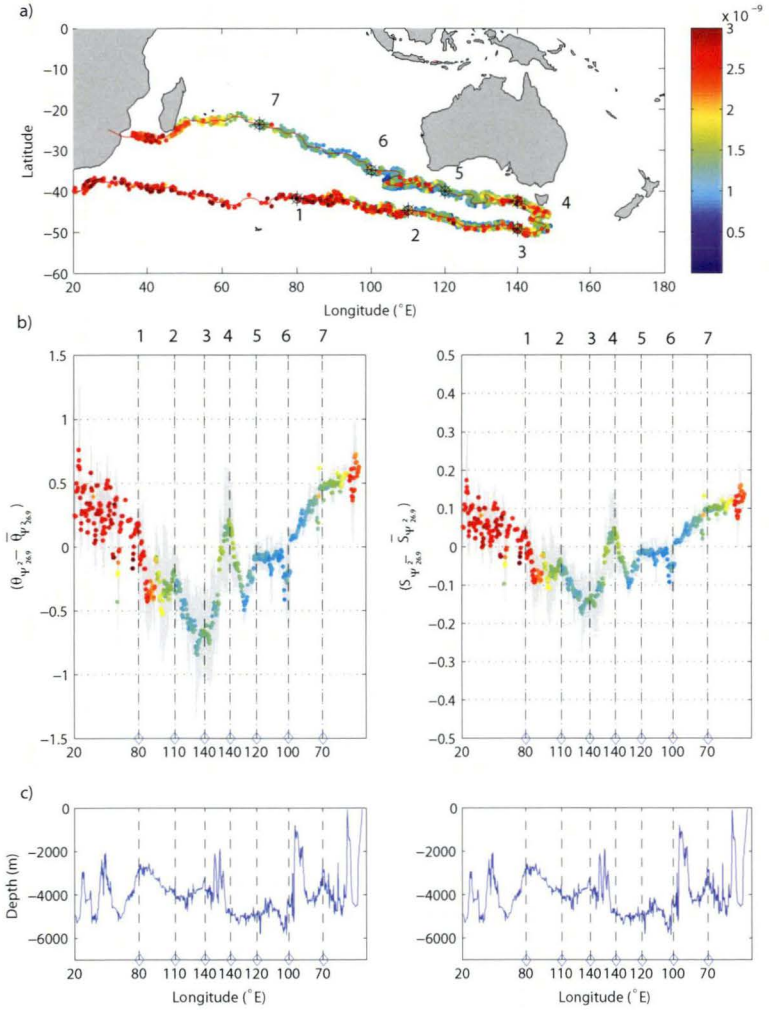

Figure 2.10: Temperature and salinity changes along $\Psi^2_{26.9}$. a) Colour–coded dots (according to the Potential vorticity) are Argo floats within 100 km from $\Psi^2_{26.9}$ (in red). Black stars where placed randomly to mark the eastward temperature and salinity anomaly changes along $\Psi^2_{26.9}$. b) Temperature and salinity anomaly along $\Psi^2_{26.9}$. Grey bars denote the standard deviation. Each dot is the mean within a 100 km radius for every position in the streamline. Vertical black dashed lines indicate the position of the black stars in (a). c) Ocean topography along $\Psi^2_{26.9}$

of streamlines south of 40°S. The remnant of the Indian subtropical gyre dominates the circulation in the western south Indian Ocean extending from the southern tip of South Africa (20°E) to approximately 70°E. The eastern SIO is described as an anticyclonic recirculation with the northwestward turning point southwest of Tasmania, as seen in the 26.8–γ^nsurface. The circulation south west and south east of Australia seem poorly represented, probably due to high mesoscale activity associated with the Leeuwin Current and East Australian Current, respectively.

SAMW PV minimum on the 26.9–γ^n surface covers vast areas of the south Indian Ocean, from southwest of Tasmania (45°S, 150°E) to the east of Madagascar (20 °S, 40 °E). Streamline contours suggest a sluggish circulation in the region between 80 °E and the region delimited by the $\Psi^2_{26\,9}$ streamline. This region seems to isolate this SAMW type. The lowest PV minimum is found between 95 °E and 120 °E, just north of the SAF and along the $\Psi^1_{26\,9}$ and $\Psi^2_{26\,9}$ streamlines (figure 2.8, black bold lines). The low PV enters the gyre in a preferred, narrow range of Ψ from the east. Southeast of the Broken Plateau (30°S, west of 100°E), the 26.9–γ^nSAMW circulation has split in two entering the central Indian Ocean. Along path one, SAMW follows the $\Psi^1_{26\,9}$ streamline northward along the western Australian coast, east of the Broken Plateau. Between 20°S and 25°S, SAMW flows westwards toward Madagascar Island where the PV minimum is eroded very quickly (following $\Psi^1_{26\,9}$). Also, the Indonesian Throughflow region acts as a high PV boundary at ~15 °S. East of Madagascar, there is evidence of an exchange of waters with high PV (moving slightly southward along the coast of Madagascar) and the low PV (moving slightly northward, east of the high PV near the coast). Along path two, following $\Psi^2_{26\,9}$, SAMW flows northwestward across the bathymetric passage, west of the Broken Plateau. There is no evidence of low PV water returning south in the western boundary, where high PV occupies the western gyre.

The erosion of the PV minimum is associated with the circulation path of SAMW. South of Tasmania, warm and salty waters carried by the remnant East Australian Current, in the

form of isolated eddies, mix with waters from the Subantarctic Zone (better seen in the higher salinity surrounding Tasmania in figure 2.9 b). The South Tasman Rise influences the regional circulation, and the properties either side of it (figure 2.10; see also Chapter 4 for more details).

SAMW Temperature and Salinity

SAMW temperature and salinity on the 26.9–γ^nsurface are shown in figure 2.9. Properties will be discussed following the two paths described above, starting where the lowest PV signature is found in the Subantarctic Zone. North of the SAF, SAMW cools and freshens as it flows eastward with the Antarctic Circumpolar Current. When it reaches south of Tasmania, SAMW temperature and salinity are: 8.6 °C – 9°C and 34.55 – 34.65 psu. Between 100 °E and 120°E, temperature and salinity increase 0.4°C and 0.05 psu, respectively (compared to south Australia values). SAMW properties increase 0.2°C and 0.05 psu near the Broken Plateau. North and northwest of the Broken Plateau, SAMW temperature has increased by 1 °C –1.5°C at 20°S, from the lowest PV region to the "end" of its export path. South of Australia and surrounding Tasmania, SAMW temperature and salinity increase from 8.6 °C – 9°C to 9.8 °C – 10°C (~1.2 °C), and from 34.55 – 34.65 psu to 34.8 – 34.85 psu (~0.35 psu) (figure 2.9).

Temperature and salinity anomalies (relative to the mean properties along $\Psi^2_{26.9}$) are followed along the streamline and compared to the PV minimum changes (figure 2.10). East of 110 °E, the PV minimum cools and freshens as it approaches the south Tasman Rise ("stations" 2 and 3), (figure 2.10, b). South of Tasmania, SAMW properties increase over 1 °C between "stations" 3 and 4, reflecting the high influence of the advection of warm and salty subtropical waters from the Tasman Sea (see Chapter 4 for a detailed description of the regional circulation and its influence over upper ocean water masses). South of the Broken Plateau (30 °S – 35 °S and 100 °E – 120 °E), between "stations" 5 and 6, mean properties are constant (error bars show the standard deviation per "station"). At

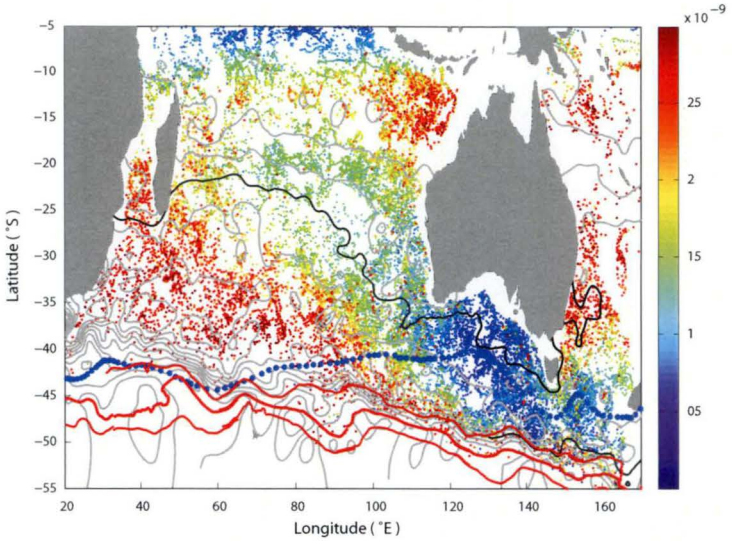

Figure 2.11: Potential Vorticity on the 26.94–γ^n surface. SAMW is identified as PV $\leq$ $1.5 \times 10^{-9} m^{-1} s^{-1}$. Modified Montgomery streamlines are depicted by grey lines. Blue dotted and red lines depict the Subtropical Front and the Subantarctic Front, respectively. Each dot represents an Argo profile.

"station" 6, temperature, salinity and PV decrease, likely reflecting the proximity of the formation region at this longitude. West of the Broken Plateau ($\sim$ "station" 6), at 100 °E, a rapid increase in SAMW temperature and salinity is followed by the erosion of the PV minima towards "station" 7 as SAMW flows over rough topography (figure 2.10, c).

SAMW on γ^n = 26.94

The streamlines and PV spatial distribution on γ^n= 26.94 show similarities with the 26.9–γ^n SAMW (figure 2.8); however, the low PV is much more restricted to south of Australia. The two pathways (northward along the western Australia coast, and west to south of the Broken Plateau) observed on the 26.9–γ^nsurface are also seen on this density surface. Note that there is a"gap" with no floats north of the Broken Plateau on both 26.9–$\gamma^n$and 26.94–γ^nsurfaces. SAMW PV minimum signal on the 26.94–γ^n surface is found south of

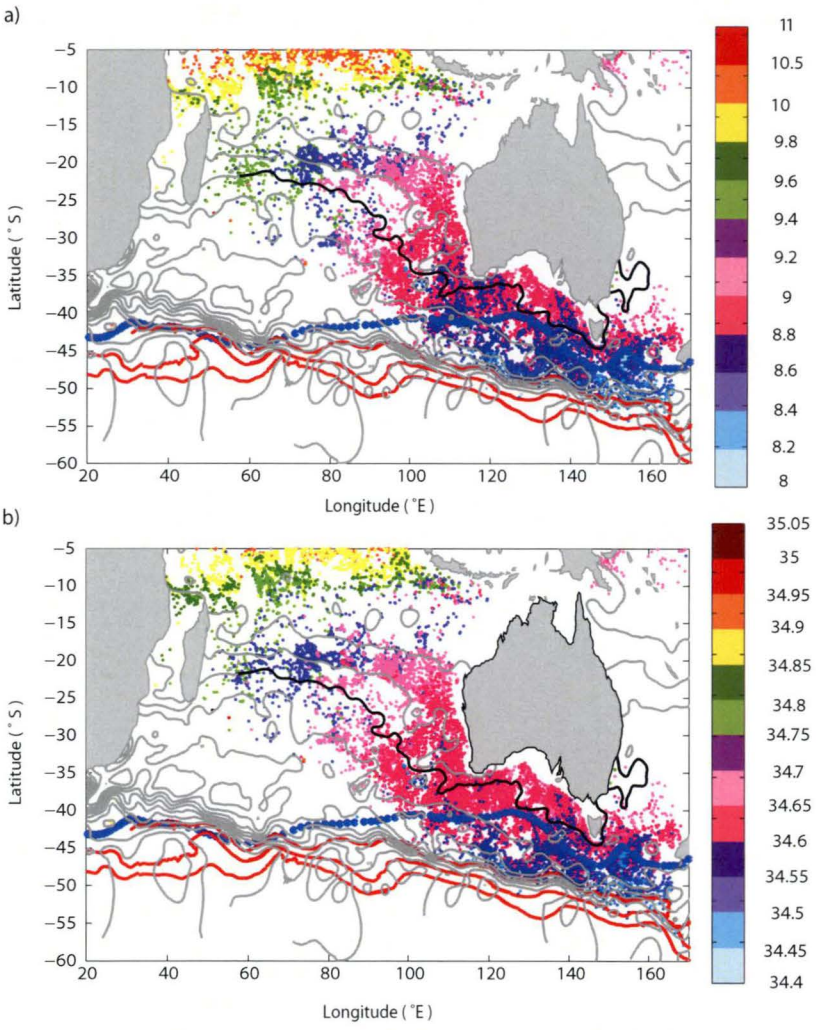

Figure 2.12: SAMW (PV $\leq 1.5 \times 10^{-9} m^{-1} s^{-1}$) temperature (a) and salinity (b) spatial variability on the 26.94–γ^n surface. Modified Montgomery streamlines are depicted by grey lines. The $\Psi_{26.94}$ streamline is shown as a thick black line. Blue dotted and red lines depict the Subtropical Front and the Subantarctic Front, respectively. Each dot represents an Argo profile.

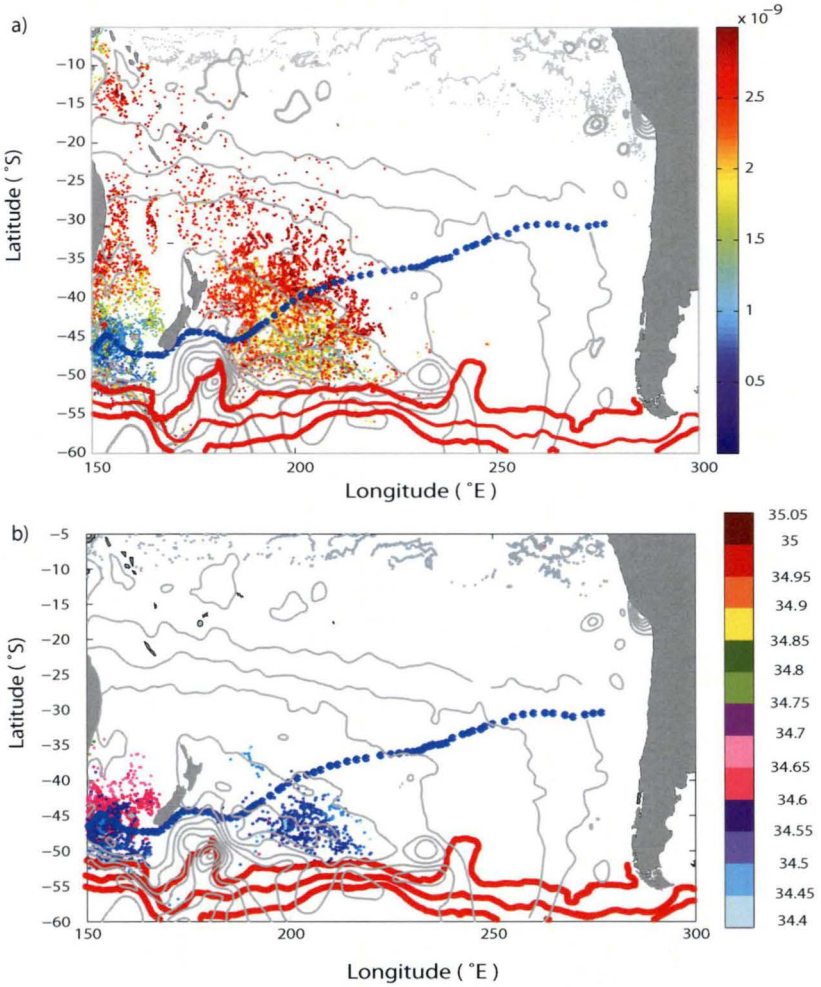

Figure 2.13: SAMW (PV $\leq 1.5 \times 10^{-9} m^{-1} s^{-1}$) potential vorticity (a) and salinity (b) spatial variability on the 26.94–γ^n surface in the Pacific sector of the Southern Ocean. Modified Montgomery streamlines are depicted by grey lines. The $\Psi_{26.94}$ streamline is shown as a thick black line. Blue dotted and red lines depict the Subtropical Front and the Subantarctic Front, respectively. Each dot represents an Argo profile.

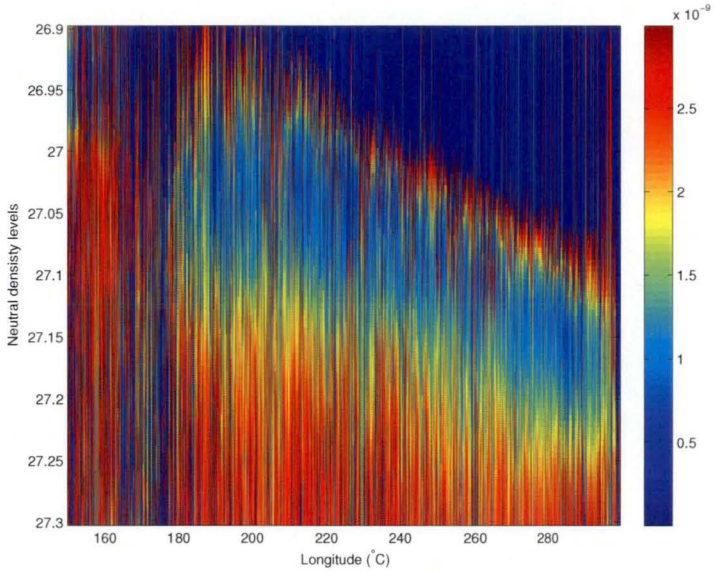

Figure 2.14: SAMW tracer, potential vorticity minimum, as a function of longitude ($^{\circ}E$) and neutral density (γ^n) in the South Pacific Ocean. This figure shows all the available profiles, sorted by longitude. The navy blue in the background just shows values out of our PV range ($[0, 3 \times 10^{-9}]\ m^{-1}s^{-1}$).

Tasmania and on either side of New Zealand (figures 2.11, 2.12, and 2.13). The evolution of properties along the northern flank of the SAF shows clearly in the salinity distribution (figure 2.12, b). The SAZ southwest of Tasmania is highly influenced by SAF waters due to the high tendency to create eddies and meanders of the SAF (more details in Chapter 4). SAMW temperature and salinity cool and freshen eastward, from southwest to southeast of Tasmania (0.2°C; 0.1 psu). The SAMW properties on either side of New Zealand show similar temperature and salinity values (8.4 °C – 8.6°C; 34.5 – 34.6 psu) on this density surface. South east of New Zealand, a cluster of SAMW is found at the turning point of an anticyclonic recirculation (40 °S – 50°S, 200 °E – 210°E)(figure 2.13).

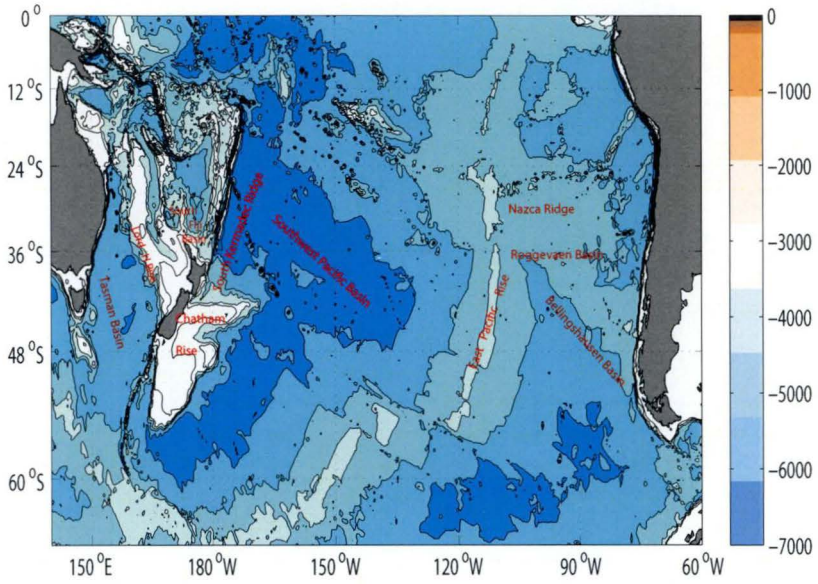

Figure 2.15: South Pacific Ocean topography. Main topographic features have been labeled.

2.3.2 SAMW in the south Pacific Ocean

SAMW (PV $\leq 1.5 \times 10^{-9} m^{-1} s^{-1}$) is found in a neutral density range of $\gamma^n \in [27, 27.2]$ in the south Pacific Ocean. Figure 2.14 depicts the PV minimum along longitude at γ^n surfaces. The region west of New Zealand has been included in this figure (longitude $\leq 180°$E). The lightest SAMW is found west of New Zealand. West of 240°E, SAMW density centers at 27.05–γ^n, with its lowest PV minimum between 220°E and 240°E. East of 240°E, SAMW becomes progressively denser as it approaches the South American continent. The lowest PV values are located at 260°E and 280°E. The local SAMW east of New Zealand is poorly represented in figure 2.14 .

Slight changes in density have strong implications for the SAMW circulation. The SAMW properties are next described on four isopycnal surfaces, $\gamma^n = [27 - 27.05]$ and, $\gamma^n \in [27.1 - 27.15]$. We have chosen to group the density surfaces in two ranges according

to their position regarding the East Pacific Rise (figure 2.15) (discussed in Section 2.4). An overview of the SAMW circulation in the Pacific Ocean will be described using the modified Montgomery streamlines for each of these density surfaces.

SAMW on 27 – 27.05

SAMW spatial variability

SAMW occupies a wide area between the Subantarctic Front (SAF) in the south and a northern limit of $\sim 30\,°S - 35°S$. SAMW pycnostad strengthens eastward along the SAF, east of New Zealand,and turns northwestward at $230\,°E - 250°E$, just west of the East Pacific Rise (figures 2.15 and 2.16). While the spatial distribution of the SAMW on the 27.0 and 27.05 surfaces show similarities (*i.e.* they are constrained to the southwest Pacific Basin – note that high PV is seen in the eastern basin), the extent of the PV minimum and so, the ventilation efficiency, differ. The lightest SAMW (27.0) is found inside the subtropical gyre, east of New Zealand, at $35\,°S - 50°S$ and, $180\,°E - 240°E$ (figure 2.16 a). Two streamlines, Ψ^1_{27} and Ψ^2_{27}, delimit the narrow zone where the 27–γ^n SAMW enters the gyre (black bold lines; figure 2.16 a, b). The 27.05–γ^n SAMW exceeds the lighter SAMW in spatial extent and pycnostad strength. It also enters the subtropical gyre in a wider region west of the East Pacific Rise.

No evidence of PV minimum water entering the Tasman Sea is seen on these density levels. The signature of the 27–γ^n SAMW PV minimum erodes abruptly between the South Fiji Basin and New Zealand ($30\,°S - 35°S$, 180°E). Similar erosion occurs to the 27.05–γ^n SAMW whose core reaches 30°S before eroding completely south of the Polynesia (figure 2.16).

SAMW Temperature and Salinity

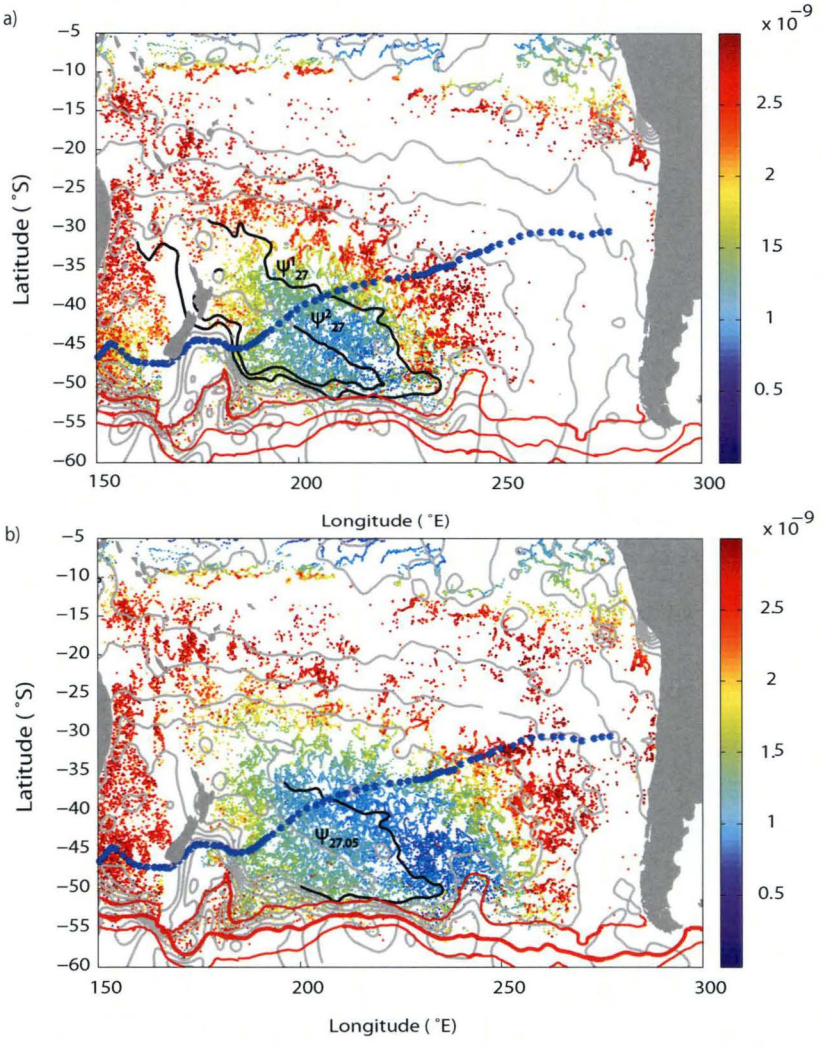

Figure 2.16: Potential Vorticity on the 27–γ^n surface (a) and 27.05–γ^n surface (b). SAMW is identified as PV $\leq 1.5 \times 10^{-9} m^{-1} s^{-1}$. Modified Montgomery streamlines are depicted by grey lines. The Ψ^1_{27}, Ψ^2_{27} and $\Psi_{27.05}$ streamlines are shown as a thick black line. Blue dotted and red lines depict the Subtropical Front and the Subantarctic Front, respectively. Each dot represents an Argo profile.

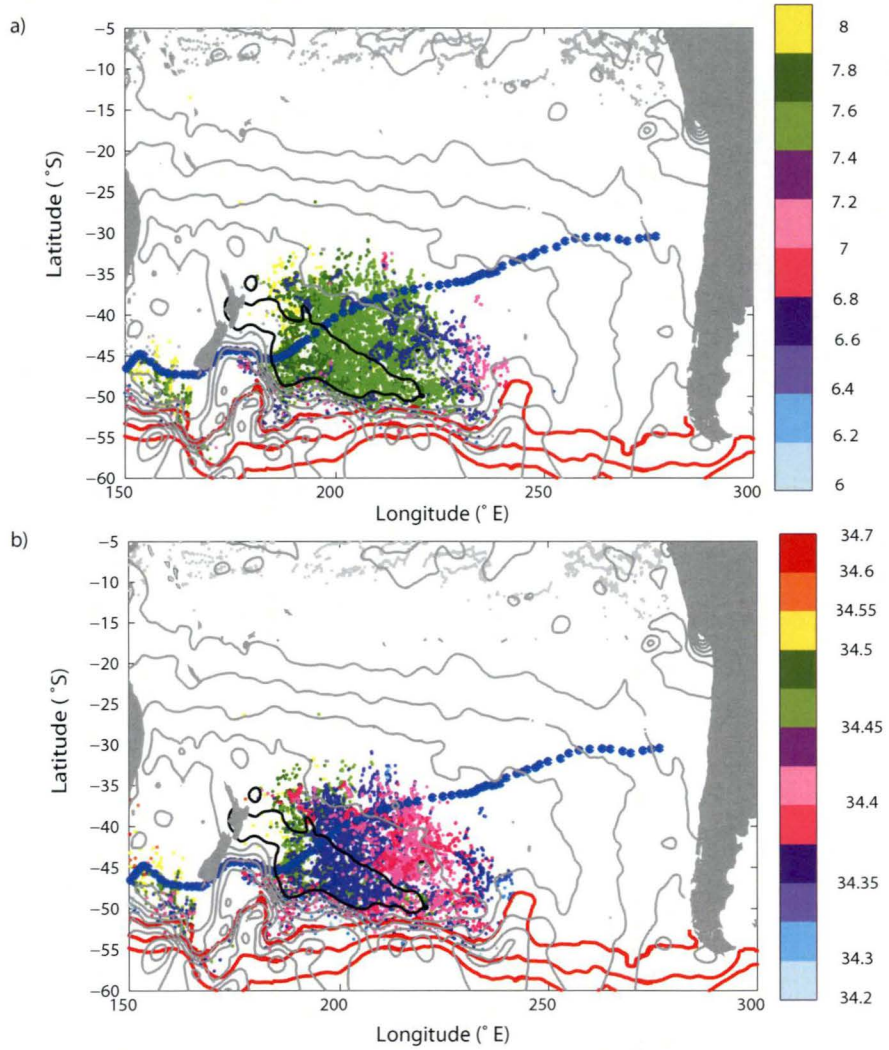

Figure 2.17: SAMW (PV $\leq 1.5 \times 10^{-9} m^{-1} s^{-1}$) temperature (a) and salinity (b) spatial variability on the 27–γ^n surface. Modified Montgomery streamlines are depicted by grey lines. Two streamlines, Ψ^1_{27} is shown as a thick black line. Blue dotted and red lines depict the Subtropical Front and the Subantarctic Front, respectively. Each dot represents an Argo profile.

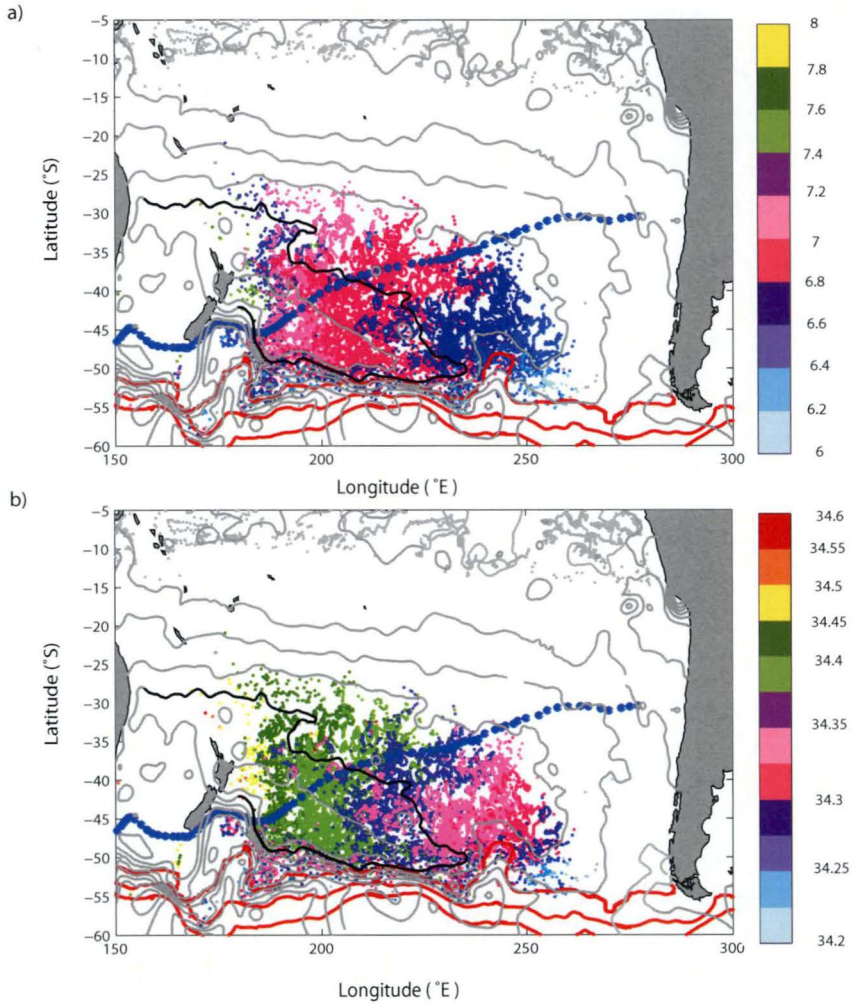

Figure 2.18: SAMW (PV $\leq 1.5 \times 10^{-9} m^{-1} s^{-1}$) temperature (a) and salinity (b) spatial variability on the 27.05–γ^n surface. Modified Montgomery streamlines are depicted by grey lines. The $\Psi_{27.05}$ streamline is shown as a thick black line. Blue dotted and red lines depict the Subtropical Front and the Subantarctic Front, respectively. Each dot represents an Argo profile.

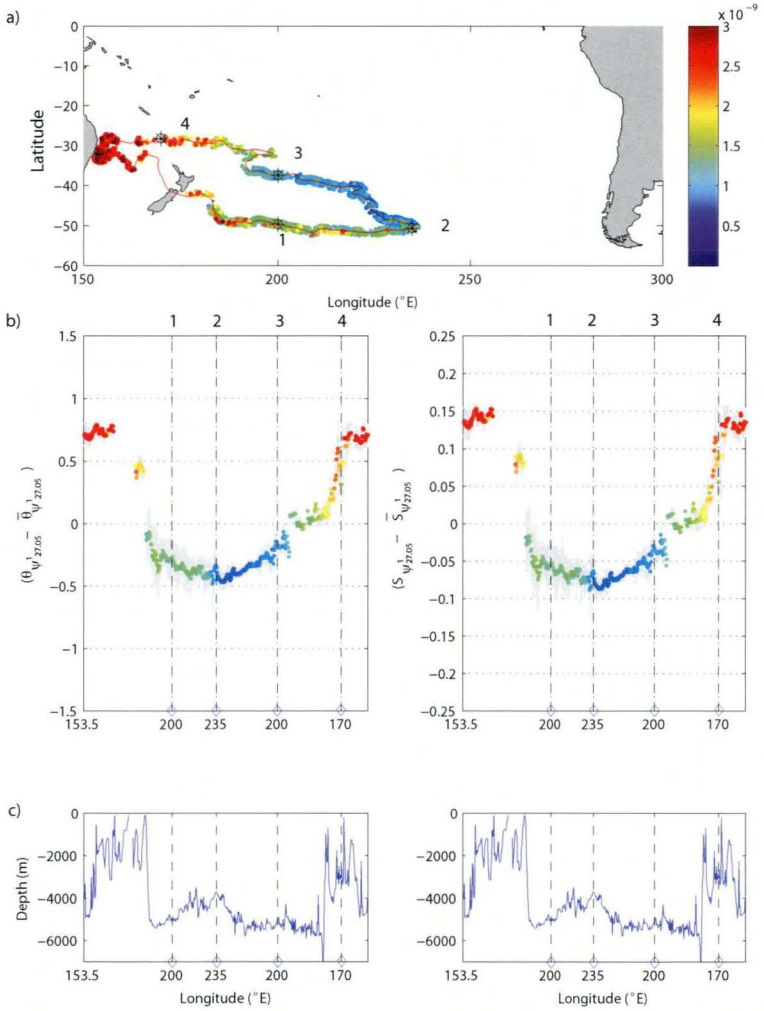

Figure 2.19: Temperature and salinity changes along $\Psi^1_{27.05}$. a) Colour–coded dots (according to the Potential vorticity) are Argo floats within 100 km from $\Psi^1_{27.05}$ (in red). Black stars where placed randomly to mark the eastward temperature and salinity anomaly changes along $\Psi^1_{27.05}$. b) Temperature and salinity anomaly along $\Psi^1_{27.05}$. Grey bars denote the standard deviation. Each dot is the mean within a 100 km radius for every position in the streamline. Vertical black dashed lines indicate the position of the black stars in (a). c) Ocean topography along $\Psi^1_{27.05}$

SAMW temperature and salinity warm and become saltier anti–clockwise along streamlines at both density surfaces (figures 2.17 and 2.18). The 27–γ^nSAMW mean temperature and salinity are 7.5°C and 34.4 psu, respectively (figures 2.17 a, 2.18 a). The closed extent of the 27–γ^nSAMW is reflected in the low variability of temperature and salinity with higher values northeast of New Zealand (7.8°C, 34.45 psu), and lower values in the eastern part of the SAMW pool (34.35 psu).

The 27.05–γ^nSAMW properties gradually change as it flows northwestward. The coldest and freshest 27.05–γ^n–SAMW patch (6.2 °C – 6.6°C, 34.2 – 34.3 psu) is found along the ACC (50 °S– 55°S) and at the eastern part of the SAMW pool (55 °S – 35°S, 220 °E – 260°E) where the Mode Water enters the main thermocline in the subtropical gyre. The temperature and salinity of the 27.05–γ^n–SAMW increase by 0.4 °C – 0.8°C and 0.15 psu respectively, warmer and saltier (relative to the SAMW core) as it flows to the west, away from the subduction area.

An example of the along–stream temperature and salinity change is shown in figure 2.19. The coldest and freshest SAMW (figure 2.19 b) is found north of the SAF where the 27.05–γ^nSAMW has its eastern–most point (figure 2.16). Compared to the Indian Ocean where the topography is more complex, in the Southeast Pacific Basin, the pycnostad is very stable. The lack of erosion of the low PV signal suggests very weak mixing, until the SAMW encounters the very steep ocean topography northeast of New Zealand, the South Kermadec Ridge (figures 2.15, 2.19 c).

SAMW on 27.1 – 27.15

SAMW Spatial Variability

The eastern south Pacific Basin is occupied by the densest SAMW spanning a neutral density range of 27.1 – 27.2 kgm^{-3}. The lowest PV minima are found east of the East

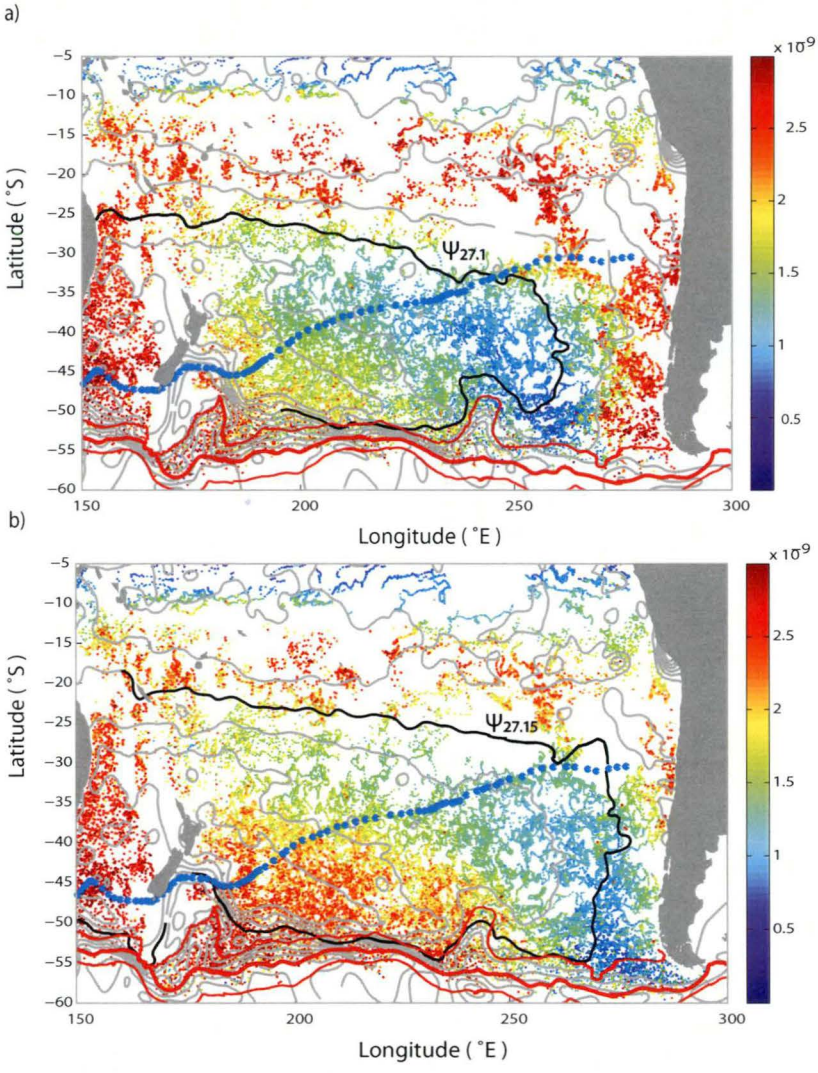

Figure 2.20: Potential Vorticity on the 27.1–γ^n surface (a) and 27.15–γ^n surface (b). SAMW is identified as PV $\leq 1.5 \times 10^{-9} m^{-1} s^{-1}$. Modified Montgomery streamlines are depicted by grey lines. The $\Psi_{27.1}$ and $\Psi_{27.15}$ streamlines are shown as a thick black line. Blue dotted and red lines depict the Subtropical Front and the Subantarctic Front, respectively. Each dot represents an Argo profile.

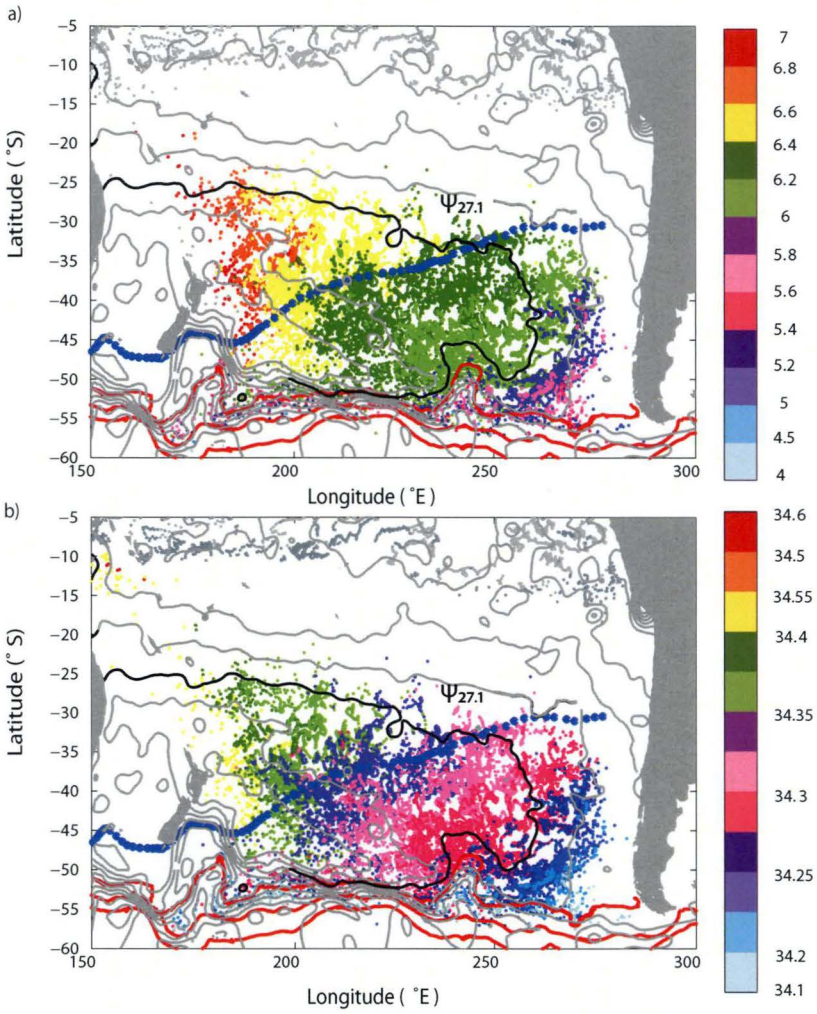

Figure 2.21: SAMW (PV $\leq 1.5 \times 10^{-9} m^{-1} s^{-1}$) temperature (a) and salinity (b) spatial variability on the 27.1–γ^n surface. Modified Montgomery streamlines are depicted by grey lines. The $\Psi_{27.1}$ streamline is shown as a thick black line. Blue dotted and red lines depict the Subtropical Front and the Subantarctic Front, respectively. Each dot represents an Argo profile.

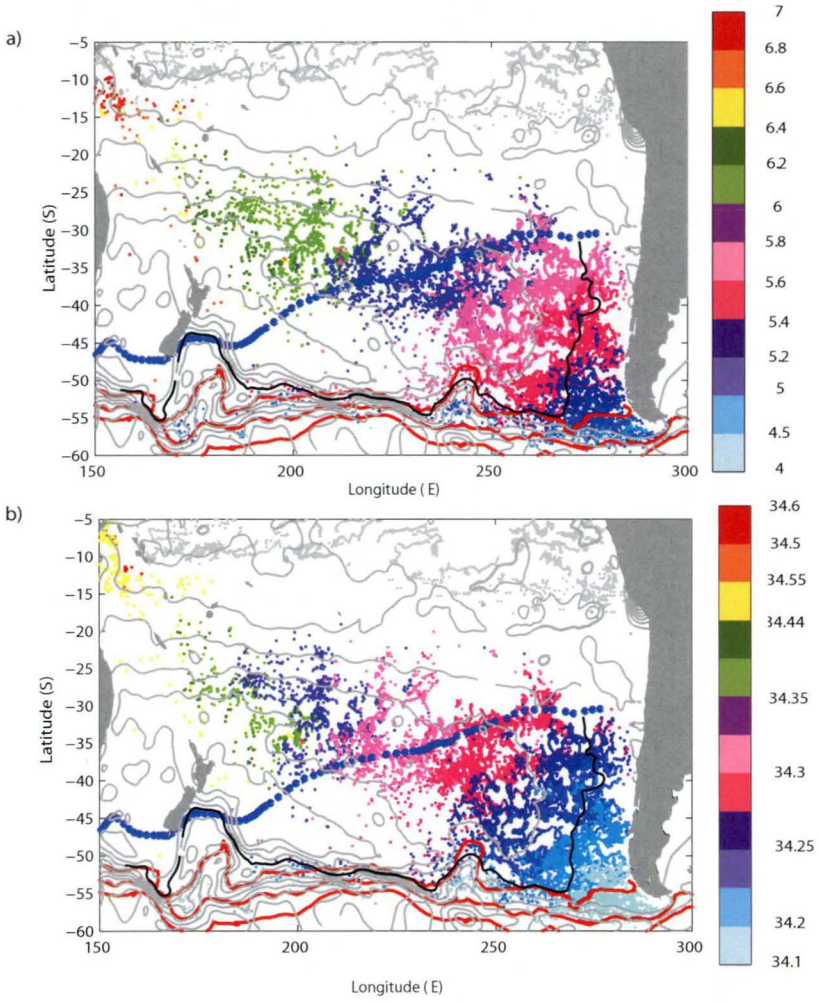

Figure 2.22: SAMW (PV $\leq 1.5 \times 10^{-9} m^{-1} s^{-1}$) temperature (a) and salinity (b) spatial variability on the 27.15–γ^n surface. Modified Montgomery streamlines are depicted by grey lines. The $\Psi_{27.15}$ streamline is shown as a thick black line. Blue dotted and red lines depict the Subtropical Front and the Subantarctic Front, respectively. Each dot represents an Argo profile.

Pacific Rise (250°E) and west of the tip of South America (280°E) (figure 2.20). The spatial distribution of the PV minimum is again very distinctive on the neutral density surface on which it lies. For the 27.1–γ^n SAMW, low PV shows a similar pattern to that seen on the 27.05–γ^n surface but with the lowest PV cluster situated east of 250°E (figure 2.20 a). A north– and northwest–ward circulation of the SAMW core can be inferred from the modified Montgomery streamlines in both neutral surfaces (figure 2.20). The erosion of the pycnostad along streamlines is very low.

A significant difference between the western and eastern Pacific SAMWs is the spatial extent of the PV minimum. While in the western SAMWs, the spatial extent is mainly defined by the SAMW core limits (where the core is defined by PV $\leq 1 \times 10^{-9} m^{-1} s^{-1}$); in the eastern SAMWs, the spatial extent of the pycnostad (PV $\leq 1.5 \times 10^{-9} m^{-1} s^{-1}$) considerably exceeds that of the SAMW, as it is the case of the 27.1–γ^nSAMW, where the PV minimum occupies the south Pacific Basin, with the exception of the Tasman Sea and the South American coast.

SAMW Temperature and Salinity

SAMW properties on the 27.1–γ^n surface occupy an extensive fan–like region of the central Pacific (50 °S – 30°S, 210 °E – 270°E) with temperature and salinity ranges of 6 °C – 6.4°C, and 34.28 – 34.32 psu, respectively (figures 2.21). Once the PV minimum core starts eroding ($\sim$ 40 °S, 230 °E), temperature and salinity change rapidly when compared to the initial properties at the formation regions. A similar behaviour is found in the 27.15–γ^nsurface. Properties of the SAMW core (5.2 °C – 5.6°C; 34.2 – 34.25 psu) propagate northward up to 40°S along the $\Psi_{27\,15}$ streamline (figures 2.21 b and, 2.22 b; black bold line) at 270 °E – 280°E from the formation region.

We have seen so far that temperature and salinity of the PV minimum become warmer and saltier as the PV minimum flows anti–clockwise from the Southern Ocean. Along the

Table 2.1: Colour–code regarding latitude–longitude of the argo profiles.

	green	*navy blue*	*red*	*pink*	*ash blue*	*black*
Latitude (°)S	≤ 50	≥ 50	≥ 50	$\in (30, 50]$	$\in [30, 50]$	~ 20
Longitude (°)E		≤ 315	$\in [315, 330]$	$\in [330, 360)$	≥ 360	
Longitude (°)W		≤ 45	$\in [45, 30]$	$\in [30, 0)$	≥ 0	

eastern side of the Tonga–Kermadec Rise (from $\sim$ 45 °S to 25 °S at 190 °E), warmer and saltier Tasman Sea waters mix with SAMW, rapidly changing its properties and eroding the PV minimum signature. This eastward flow is inferred from the increased temperature and salinity along $\sim$35 °S (between 190 °E and 200 °E) and followed by the streamlines (also observed on previous density surfaces) (figures 2.20 a, 2.21). PV minimum waters with similar temperature and salinity values to those in the southeast Pacific Ocean are also found in the SAF further west, but are not exported to the subtropics at these longitudes.

2.3.3 SAMW in the south Atlantic Ocean

Contrary to what we found in the south Indian and south Pacific Oceans, there is no clear PV minimum "pool" associated with a specific density surface in the South Atlantic Ocean (figures 2.3 and, 2.14). The PV minimum was plotted on neutral density surfaces spanning from 26 to 28 kgm^{-3}. Two γ^n ranges, 26.5 – 26.6 and 27.2 – 27.3, showed a layer of PV minimum. The lighter PV minimum layer is associated with a narrow region where deep mixed layers are found (30 °S – 40°S; 30 °W – 40 °W). The range of temperature and salinity values in this layer is narrow: 14 °C – 15°C and $\sim$ 35.5 psu, respectively (not shown). These properties coincide with the Subtropical Mode Water defined in previous studies (e.g. *McCartney* (1977, 1982), *Provost et al.* (1995)). Here we will focus mainly on the denser PV minimum waters.

Argo profiles along the modified Montgomery streamlines are now followed for the 27.25–γ^nisopycnal surface. The location of the PV minimum in the temperature and

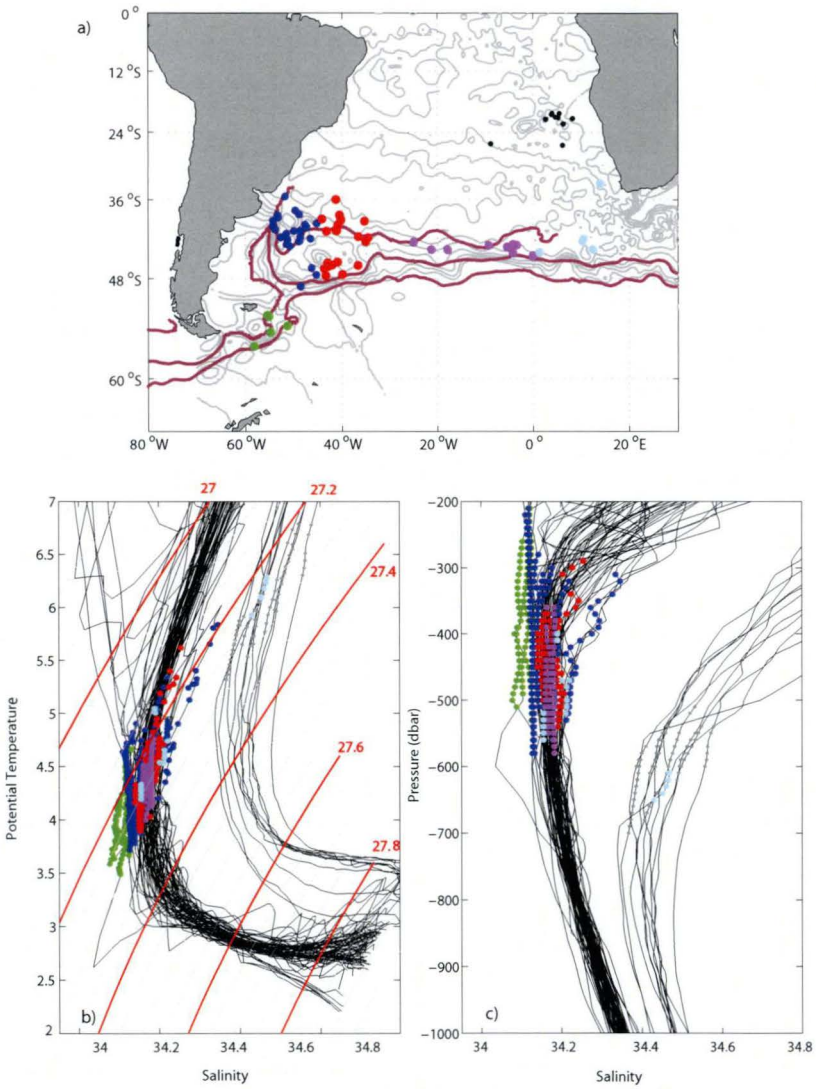

Figure 2.23: (a) Modified Montgomery streamlines at 27.25–γ^nsurface. Argo floats are shown with a location colour–code (see Table 1). (b) Potential temperature – salinity relationship. Dots depict the portion of the profile where PV $\leq 1.5 \times 10^{-9} m^{-1} s^{-1}$. (c) Salinity versus depth.

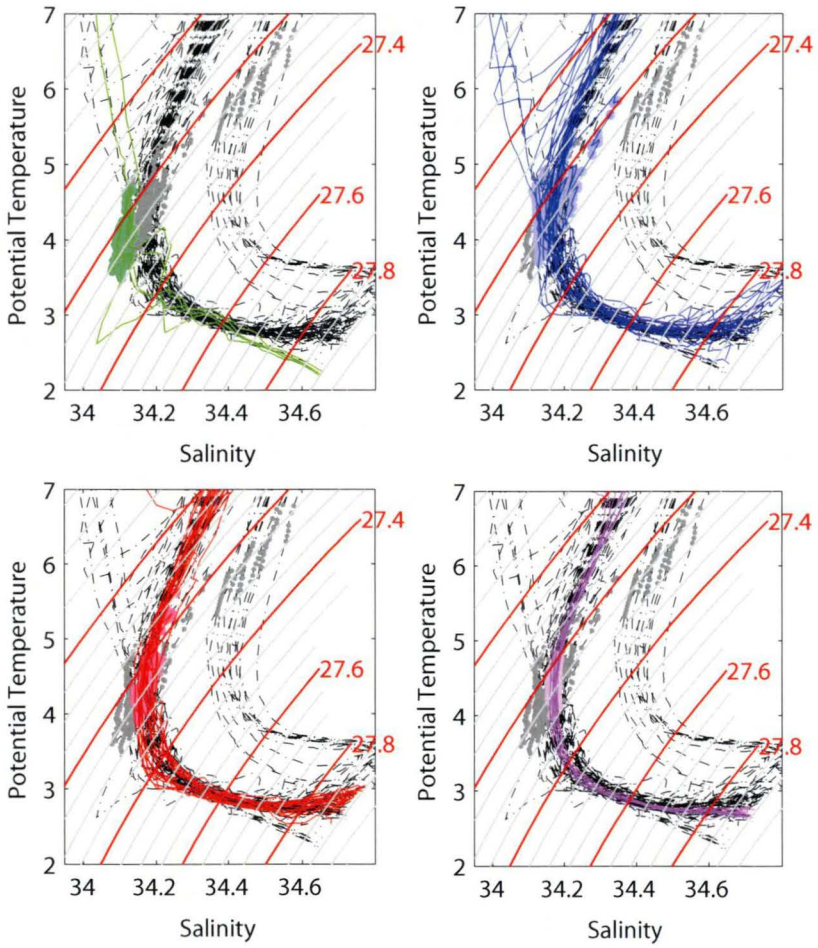

Figure 2.24: Eastward evolution (green→ blue→ red→ pink) of the PV minimum (in dots) along the streamline range. Following Table 1, colour–coded profiles, depicted by the coloured line) are highlighted in every panel regarding their location. All the selected profiles appear in the background as grey dotted lines. Grey dots show the location of the PV minimum in the profile.

salinity profiles is followed as the streamlines flow from Drake Passage toward the south Atlantic Ocean (figure 2.23). The temperature and salinity profiles are colour–coded depending on their position to clarify the region where changes in the depth (density level) of the PV minima occur (table 2.1). Floats found where the Brazil Current and the Malvinas current meet, known as the Brazil–Malvinas Confluence (BMC) are shown in navy blue. The Subtropical Convergence has been divided in 3 regions (red, pink, and ash blue) (figure 2.23). No distinction between seasons was made[2].

SAMW becomes slightly denser reaching γ^n= 27.3 kgm^{-3} east of Drake Passage and spreads eastward as a salinity minimum layer. Figures 2.23 to 2.24 show the stream–wise evolution of SAMW temperature and salinity from Drake Passage into the southwestern Atlantic Ocean. At Drake Passage, the PV minimum layer (4 °C – 5°C, 34.1 – 34.2 psu) with a density shifts from 27.2 to 27.3 kgm^{-3} (green profiles, figure 2.23). The region between Drake Passage and the BMC is interrupted due to lack of data. At the BMC, warm and salty waters of the Brazil Current occupy the top 200 – 400 metres, below which SAMW lies and forms the salinity minimum layer, namely Antarctic Intermediate Water (AAIW) (figure 2.24 b; grey dots in navy blue profiles). East of the BMC, SAMW is embedded in an eastward flow at the salinity minimum layer (400 – 700 metres) (figure 2.24 c, d). The top of the PV minimum layer erodes faster as it moves eastward, and it is almost absent east of 30 °W (figures 2.23 c, 2.24 d, e; grey dots in pink and ash blue profiles). So, our results evince that the salinity minimum layer in the south Atlantic Ocean is supplied by the potential vorticity minimum imported from the south Pacific Ocean. Worth noting that apparently this is not the case for deeper waters ($\leq$4 °C; see figure 2.23, b).

Near the Angolan coast (20°S, 0–10°E) a PV minimum layer of the same density/depth rage is found (black lines, figure 2.23) but with relatively higher temperature and salinity

[2]Note again that the first 200 dbar are excluded in our analysis.

(5.5 °C – 6.6°C, 34.4 – 34.5 psu) (figure 2.23 b). The first top 600 metres are of similar properties as the profiles flowing with the south Atlantic Current. Below 600 metres, temperature and salinity are relatively higher. Low PV signal spreading southward along the eastern African coast as part of the Angolan Current seems to be the origin (eastern boundary of the Angola gyre) (*Stramma and England*, 1999; *Lass and Mohrholz*, 2007); Properties are those of the south Atlantic Central Waters.

2.4 Discussion

SAMW properties have been described using CARS Climatology and Argo float temperature and salinity profiles (Sections 2.2 and 2.3). We compare our results with previous studies on SAMW properties and circulation, mainly carried out as part of the World Ocean Circulation Experiment (WOCE) and before the Argo program started. Firstly, SAMW types and circulation patterns in the Southern Hemisphere are discussed. Next, *McCartney*'s (1977) view of SAMW formation and evolution eastward along the Antarctic Circumpolar Current is also revised, followed by a review of previous ventilation and subduction studies.

2.4.1 SAMW modes and circulation

Different types or modes of Subantarctic Mode Water have been identified according to the PV minimum associated with a specific γ^nsurface. Here, SAMW properties and circulation will be exposed from the lightest to densest modes, progressively.

In the south Atlantic, different definitions have been given for the Mode Water at this location (e.g., *McCartney*, 1977; *Maamaatuaiahutapu et al.*, 1994; *Tsuchiya et al.*, 1994; *Provost et al.*,1995; *De Miranda et al.*, 1999; *Mémery et al.*, 2000), alternating between Subantarctic Mode Water or Subtropical Mode Water (STMW). The boundary between waters north or south of the STF is complicated at the Brazil–Malvinas Confluence Zone.

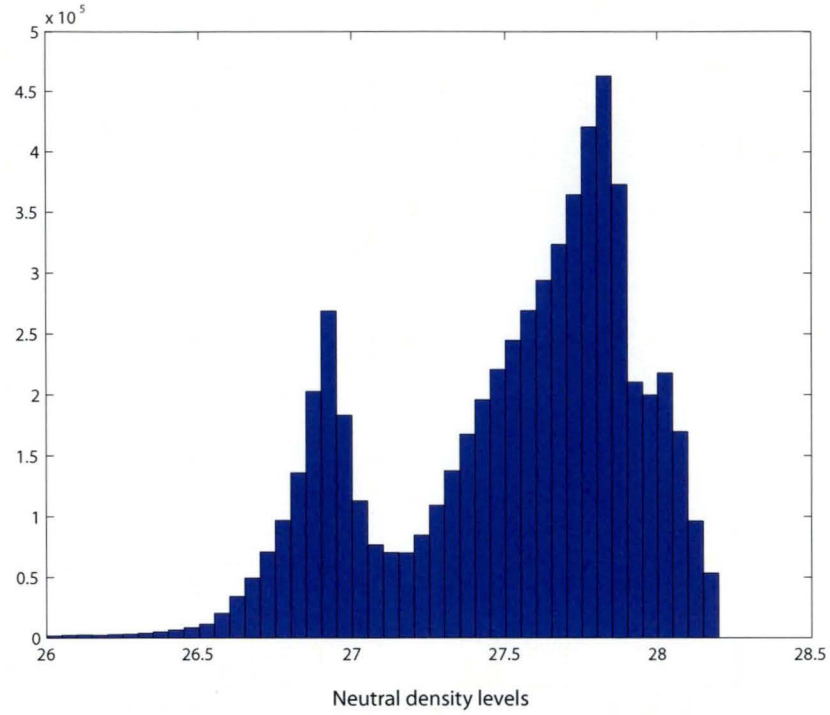

Figure 2.25: Neutral density distribution for the PV minimum in the south Indian Ocean.

This region is perhaps one of the most mesoscale energetic region in the world ocean (*De Miranda et al.*, 1999). Here, the lightest PV minimum waters with a neutral density range of 26.5 – 26.6 kgm^{-3} are found with a temperature and salinity of 14 °C – 16°C and 34.5 psu, respectively. The location of the SAMW, inferred from the PV minimum, shows a very narrow region (30 °S – 40 °S, 30 °W – 40 °W) where deep mixed layers are found. The PV minimum signature associated with this light mode water disappears very quickly east of 25°W to form part of the South Atlantic Current as South Atlantic Central Water. Strong eddy lateral mixing and stratification of the upper water column is apparent in the rapid erosion of the PV minimum, noted also by *Tsuchiya et al.* (1994). Isolated profiles showed PV minimum signals east of the Brazil–Malvinas Confluence , probably flowing eastward by being trapped in long–lived mesoscale features also noted by *Provost et al.* (1995).

In the Indian Ocean, four types of SAMW are found with specific circulation patterns, one more than identified in previous studies (*McCartney*, 1982; *Fine*, 1993; *McCarthy and Talley*, 1999). A histogram of the neutral density classes associated with a minimum in potential vorticity shows two main peaks centered at 26.9 kgm^{-3} and 27.8 kgm^{-3}. The latter corresponds to the boundary between the lower thermocline and deep waters. The peak at the lighter densities lies over the SAMW density range, with the 26.9–γ^nclass as the largest volumetric type (figure 2.25). The distribution of the three largest volumetric types of SAMW is shown in figure 2.26 in different greens over the main ocean topography. The size of the marker is inversely proportional to the PV minimum, that is, the smaller the PV, the bigger the marker. The northern branch of the SAF marks the southern boundary of the SAMW formation. *McCartney* (1982) pointed out the isolated distribution of the lighter SAMWs, confined to the southwest part of the subtropical gyre, in agreement with our observations. The 26.75–γ^n SAMW is found in a narrow region just west of the Southeast Indian Ridge, limited in the south by the SAF (not shown in figure 2.26). A change in the mixed layer depth east of the Southeast Indian Ridge marks the transition toward the 26.8–γ^n SAMW, expanding from 80 °E to 100°E (figures 2.26, and 2.31 a – see Section 2.4.2). Air–sea fluxes, eddy diffusion and northward Ekman transport are responsible for the preconditioning and formation of deep mixed layers associated with SAMW east of 80°E (*Sallée et al.*, 2006). This SAMW type is confined between the Broken Plateau and the Southeast Indian Ridge (figure 2.26, violet). Export of SAMW in this density class seems to happen in this same region, by tracing the PV minimum as far as north of 30°S and southeast of the Madagascar Basin. The effectiveness of this export in terms of ventilation of the ocean interior is likely to be low as the SAMW core PV minimum erodes very quickly close to the formation regions.

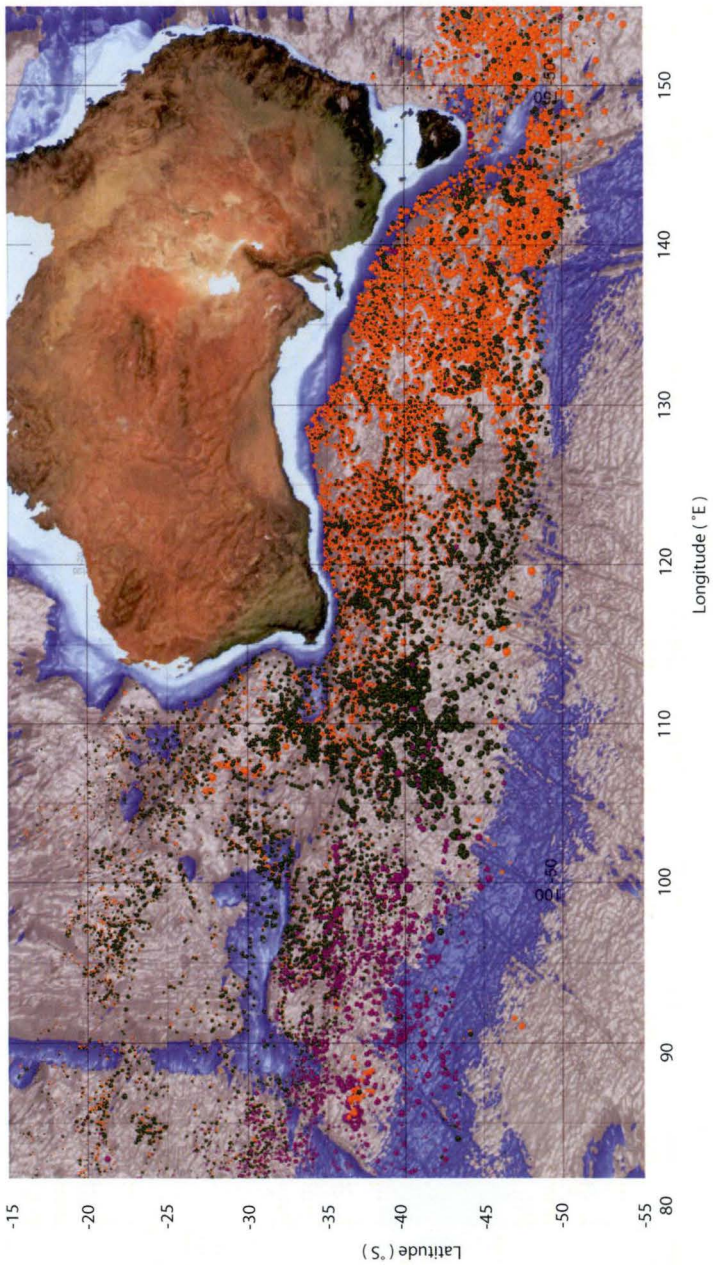

Figure 2.26: From east to west: 26.8–γ^n(violet), 26.9–γ^n(dark green), and 26.94–γ^n(orange) SAMW types). The size of the dots is inversely proportional to the PV minimum value.

Further east, between 100 °E and 120°E, the mixed layer depth increases at the same location as the PV minimum layer thickness (figure 2.31). This region is related to the 26.85–γ^n SAMW (not shown here). The SAMW core PV minimum can be traced from 50°S, 120°E diagonally northwestward to 30°S, 80°E with minimum PV change (figure 2.26) into the subtropical gyre. Consequently, we conclude the subduction of SAMW to be highly effective in the SAZ southwest of Australia, between 100 °E – 120°E, in agreement with previous studies (*Fine*, 1993; *Sallée et al.*, 2009; accepted by JPO). The trace of this SAMW class can be followed up to 20°S, east of Madagascar Island, before it is completely mixed (i.e. the low PV layer is eroded).

South of Australia, the 26.9–γ^n SAMW constitutes the largest volumetric SAMW class of the south Indian Ocean (figure 2.8). The core of the SAMW is located north of the SAF and centered at ~110°E. It is in this region where two SAMWs coexist (26.85– and 29.9–γ^n SAMW) and subduct to form part of the lower thermocline and feed Indian Central Water (*You and Tomczak*, 1993). Although they subduct in similar regions, the export paths followed are different. While the lighter SAMW enters the subtropical gyre following a northwestward geostrophic flow, the denser SAMW is forced to follow two routes as it encounters the Broken Plateau (figure 2.26). The influence of the Broken Plateau is highlighted by the fact that very few Argo profiles are found north of the Plateau. The encounter of the flow with this bathymetric feature likely enhances mixing, inferred from the change in the PV minimum (also in temperature and salinity) seen along streamlines (figures 2.7 and 2.10).

Two zonal westward flows describe the export of SAMW on the 26.9–γ^nsurface. The first one joins the subtropical gyre west of the Broken Plateau. On the other hand, SAMW flows northward along the western Australian coast. *Reid* (2003) used World Ocean Circulation sections to map the large–scale geostrophic flow in the Indian Ocean at various depths. He inferred poleward flow along the western coast of Australian at depths from 0 to 3000 dbar. Our observations, on the other hand, suggest an equatorward

flow along the western Australian Coast. *Domingues et al.* (2007) proposed a new 3–D view of the upper–circulation of the Southeastern Indian Ocean in which the net anticyclonic movement of the Subtropical Gyre is, in fact, formed by a combination of dominant zonal flows – a latitudinal succession of near surface eastward jets and deeper westward jets – linked with the equatorward boundary flow of the Leeuwin Undercurrent (LUC), along the west Australian continental slope. Near Cape Leeuwin (35 °S), the LUC transports South Indian Central Water (SICW), SAMW and AAIW. Only a smaller fraction of the deeper water masses, SAMW and AAIW, remains coastally–trapped and is advected towards lower latitudes by the LUC. The salinity distribution on the 26.9–γ^nsurface (figure 2.27) reveals an eastward flow of relatively saltier waters surrounded by the two westward flows of fresher SAMW described above, in agreement with the subtropical gyre system proposed by *Domingues et al.* (2007). These zonal flows are also clear in the vertical distribution of oxygen[3], in which two clusters of high oxygen are found at 30 °S – 25 °S and at $\sim$ 20 °S, where SAMW flows westward (figure 2.28, black horizontal lines).

The strongest PV minimum associated with SAMW is found in the Australian Basin (figure 2.11). As observed in Section 2.3.1, a strong PV minimum signal extends from 120 °E to south of Tasmania. SAMW likely subducts south of Tasmania but it is between 100 °E – 120 °E that it gets exported into the subtropical gyre (*Sallée et al.*, 2009, accepted by JPO) following a similar route as the 26.9–γ^nSAMW (figure 2.8). This SAMW type is also found east and west of New Zealand. Temperature and salinity ranges are of similar magnitude in both SAMW clusters, suggesting that these two clusters are formed locally under similar forcing rather than downstream evolution of properties (at least at the 26.94–γ^nsurface). West of New Zealand, the SAMW is warmer and saltier in the northern side of the Subantarctic Zone due to the strong subtropical influence over the

[3]Oxygen data corresponds to the World Ocean Circulation Experiment section I08N, along 80 °.

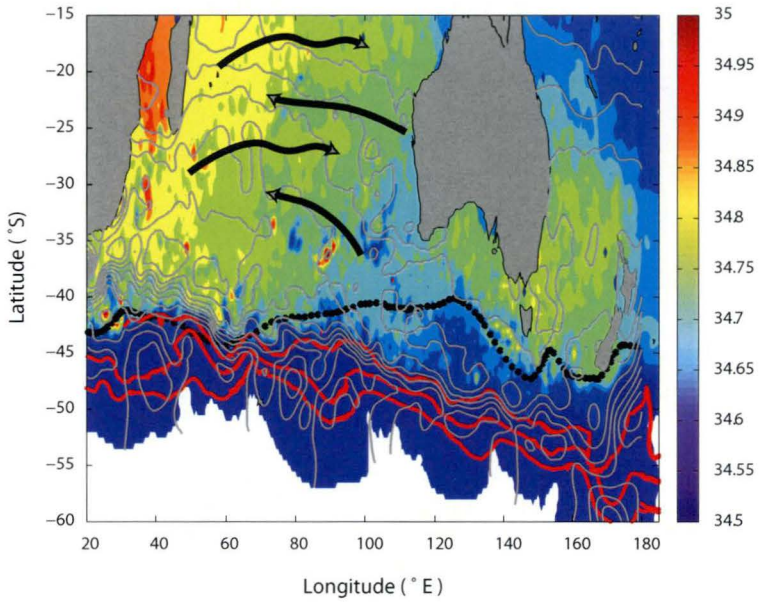

Figure 2.27: Salinity map on the 26.9–γ^nsurface from Argo data. Grey lines depict the modified Montgomery streamlines. Blue dotted and red lines depict the Subtropical Front (STF) and the Subantarctic Front (SAF), respectively. Black arrows show the eastward/westward jets flow.

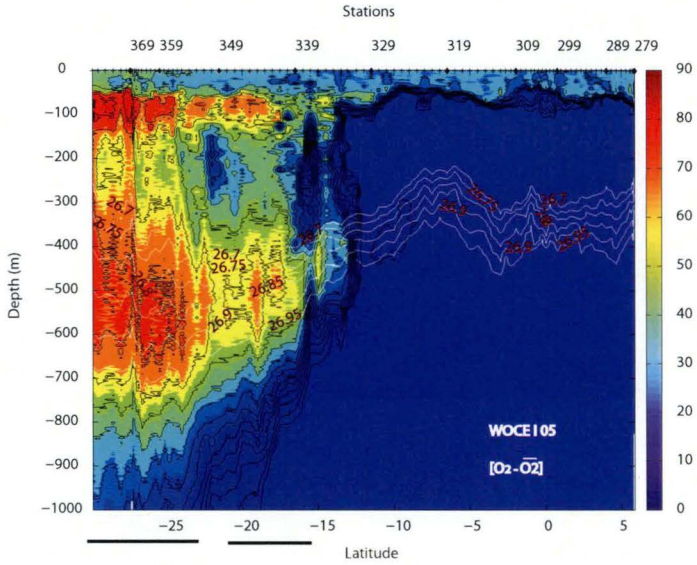

Figure 2.28: Oxygen anomaly (from the mean oxygen concentration of the section) along the World Ocean Experiment section I08N (at 80 °). Stations number appear above the section. The region where the two branches of 26.9 γ^nSAMW are indicated by the black lines below the x–axis. White lines show the neutral density surfaces crossing the deep oxygen anomaly maximum. Values lower than 0 appear as dark blue as they are out of the colour bar range.

SAZ, east/southeast Tasmania (see Chapter 4).

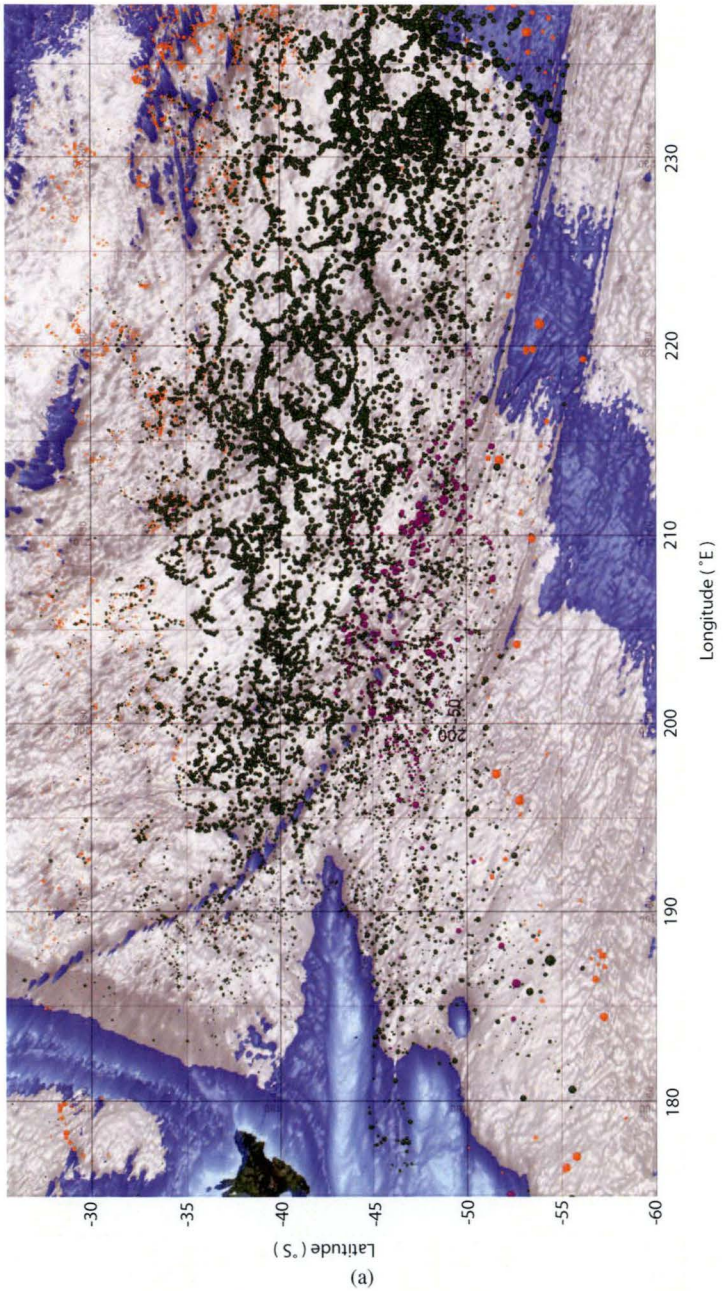

(a)

Figure 2.29: Southwest Pacific Ocean SAMW. From east to west: 26.94–γ^n(violet), 27.05–γ^n(dark green), and 27.15–γ^n(orange) SAMW types). The size of the dots is inversely proportional to the PV minimum value.

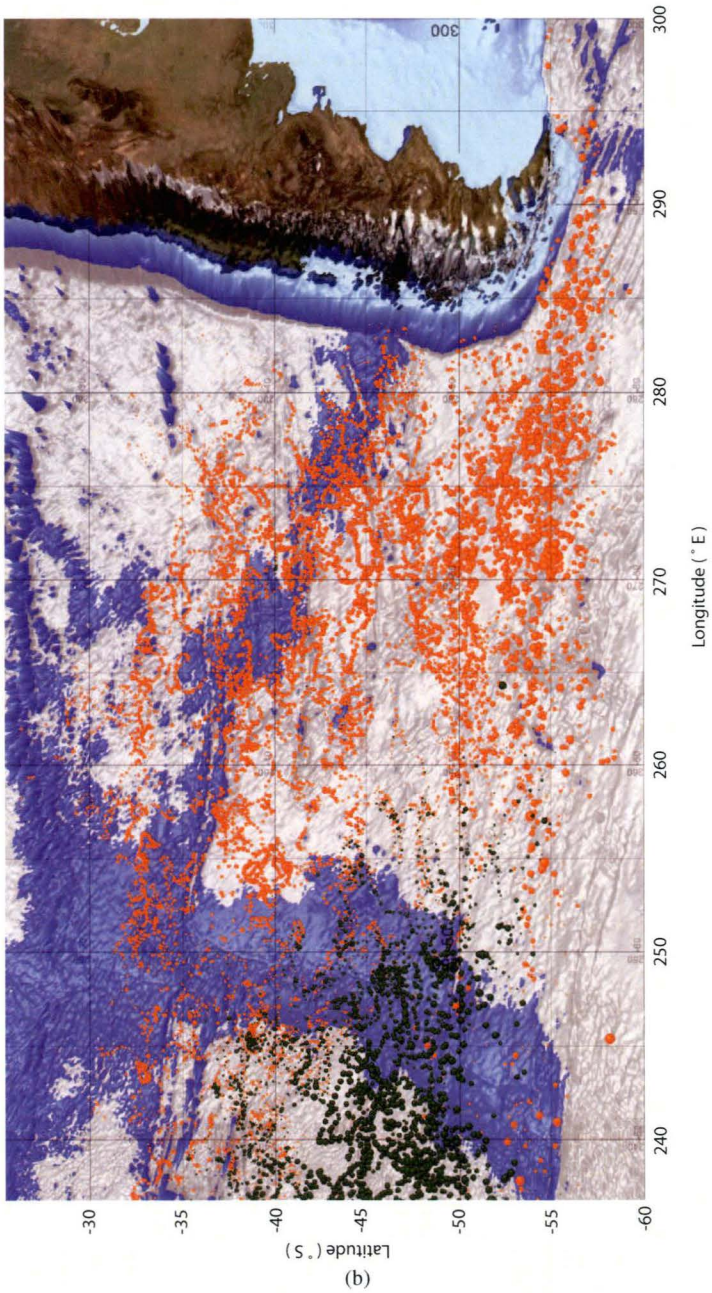

(b)

Figure 2.29: Southeast Pacific Ocean SAMW. From east to west: 27.05–γ^n(dark green), and 27.15–γ^n(orange) SAMW types). The size of the dots is inversely proportional to the PV minimum value.

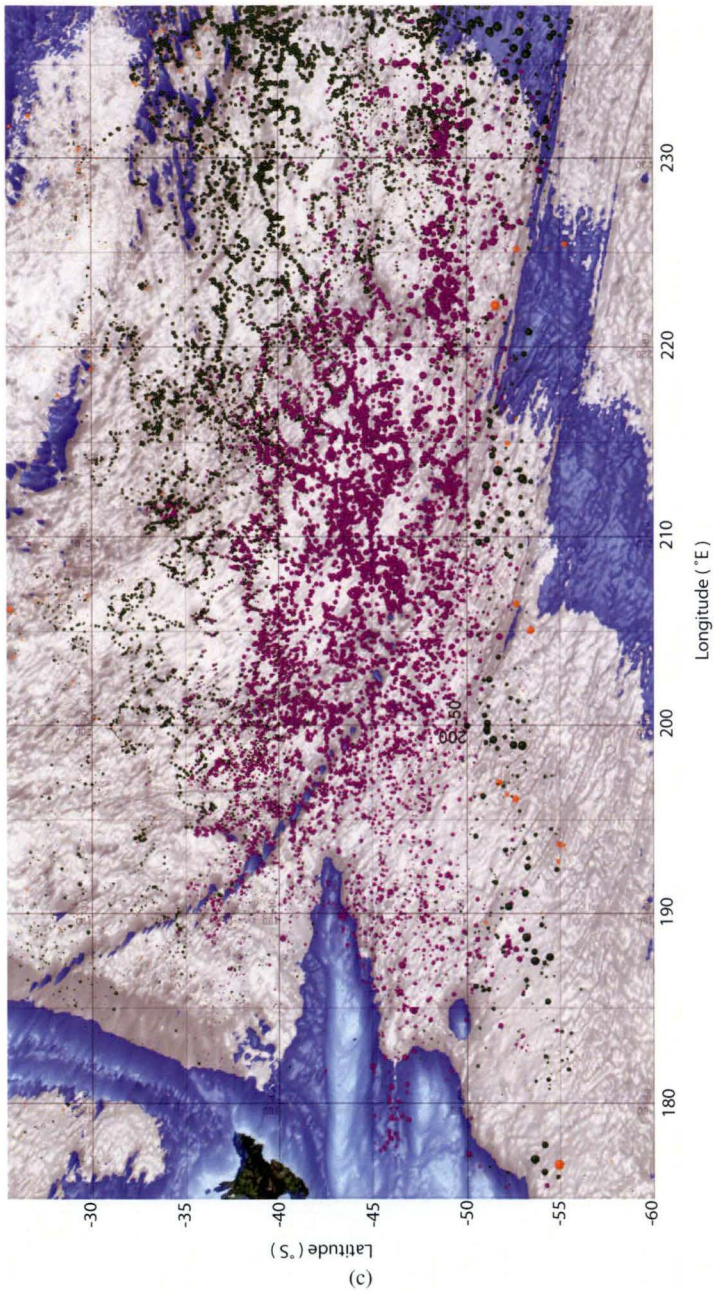

Figure 2.29: Southwest Pacific Ocean SAMW. From east to west: 27–γ^n(violet), 27.1–γ^n(dark green), and 27.2–γ^n(orange) SAMW types). The size of the dots is inversely proportional to the PV minimum value.

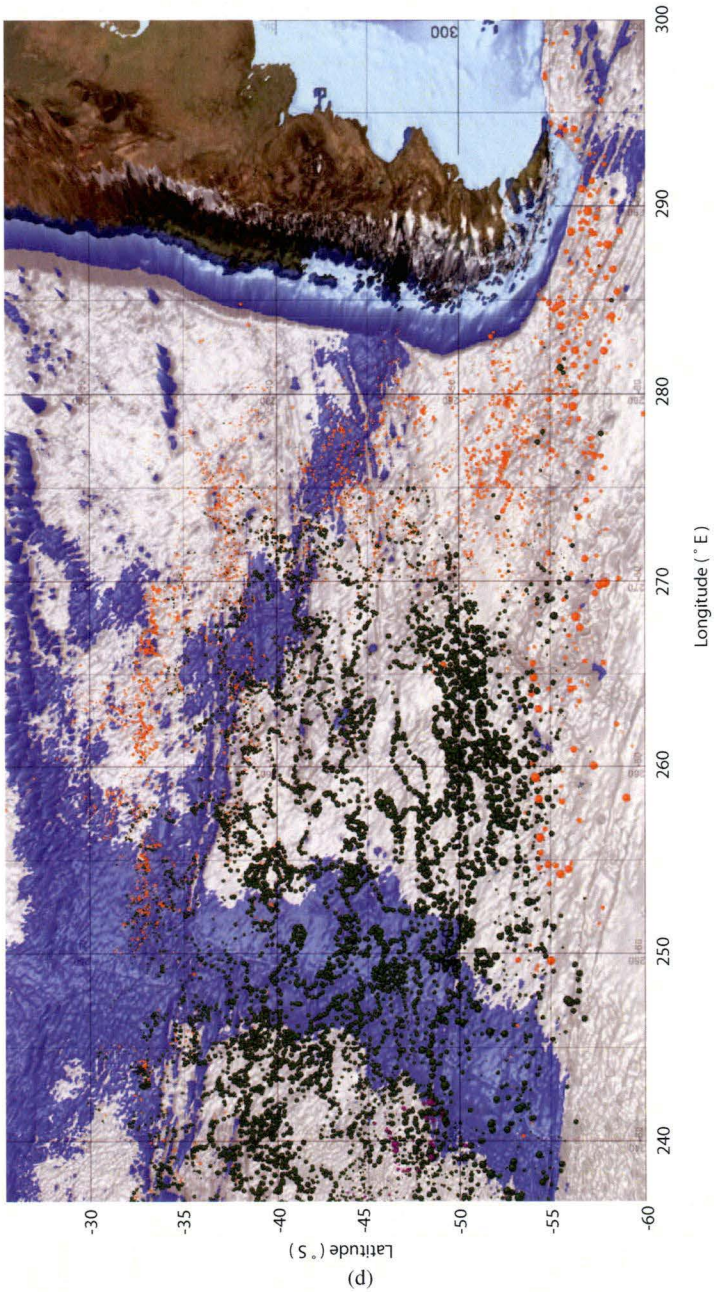

(d)

Figure 2.29: Southeast Pacific Ocean SAMW. From east to west: 27–γ^n(violet), 27.1–γ^n(dark green), and 27.2–γ^n(orange) SAMW types). The size of the dots is inversely proportional to the PV minimum value.

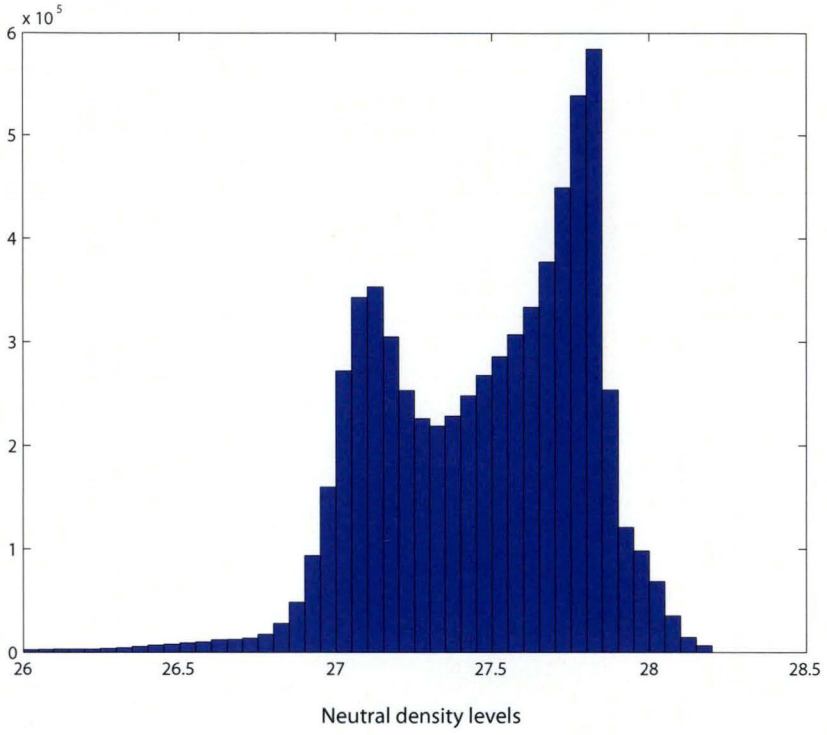

Figure 2.30: Neutral density distribution for the PV minimum in the south Pacific Ocean.

The south Pacific Ocean holds the densest SAMW, with four different types of SAMW distinguished by the spatial extent of their properties (figure 2.29). Even though the south Pacific Ocean holds SAMW of similar densities as the Indian SAMWs, the densest SAMWs overcome them in volume (figure 2.30). In previous studies, the lightest Pacific SAMWs were shown to be limited to the western Pacific (the Tasman Sea and east of New Zealand), while the densest SAMWs were found in the southeast Pacific (*McCartney and Baringer*, 1993; *Sokolov and Rintoul*, 2000). Two branches had been suggested to account for the circulation of densest SAMWs formed east of the South Pacific Rise. The northern branch spreads northwestward with the outer subtropical gyre and enters the Coral Sea north of Vanuatu (*Sokolov and Rintoul*, 2000). The southern branch was inferred by *McCartney and Baringer* (1993) and it is limited to the western Pacific, south

of 35 °S. Here we propose a variant for this two–branch circulation in which three main routes describe the SAMW circulation in the South Pacific and a fourth, the export of SAMW through Drake Passage.

Route 1. The lightest (γ^n= 27 kgm^{-3}) of the South Pacific SAMW is found east of New Zealand (figure 2.29b, green dots). Deep mixed layers (ML) are first developed east of 220 °E, with a neutral density of $27kgm^{-3}$ at the base of the ML coincident in space (50 °S – 55 °S and 220 °E (140 °W)) with the 27–γ^nSAMW core (figure 2.31). The Montgomery streamlines and 27–γ^nproperties suggest a nearly closed recirculation east of New Zealand, leaving this type of SAMW restricted to the centre of the subtropical gyre. Also, warmer and saltier 27–γ^nSAMW turns poleward into the gyre, east of New Zealand (figures 2.17, and 2.18). High potential vorticity values and low oxygen concentrations[3] also suggest a closed recirculation, restricting 27–γ^nSAMW to the interior of the subtropical gyre and separating it from the circulation in the Tasman Sea.

Route 2. The south western Pacific Basin is dominated by the 27.05–γ^nSAMW. It resembles the circulation pattern of the 27–γ^nSAMW but with a wider zonal and meridional extension. The most prominent feature of the 27.05–γ^nSAMW is the strong PV minimum signal associated with the core of the mode water (figure 2.16). The large northwestward extension of the SAMW core suggests a very efficient export of 27.05–γ^nSAMW into the subtropical gyre, likely subducting north of the SAF at 240 °E, in agreement with *Sallée et al.* (2009, accepted by JPO). The export of the 27.05–γ^nSAMW corresponds to the southern branch described in previous works (*McCartney and Baringen*, 1993; *Sokolov and Rintoul*, 2000), although we claim the origin to be in the western Pacific rather than a diversion of flow of the denser SAMWs from the southeastern Pacific. An oxygen maximum layer associated with a PV minimum was identified at a neutral density level of 27.1 – 27.2 along 32 °S (*Wijffels et al.*, 2001),

[3]Oxygen concentrations obtained from the Southern Ocean Data Base, http://wocesoatlas.tamu.edu/Sites/html/atlas/SOA_DATABASE.html.

supporting our claim that the lighter south Pacific SAMWs do not extend as far north as 30 °S (figure **??**).

SAMW formed east of the South Pacific Ridge fills the lower thermocline of the South Pacific Basin as part of the wind–driven circulation, from the American continent to the Australian coast. The 27.1–γ^nSAMW core spreads northward from north of the SAF to just south of 40 °S before it turns northwestward. This path resembles the one followed by the 27.05–γ^nSAMW although the relatively denser SAMW reaches further north and west. Thus, the ventilation of the south and, especially, the equatorial Pacific depends mainly on the formation and circulation of the 27.1–γ^nSAMW.

Route 3. The last of the circulation paths of the Pacific SAMW occurs along the outer subtropical gyre. The PV minimum core at γ^n= 27.15 has a distinctive northward circulation from the formation region along 55 °S, between 270 °E – 280 °E (80 °W – 90 °W). The flow turns westward at approximately 25 °S. This northward flow resembles the export path of AAIW described by *Iudicone et al.* (2007), in which AAIW is injected in the subtropical gyre east of 90 °W.

The southeastern SAMWs appear to join the South Equatorial Current in its westward flow. Geostrophic circulation maps at 500 and 800 dbar (*Reid*, 1997) show a westward circulation between 15 °S and 25 °S, consistent with the circulation of the (27.1 – 27.15)–γ^nSAMW. The South Equatorial Current splits into jets when it encounters the complex topography of the southwest Pacific (*Sokolov and Rintoul*, 2000). Part of the eastern SAMW flows cyclonically around the Gulf of Papua New Guinea to ultimately enter the Solomon Sea. The remaining SAMW turns southward feeding the East Australian Current (*Sokolov and Rintoul*, 2000). In our PV minimum map at 27.1–$\gamma^n$and 27.15–γ^nsurfaces (figure 2.20), the PV minimum gets eroded very fast due to the vigorous stirring of the eddy field that homogenizes temperature and salinity along isopycnals west of the Tonga–Kermadec Ridge (*Sokolov and Rintoul*, 2000).

Route 4. Several studies have agreed that SAMW is a precursor for the formation of Antarctic Intermediate Water (AAIW) in the southeast Pacific (e.g., *McCartney*, 1977; *Talley*, 1996). On the other hand, *Naveira–Garabato et al.* (2009) claimed that the inter–annual variability of the southeastern Pacific AAIW properties is primarily driven by changes in Antarctic Surface Water (AASW) properties rather than SAMW variability. In the South Atlantic, there is an overall agreement that the densest SAMW contributes to AAIW formation, after SAMW enters Drake Passage. *Naveira–Garabato et al.* (2003) applied an inverse model along the rim of the Scotia Sea. The surplus of AAIW/AASW in the out–flowing ACC from the Scotia Sea was hinted to be due partly to an uncertain interior conversion of SAMW to AAIW, driven primarily by upper–ocean mixing processes (effective diffusion). By following the PV minimum signature of SAMW with $\gamma^n \in$ [27.15, 27.2] along its flow into the south Atlantic Ocean, the conversion of the SAMW into a denser salinity minimum layer could be followed (Section 2.3.3, figure 2.23) although the Malvinas Current is not represented (as yet) by Argo data. As SAMW flows through the Drake Passage, north of the SAF, the pycnostad is also a salinity minimum layer. Once it reaches 40 °S, the northward Antarctic flow encounters the surface warm, salty waters of the Brazil Current. This leads to the subduction of the cool and fresh PV minimum underneath the light Brazil Current waters and the mixing with "old" AAIW which is ventilated and renewed.

2.4.2 SAMW in the Subantarctic Zone

The combination of several physical mechanisms make the Subantarctic Zone the ideal place for Mode Water formation. The zero wind stress curl lies almost centred on the ACC circulation, north of which the Ekman layer converges and pumping occurs. The rapid deepening of the isopycnals at the Subantarctic Front (SAF) preconditions the Subantarctic Zone to the north to form deep mixed layers. If the air–sea interaction is added, wintertime convective mixing due to buoyancy loss from the ocean surface

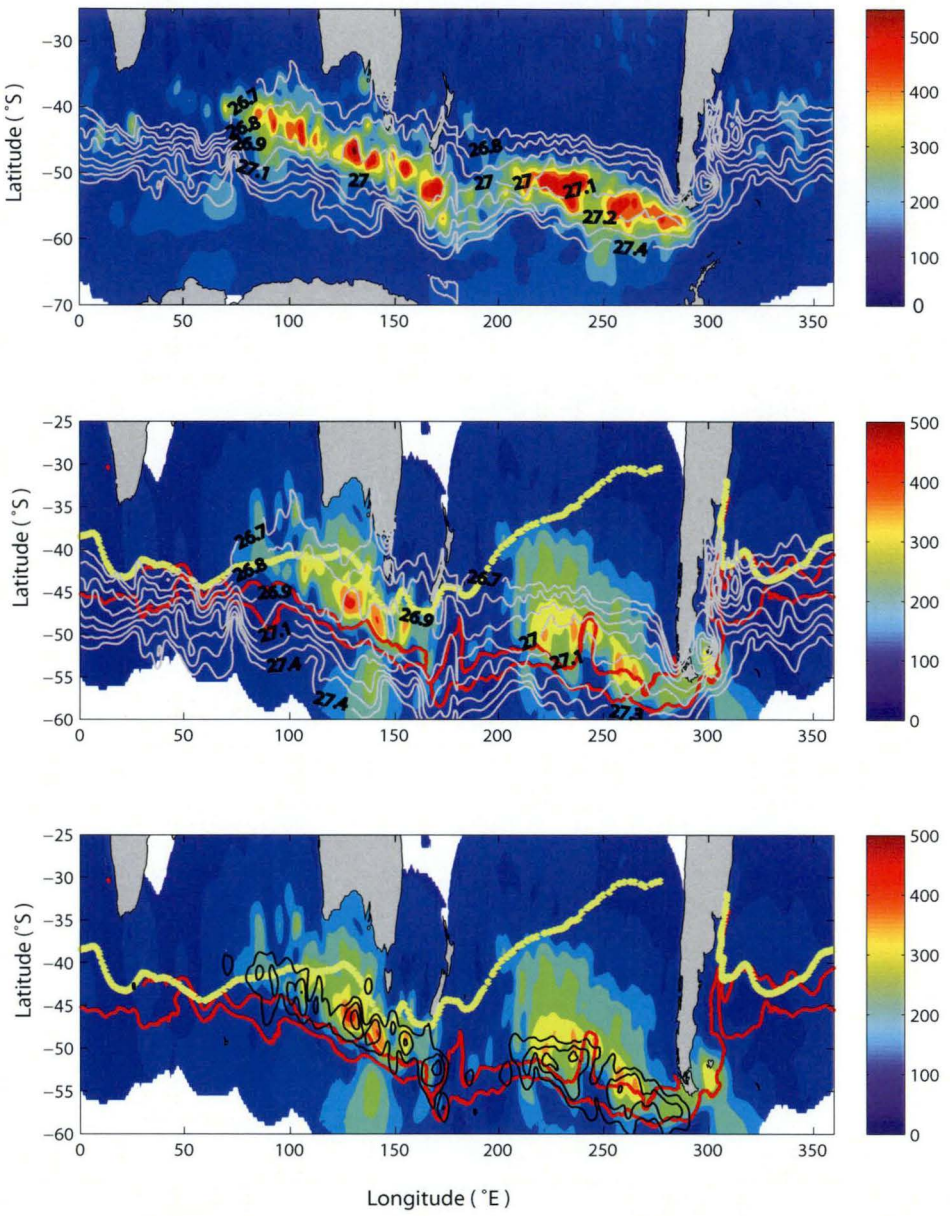

Figure 2.31: (a) Mixed layer depth calculated following a density difference criterion with a threshold of 0.03 kgm^{-3} from Argo floats, during late winter conditions (September). (b) PV minimum thickness during late winter conditions (September). Grey lines depict the potential density at the base of the mixed layer. (c) Same as in (b) plus the 300-400 metres mixed layer depth location (black lines). Yellow and red dot lines show the location of the Subtropical Front and the Subantarctic Front.

will enhance the formation of Mode Water in the Southern Ocean. *McCartney* (1977) found that SAMW was formed on the northern flank of the SAF (and south of the STF) with properties evolving eastward downstream of the ACC, accompanied by progressive cooling and freshening of SAMW properties from the south Atlantic Ocean to the south Pacific Ocean (figure 2.1).

SAMW occupies a wide neutral density range spanning from 26.7 to 27.2 kgm^{-3}. The evolution of the winter mixed layer depth and SAMW core thickness is compared to the eastward evolution of SAMW properties. The mixed layer depth has been calculated using a density difference criterion with a threshold of 0.03 kgm^{-3}, from Argo profiles under late winter conditions (September) (figure 2.31). SAMW core thickness is calculated using the thickness[4] of the PV minimum layer (PVmL) defining the SAMW core (PV $\leq$ $1\times\ 10^{-9}\ m^{-1}s^{-1}$ at $\gamma^n \in$ [26.75, 27.2]) in winter (figure 2.31 b). The neutral density at the base of the mixed layer is depicted by grey lines. Deep mixed layers and thick PVmLs are found just north of the SAF but the spatial distribution of both is patch–like rather than a continuous circumpolar layer. In the Indian Ocean, mixed layer depths deeper than 400 metres are seen in two main locations: between 80 °E – 90 °E and 110 °E; and, south of Australia on either side of Tasmania ($\sim$ 140 °E). The latter coincide in location with the thickest PVmL. In the Pacific Ocean, two regions stand out as the deepest layers, separated from each other by the northern branch of the SAF (SAF–n) (figure 2.31 c, red lines). The SAF–n acts as the southern–most boundary for the formation of these deep layers with a single exception, the eastern south Pacific. The discontinuities seen in the circumpolar distribution of deep mixed layers and thick PV minimum layers seem to coincide with changes in the neutral density at the base of the winter mixed layer. We will see that the discontinuities mark the transition between types of SAMW, and also "hot spots", where SAMW enters the main thermocline.

[4]Note that the top 200 metres are not used in our analysis

2.4.3 Subduction and the role of SAMW in the ocean interior ventilation

The subduction/ventilation of mode and intermediate waters has been of great interest since the 1990s as they ventilate the permanent thermocline in regions away from their formation areas in the Southern Ocean (e.g., *Talley*, 1999; *You*, 1998; *Fine*, 2001; 2008; *Karstensen an Quadfasel*, 2002 a, b; *Qu et al.*, 2008; *Sallée et al.*, 2009, accepted by JPO).

The strongest PV minimum signatures are related to the denser types of SAMW (γ^n= 26.9 – 26.95 kgm^{-3}) in the southeast Indian Ocean. Our results agree with the location of a layer of young SAMW (approximately 5 years–old) by *Karstensen and Tomczak* (1997). High CFC concentrations observed in the southeast Indian Ocean indicate this region as the source for recently–ventilated thermocline water entering the north Indian Ocean mainly through the eastern Indian Ocean (e.g., *Wyrtki*, 1971; *Stramma and Lutjeharms*, 1997; *Fine et al.*, 2008; *Sloyan and Rintoul*, 2001).

SAMW occupies a vast area of the south Pacific with a considerable export at several locations, each reaching different subtropical gyre regimes. The ventilation flux of SAMW and AAIW was estimated to be around 8 Sv each (*Fine et al.*, 2001; *Schmitz*, 1996), highlighting the south east Pacific as an important region of exchange with the subtropical gyre. Either side of the South Pacific Ridge (figure 2.15), a tongue of low PV minimum at two density levels (γ^n= 27.05 and 27.1 kgm^{-3}) suggests this site to be important in exporting SAMW into the gyre.

SAMW export "hot spots" coincide with the discontinuity of the SAMW thickness (figures 2.5, 2.8, 2.16, and 2.20). In the South Indian Ocean, the spread of PVmL from the Southern Ocean to the subtropical gyre occurs in two regions (40°S, 100°E; and, 50°S, east of 150°E) at the 26.8–γ^n and 26.9–γ^n surfaces, respectively (figure 2.31). In the south Pacific Basin, SAMW is exported from the Southern Ocean east and west of

the East Pacific Rise ($\sim$ 250°E). East of Drake passage, in the south Atlantic Ocean, a thick PVmL cluster, not seen in the mixed layer depth distribution, is found east of the Scotia Sea. Its thickness decreases north of 50°S as it enters the salinity minimum layer at higher densities. These "hot spots" are consistent with the Southern Ocean thermocline ventilation estimates by *Sallée et al.* (2009, accepted by JPO), where subduction along the ACC also shows high regional variability.

2.5 Conclusions

We have determined SAMW properties and export pathways from the formation areas of the Southern Ocean by tracking a PV minimum signature using Argo temperature and salinity profiles mapped onto isopycnal surfaces. Argo floats have provided an excellent data set, especially of those regions so long under–sampled (e.g., south Pacific and Southern Oceans). Our major results are summarized below.

- *McCartney* (1977) suggested that SAMW varieties, from the warm–salty SAMW variety in the south Atlantic Ocean to the cold and fresh SAMW in the southeast Pacific Ocean, are explained by the progressive eastward cooling and freshening of SAMW properties as the water mass is advected to the east on the northern flank of the ACC. Discontinuities in the winter mixed layer depth and PV minimum layer thickness, associated with SAMW, suggest that SAMW is not entirely continuous around the ACC. These discontinuities coincide with the injection of different SAMW into the ocean interior at specific regions along the ACC.

- The injection of SAMW into the main thermocline occurs at specific locations or "hot spots". The thickness of the PV minimum layer during late winter conditions showed discontinuities along the ACC associated with the equatorward export of the PV minimum feature. Two regions require special attention as the low PV tongue

(PV $\leq 1 \times 10^{-9} m^{-1} s^{-1}$) extends far to the north reaching subtropical latitudes. These regions are: 100 °E – 140 °E in the southeastern Indian Ocean and, the vicinity of the East Pacific Rise (240 °E – 260 °E) in the south Pacific Ocean. These regions provide a window for efficient transfer of highly ventilated and relatively new SAMW into the main thermocline.

- As previous studies claimed, we find that the densest SAMW types in the southeast Indian and Pacific Oceans are likely to play a major role in the ventilation of the main thermocline. The density distribution at the PV minimum range shows 2 main density ranges for the SAMW types. In the south Indian Ocean, the 26.9–γ^nSAMW dominates the other SAMW types. In the south Pacific, on the other hand, the 27.05–$\gamma^n$and 27.1–γ^nSAMW types are equally important. These SAMW types also occupy a wide zonal and meridional extent in their respective oceanic basins.

- The densest SAMW renews and ventilates the salinity minimum layer and enters the south Atlantic as part of the cold return route closing the thermohaline circulation. The south Atlantic salinity minimum layer is supplied by the potential vorticity minimum layer passing through Drake Passage from the south Pacific Ocean. The advection of the well ventilated AAIW as a potential vorticity minimum signature from the Scotia Sea is mainly equatorward toward the Malvinas–Brazil Confluence Zone, where the main flow is eastward.

A new view of Subantarctic Mode Water spatial variability has been described. In earlier studies, SAMW was presented as a continuous water mass with gradual downstream evolution of its properties north of the Subantarctic Front. The export to the subtropics occurred more or less gradually across the basin and the within–subtropical gyre circulation was thought to be at a uniform broad (basin–wide) scale. Our results show that SAMW consists of different modes or types in each oceanic basin. Changes in their properties are related to circulation. SAMW subduction takes place in "hot spots" where

each SAMW variety is exported to the subtropics following narrow pathways, influenced by topography.

Chapter 3 Subantarctic Mode Water Variability Influenced by Mesoscale Eddies South of Tasmania

3.1 Introduction

Subantarctic Mode Water (SAMW) is a thick near–surface layer which occurs in the Subantarctic Zone (SAZ), the region defined between the Subantarctic Front (SAF) and the Subtropical Front (STF). It is formed in the winter mixed layer of the ocean, which reach to depths as great as 700 m and, it is characterized by high oxygen concentration (*McCartney*, 1977). While SAMW is observed in each of the oceanic basins around Antarctica, the temperature and salinity properties vary along the circumpolar path: the warmest SAMW (15 °C, 35.8 psu, 26.5 σ_θ), which is the same as the main Subtropical Mode Water discussed by *Provost et al.* (1999), is found where the SAF is furthest north, in the western Atlantic; the coldest mode water (4 °C – 5 °C, 34.5 psu, 27.1σ_θ) occurs just west of Drake Passage (*Hanawa and Talley*, 2001).

The formation and export of SAMW from the Southern Ocean to the subtropical gyres as part of the overturning circulation are of high relevance for climate change studies. SAMW ventilates the subtropical thermocline and transports atmospheric gases, like carbon dioxide, into the ocean interior (*Metzl et al.*, 1999; *Sabine et al.*, 2004). The export of nutrients in the SAMW supports ocean productivity at low latitudes (*Sarmiento et al.*, 2004). Furthermore, SAMW properties (e.g. low potential vorticity) serve as useful tracers because they are retained for great distances, keeping a record of surface conditions at the time of formation (*Hanawa and Talley*, 2001).

Previous studies of SAMW have revealed mechanisms that may contribute to its variability. Air–sea fluxes of heat and freshwater in the SAZ sufficient to drive changes in the SAMW properties were first suggested by *McCartney* (1977; 1982). However, it has been reported that air–sea fluxes alone are not enough to explain the variability of SAMW. Northward Ekman transport across the fronts also contributes to SAMW formation and hence, its variability (*Speer et al.*, 2000; *Sloyan and Rintoul*, 2001; *Rintoul and England*, 2002). Eddy heat diffusion was recently shown to modify the action of Ekman and air–sea fluxes causing local heating/cooling of the SAMW (*Sallée et al.*, 2008).

Changes in the ocean heat and freshwater budget have been a topic of great interest in the last decade as a result of climate changes. Several studies have concluded that changes have occurred in recent decades. Southern Ocean temperatures in the depths between 700 and 1100 metres have warmed approximately $0.17 \pm 0.06\,^{\circ}\mathrm{C}$ between the 1950s and the 1980s, with the highest rise found near the Antarctic Circumpolar Current (ACC) (*Gille*, 2002). SAMW warming is consistent with subduction of warmer surface waters from south of the ACC (*Wong et al.*, 2001; *Aoki et al.*, 2003). On density surfaces and in the formation areas, SAMW shows a freshening and warming in the Indian and Pacific sectors of the Southern Ocean between the 1960s and the 1990s (*Bindoff and Church*, 1992; *Bindoff and McDougall*, 2000; *Johnson and Orsi*, 1997; *Wong et al.* 1999; *Bryden et al.*, 2003) and has been linked to anthropogenic carbon dioxide emissions (*Banks et al.*, 2000). However, the salinity in the Indian Ocean returned to the 1960s values in 2002 (*Bryden et al.*, 2003). Some studies using oceanic models suggest the observed changes may reflect natural or internal variability in the Indian Ocean sector rather than a long–term trend (*Stark et al.*, 2006). The Pacific and Atlantic sector of the Southern Ocean also show freshening in the periods between the 1980s – 1990s and 1950s – 1960s (*Curry et al.*, 2003; *Wong et al.*, 2001). However, most earlier studies have relied on infrequent repeats of hydrographic sections, which may alias short–term variations in water properties. A recent work examining a time series of SAMW properties in the Drake

Passage between 1969 and 2005 showed high variability on interannual to interdecadal time scales, with warming (by $\sim 0.3\,^{\circ}C$) and an increase in salinity (by ~ 0.04 psu) during the 1970s, and cooling and freshening trends between 1990 and 2005 (*Naveira–Garabato et al.*, 2009). The interdecadal variability in SAMW properties was primarily driven by trends in the major modes of southern hemisphere climate variability (the Interdecadal Pacific Oscillation, Southern Annular Mode, and the El Niño Southern Oscillation). The lack of continuous time series of hydrographic measurements at key formation areas in the Southern Ocean and the poor understanding of the physical processes that imprint the temperature and salinity signal to the mode waters at the surface make it difficult to interpret changes observed in areas far from where SAMW subducts.

In regions south of Australia, Subantarctic Mode Water forms a thick layer of uniform density (a pycnostad) from 26.8 to 26.95 kgm^{-3}, and thus, a layer of very low potential vorticity. The vertical extent can reach 450 – 700 dbar from the surface and it can be found between 45°S (STF mean position) and 50°S – 53°S (SAF mean position) (*Sokolov and Rintoul*, 2002). No SAMW has been found further north than 36°S in the Tasman Sea (*Sokolov and Rintoul*, 2000). To the east, the Campbell Plateau (160°E – 165°E) prevents the type of SAMW found at the WOCE SR3 ($\sim$145°E) transect from entering the Pacific Basin (*Rintoul and Bullister*, 1999). It is often assumed that there is a single mode or type of mode water at each location. We show how the SAMW south of Tasmania can be composed of different modes and discuss their origin.

The intra–and inter–annual variability of SAMW has been examined south of Tasmania. Temperature and salinity properties of SAMW are described in Section 3.3.1, followed by the SAMW core temperature time series. SAMW variability is described in more detail by considering several case studies in Section 3.3.3, to end with a brief description of the seasonal evolution of the SAMW properties.

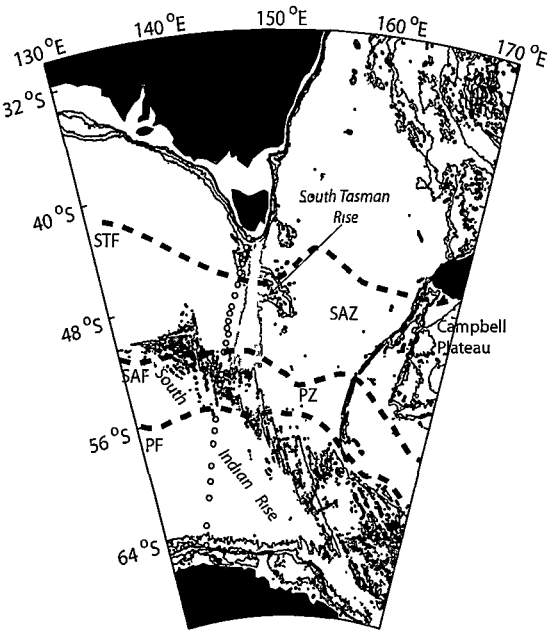

Figure 3.1: Location of hydrographic sections in the Subantarctic Zone (SAZ): WOCE SR3 CTD sections (open circles) and *l'Astrolabe* XBT sections (grey full circles). Southern Ocean Fronts south of Tasmania are indicated by dotted lines. STF: Subtropical Front (Southern Ocean Data Base); SAF: Subantarctic Front; PF: Polar Front; SAZ: Subantarctic Zone; PZ: Polar Frontal Zone.

3.2 Data analysis

Conductivity–Temperature–Depth (CTD) recorder and eXpendable BathyThermograph (XBT) data sets were used to determine the magnitude and cause of temporal variability of the Subantarctic Mode Water south of Tasmania. Seven repeat CTD transects from the World Ocean Circulation Experiment (WOCE) SR3 sections were collected during voyages of the research vessel R/V *Aurora Australis*. Data were retrieved in several years: November 1991, March 1993, January 1994, January 1995, July 1995, September 1996, and November 2001, covering temporal sampling across most seasons. Stations along SR3 were generally about 55 km apart in the Subantarctic Zone. Useful information on WOCE SR3 sections can be found in *Rintoul and Bullister* (1999); *Sokolov and Rintoul* (2002); and *Rintoul et al.* (2002).

The second data set used comes from the joint XBT program between France, Australia, and the United States from the French vessel *l'Astrolabe* (SURVOSTRAL) between Tasmania and the French Antarctic base Dumont D'Urville (66°E, 140°E). XBT temperature profiles from repeat sections were taken 6 times per year, when weather conditions made it possible, during austral summers between December 1993 and January 2007. The SURVOSTRAL Program is on–going although we limited our analysis to the above dates. The homogeneity of mode water properties in the vertical allows us to use vertical temperature gradients from XBT profiles to reliably identify the mode water core. Figure 3.1 shows the location of the CTD and XBT transects south of Tasmania and the mean position of the SAF and STF (*Orsi et al.*, 1995). The SURVOSTRAL XBT lines provide the longest available time series of temperature sections across the Southern Ocean. This time series allows us to examine the variability and the mechanisms driving changes in the SAMW properties. Faulty probes and poor weather caused gaps in some of the XBT sections. We restricted the analysis to sections where the distance between adjacent good profiles was less than 100 km. A total of 44 out of 89 sections met this criterion.

Sea surface height (SSH) maps provide insight into the processes responsible for SAMW formation and variability and allow our sections to be placed in a wider regional and temporal context. Satellite altimetry data have previously been used to study the mesoscale features and energetics of the ACC, in particular those associated with the SAZ (*Hughes and Ash*, 2001; *Morrow et al.*, 2003; *Sokolov and Rintoul*, 2007). For the SSH mean field (relative to 2500 dbar), we used *Olbers et al.* (1992) climatology and, for the SSH anomaly, the CLS/AVISO "Mean Sea Level Anomaly" (MSLA) maps, which are produced by mapping data from the Topex/POSEIDON, ERS–1 and ERS–2 satellite altimeters (*Le Traon et al.*, 1998). We follow a sequence of SSH maps of the Southern Ocean to identify the mesoscale features that cross our hydrographic sections south of Australia at the time of the sampling.

SAMW is formed south of Tasmania between the Subtropical Front and the Subantarctic Front (figure 3.1). Strong horizontal gradients in water mass properties are associated with fronts of the ACC (*Orsi et al.*, 1995; *Belkin and Gordon*, 1996); hence isotherms can be used to identify the boundary of the SAMW region. The STF can be identified by the 11°C–isotherm at 150 dbar; and the northern branch of the SAF, by the 6°C – 8°C isotherm at 400dbar (*Sokolov and Rintoul*, 2002, Table 6).

Based on the 17 years of XBT and CTD, we found that the local SAMW core around 140°E is well monitored by criteria based on temperature and vertical temperature gradient. A running mean average over 20 m in the vertical was used to smooth the temperature profiles prior to the calculation of the vertical gradient over approximately 40 m. We define the local variety of SAMW core as water with a temperature between 8°C – 9.5°C and a vertical gradient, $|\Delta\theta/\Delta z|(\Delta z \sim 40$ m) = 0.005°C/m. In order to compare XBT and CTD sections, the same analysis has been applied to both data sets. Therefore, the results are expressed mainly as a function of temperature and the vertical gradient of temperature.

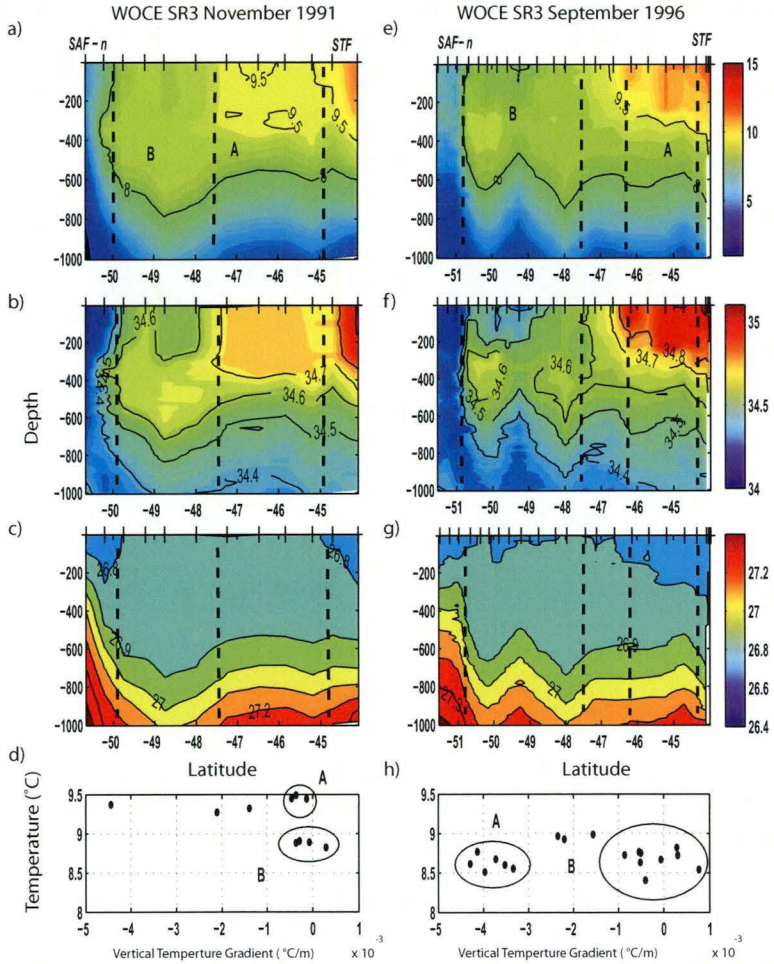

Figure 3.2: Vertical distribution of temperature (a, e), salinity (b, f) and density (c, g) for the hydrographic sections corresponding to WOCE SR3 November 1991 and September 1996, south of Tasmania. SAMW (Mean Temperature per station *vs.* mean $d\theta/dz$ per station) diagram (d, h). Each dot represents the mean temperature of the local SAMW at each station. Stations are depicted by black crosses. Black dotted lines delimit regions of distinct SAMW characteristics (see Section 3.3.3).

3.3 SAMW Variability

3.3.1 Temperature – Salinity Properties

Figure 3.2 shows an example of the vertical distribution of SAMW properties (potential temperature (θ) (a, e), salinity (S) (b, f), potential density (kgm^{-3}) (c, g), and θ *vs.* $|\Delta\theta/\Delta z|$ (d, h)) corresponding to two austral spring sections: WOCE SR3 November 1991 and September 1996 (figure 3.2, left and right panel, respectively). The bottom of the pycnostad reaches to 600 dbar in both sections. Density plots suggest there is a single pool with density between 26.8 and 26.9 kgm^{-3}. But temperature and salinity sections suggest the SAMW pool is not completely homogeneous. This apparent heterogeneity in properties in the SAMW pool is clearer when θ is plotted against $\Delta\theta/\Delta z$ (same for salinity, not shown) (figure 3.2 d, h). Each black dot in these two plots represents the mean temperature and mean $\Delta\theta/\Delta z$ for the local variety of SAMW at each station.

The repeat WOCE SR3 CTD sections were used to evaluate the inter–annual variability of the SAMW properties south of Tasmania. *Rintoul and England* (2002) studied the variability of the SAMW properties using an area–weighted potential temperature–salinity (θ–S) plot. Here we have reproduced their figure 1 with an additional section, SR3 November 2001 (figure 3.3). We also added a histogram (in red) of the XBT temperature from the local variety of SAMW over the 15–year–record. The majority of points fall in a cluster defined as: $\theta \in$ [8.5 °- 9]°C (coincident with the maximum XBT temperature frequency); S $\in [34.58 - 34.68]$ psu. There are two periods with strong modes which lie outside the central cluster. The XBT histogram highlights how uncommon these 2 modes are, as they lie within the tails of the XBT temperature frequency distribution. November 1991 shows a strong warm and salty mode (θ = 9.5 °C, S = 34.75 psu); July 1995 shows a strong cold and fresh mode (θ = 8.2 °C, S= 34.45 psu) and a second weak mode close to the main cluster. A second minor peak in the XBT histogram is also found close to 8 °C.

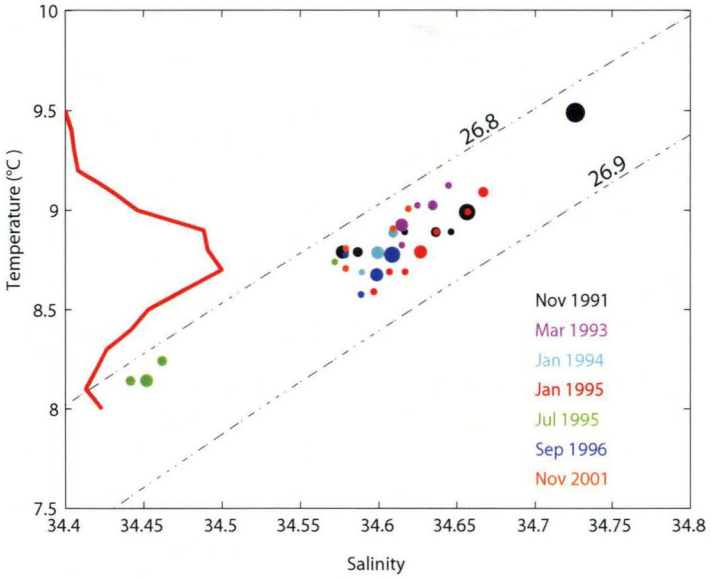

Figure 3.3: Variability of SAMW properties south of Australia. (Figure 1 in *Rintoul and England* (2002) plus WOCE SR3 section November 2001). The cross–sectional area of water in each 0.1°C by 0.01 psu θ–S class is shown by a filled circle, with the size of the circle proportional to the area. Only the large volume ($\geq 10^7 m^2$) modes are shown. Potential density contours are shown by black dotted lines. A histogram showing the XBT temperature distribution of the local SAMW over the 15 years is seen on the left (thick red line).

3.3.2 Core Temperature

A 17–year record of SAMW temperature from CTD and XBT data is used to study the inter–annual SAMW variability south of Tasmania. XBT data are available in each austral spring–summer from October to March. The observed monthly mean temperature of the local variety of SAMW core is depicted in figure 3.4. The mean temperature plotted in figure 3.4 is the monthly mean of all those observations satisfying the criteria for the local SAMW core: $T_{SAMW} \in [8 - 9.5]$ °C and $|\Delta T/\Delta z|_{SAMW} = 0.005$ °C/m. The mean temperature over the 17 years is 8.8 ± 0.3 °C, consistent with the main cluster observed on the hydrographic sections in Section 3.3.1 (figure 3.3). The error bars represent the standard deviation of temperature per month. While there are some abrupt jumps in temperature, e.g. summer 1995 – 1996, 1999 – 2000, 2004 – 2005, and 2006 – 2007, the variability is generally within the error bars and there is no significant trend observed. These temperature changes are due mainly to cooling episodes. November 1991 is the warmest SAMW core in our time series, followed very closely by the beginning of summer in 1999. Air–sea fluxes or changes in the horizontal wind stress cannot explain entirely the variability observed in figure 3.4, or the abrupt temperature changes, as discussed below. Different mechanisms have been claimed to drive SAMW variability: air–sea fluxes of heat and freshwater (*Bindoff and Church*, 1992; *Johnson and Orsi*, 1997; *Wong et al.*, 1999; *Banks and Bindoff*, 2003); northward Ekman transport (*Rintoul and England*, 2002); and eddy heat diffusion modifying the action of Ekman and air–sea fluxes (*Sallée et al.*, 2008). An alternative hypothesis to describe the cause of the changes in the SAMW is the advection of anomalous water into the SAZ by eddies and meanders from the SAF, discussed next.

3.3.3 SAMW: Multiples Modes

The vertical sections of θ and S revealed heterogeneity of SAMW properties not seen in the vertical distribution of potential density (figure 3.2). Moreover, the volumetric

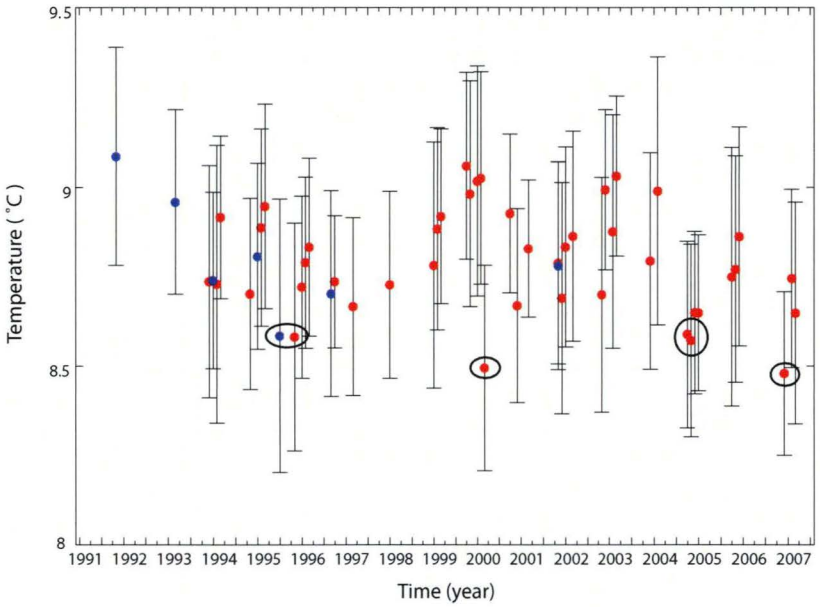

Figure 3.4: Monthly mean temperature of the SAMW core as a function of time. Blue dots depict the WOCE SR3 hydrographic sections and red dots, XBT sections. Errors bars indicate the standard deviation of temperature per month (or section). XBT data are available from October to March in each austral summer. Sections influenced by SAF–eddies or SAF–meanders have been highlighted (ellipses).

analysis of the θ–S properties in figure 3.3 showed two sections, WOCE SR3 November 1991 and WOCE SR3 July 1995, with strong anomalous modes lying outside the main cluster. Similarly, we observed abrupt jumps in the SAMW core mean temperature during the summers of 1995 – 1996, 1999 – 2000, 2004 – 2005, and 2006 – 2007 from the analysis of the XBT sections (ellipses, figure 3.4). In this Section, we examine in more detail the SAMW heterogeneity found in the previous figures by considering a number of case studies.

a) WOCE SR3 July 1995

Figure 3.5 (a) shows the vertical salinity section corresponding to WOCE SR3 for July 1995. Within the SAMW pool observed on the SR3 section, we can easily distinguish the unusual cold/fresh mode in figure 3.3 from the rest of the SAMW pool. Figure 3.5 (b) depicts the mean θ *versus* the mean dθ/dz of the local variety of SAMW at each station. The SAMW properties fall into three clusters. The temperature of modes **A** and **B** is consistent with the central cluster in figure 3.3; the anomalously cool and fresh SAMW type (mode **C**) is found in the southern SAZ, north of the SAF. Modes **A** and **B** have similar temperatures, but different vertical temperature gradients. The larger vertical gradient in the subducted mode water north of 46°S, labeled **A**, indicates that mixing has eroded the pycnostad of this mode, which may have formed in the previous winter while temperature mode **B** has a well developed thermostad and is located at 46°S – 47.5°S.

What caused the particularly cold, fresh mode observed in July 1995 (mode **C**, figure 3.5)? The computed monthly mean ocean heat loss in July 1995 over the SAZ along the SR3 line is about 137 Wm^{-2} (data taken from the NCEP reanalysis; 161 Wm^{-2}, from JRA–25 (*Onogy et al.*, 2007)) and the evaporation minus precipitation flux is 0.003 m/month (data taken from NCEP/NCAR reanalysis). To cool and freshen a 300 meter–thick by 1 m^2 column by 0.5°C and 0.1 psu (the difference between modes **B** and **C**), requires a heat loss of about 238 Wm^{-2} (using ρ_0 = 1026.85 kgm^{-3}, and c_p = 3986 Jkg^{-1} C^{-1}) and a

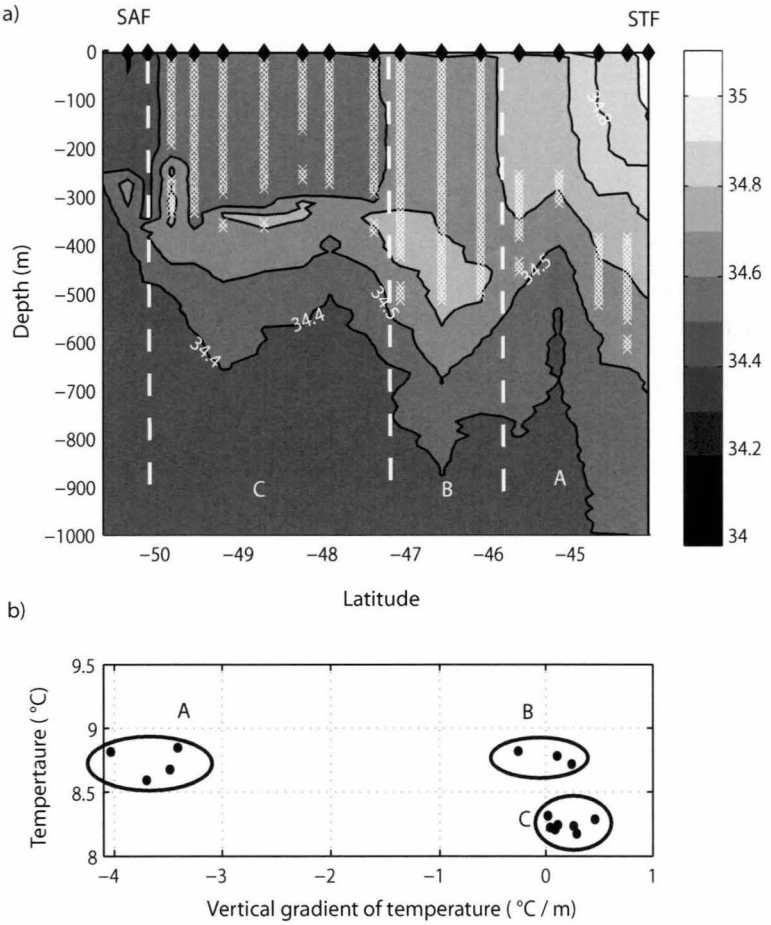

Figure 3.5: Vertical distribution of salinity during the World Ocean and Climate Experiment (WOCE) SR3, July 1995 (a). Yellow crosses depict regions where the criteria used to define SAMW (θ /(dθ /dz) ≤ 0.005 and $\theta \in [8, 9.5]°C$) are satisfied. Stations are shown by black diamonds at the top of the contour. (b) Classification of the water types that satisfy the SAMW criteria, based on the mean temperature and vertical temperature gradient.

freshwater input of about 0.9 m, maintained for a month. This suggests that local air–sea forcing is insufficient to account for this change.

Topex/Poseidon SSH maps at the time of the section and for the previous 3 months are shown in figure 3.6. In April, two cold–core meanders of the SAF are present at 143°E and 150°E. The meanders grow in subsequent months and wrap around a warm (high SSH) feature near 50°S, 146°E. The cold, fresh mode **C** is observed where the July section crosses the low SSH features that originated as cold meanders of the SAF. Figure 3.7 (b, d) shows the θ–S relationship for WOCE SR3 July 1995. The SAMW potential density class is found between 26.8 and 26.9 kgm^{-3} (black dots). There is no density barrier between the SAF waters (in red) and mode **C** (dark blue) which allows rapid cooling and freshening by mixing along isopycnals to occur in the SAMW where the cold meanders were seen. Note that the SAMW θ–S curves show a sharp "hook" toward cooler and fresher values near the sea surface, consistent with mixing with water to the south. The horizontal wind stress for July 1995 is not significantly different from the mean in this region. The proximity of the anomalous mode water to the SAF meander in the SSH map suggests that the advection of cold fresh water from the SAF by the meander, rather than northward Ekman transport, was responsible for the unusually cold, fresh mode water observed – see figures 3.3, 3.5.

We find a similar distribution of water properties on the WOCE SR3 transect in November 1991 (figure 3.2, left panels). Two distinct modes can be seen in the section: **A** (45°S – 47.5°S; with 9.4°C, 34.725 psu) and, **B** (47.5 – 50°S; with 8.3°C, 34.65 psu) (figure 3.2) (Note that we use the letters (**A**, **B**,) to refer to distinct SAMW types observed on each individual section; there is no connection between mode **A** on different sections). *Rintoul and Bullister* (1999) showed that water masses can be influenced by subtropical water carried by the westward Tasman Outflow south of Tasmania (around 44°S). The shaded area in figure 3.7 (a, b) represents the envelope of θ–S curves observed at 43°S in the Tasman Sea and shows the θ–S range influenced by the Tasman Outflow from the repeats

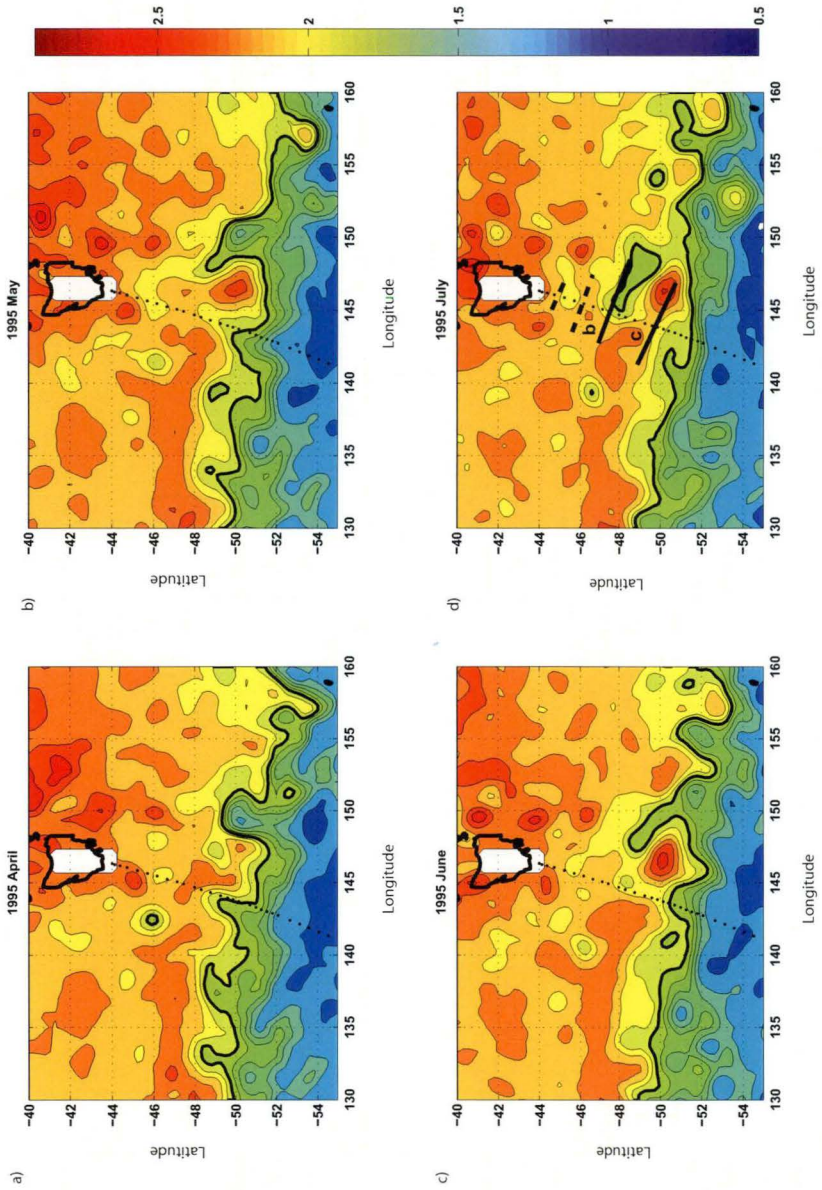

Figure 3.6: Sea Surface Height maps (m) south of Tasmania at the time of the World Ocean and Climate Experiment (WOCE) SR3 section held on July 1995. Black bold line correspond to the 1.9 m steric height as the position of the time–varying SAF (calculated from the Olbers 0/2500 m mean steric height plus the sea level anomalies from the Topex/Poseidon + ERS1–2 altimetry data defined by *Sokolov and Rintoul* (2002)).

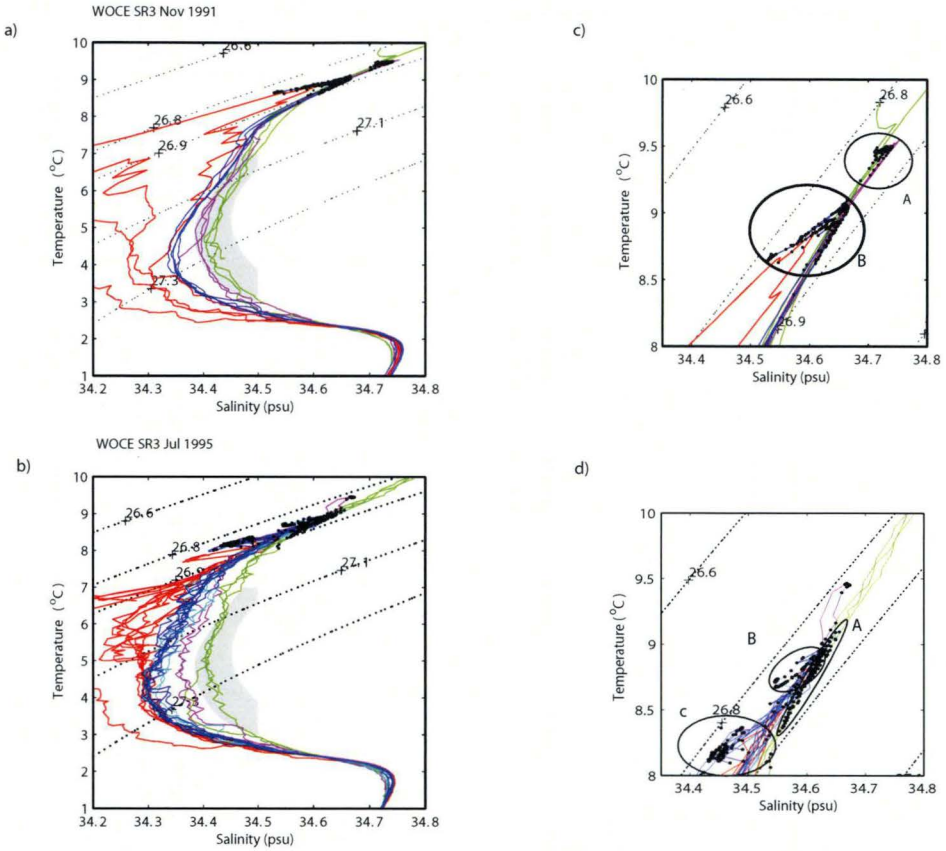

Figure 3.7: Potential temperature *vs.* salinity relationship for World Ocean and Climate Experiment (WOCE) SR3 November 1991 (a, c) and July 1995 (b, d). Black dots represent SAMW properties. Colour–code for WOCE SR3 Nov1991: green, stations northern STF; magenta, mode **A**; blue, type **B**; red, stations at/south of the SAF. Colour–code for WOCE SR3 Jul1995: green, just south of the STF; cyan, mode **A**; blue, type **B**; red, stations at/south of the SAF.

of the SR3 hydrographic section (see figure 3.6 from *Rintoul and Bullister*, 1999). Profiles north of the STF (figure 3.7 a, c, in green) and of the SAMW mode **A** (figure 3.7 a, c, in magenta) are inside the shaded area, reflecting their subtropical influence. Sea Surface Temperature (SST) satellite images (not shown) show southward penetration of a warm temperature anomaly, likely the result of an eddy formed from the East Australian Current Extension. We used SST because no SSH maps exist prior to 1992. Similarly, monthly mean temperatures exceeded 9°C during the summer of 1999 (figure 3.4). This relatively warm SAMW is associated with high SSH features moving southward following the East Australian Current flow, and advecting warm/salty waters into the SAZ. Warm and salty anomalies carried by the eddy and homogenised by deep winter mixing could explain the near 9.5°C core seen in figure 3.3.

b) WOCE SR3 November 2001

Generally, SAMW temperature progressively cools and freshens from the STF to the SAF. However, in WOCE SR3 November 2001 the warmest/saltiest cluster (**B**) is situated closer to the SAF (figure 3.8, a, b). Although the difference between **A** (47°S – 48°S; 8.7°C, 34.57 psu) and **B** (48°S – 49°S; 8.9°C, 34.61 psu) is not as extreme as in the previous examples, it is important to understand the origin of this reverse distribution of the horizontal temperature in the SAMW pool to improve our knowledge of the processes driving SAMW variability.

We use the SSH maps from different months once again to describe the origin of clusters **A** and **B** (figure 3.9). The CTD section crosses the eastern edge of a low dynamic height feature between 47°S and 48°S (figure 3.9 d), corresponding to cluster **A** in figure 3.8. During August, a path of high dynamic height can be seen from 42°S to 50°S (figure 3.9 a, white line). The path splits into 3 eddies in August. The first eddy (45°S, 147°E) moves slowly westward and is crossed by the November section at 46°S. The second eddy (47.5°S, 144.5°E) moves more rapidly to the west. The third feature appears to

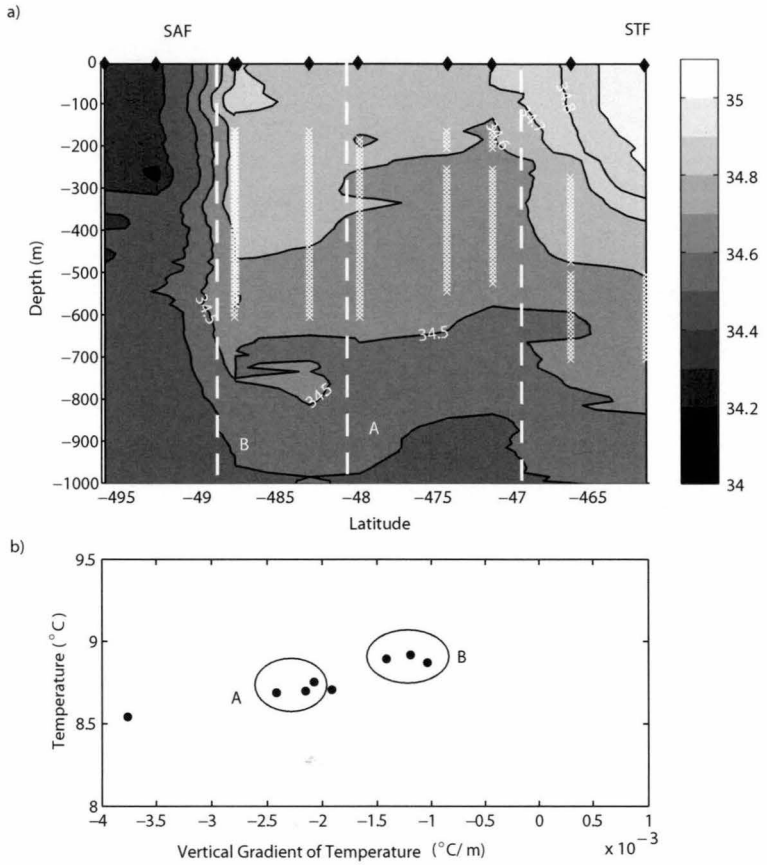

Figure 3.8: SAMW vertical distribution of Salinity during the World Ocean and Climate Experiment (WOCE) SR3, November 2001 (top figure). Yellow crosses depict regions where the criteria used to define SAMW ($\theta/(\mathrm{d}\theta/\mathrm{dz}) \leq 0.005$ and $\theta \in [8,\ 9.5]$°C) are satisfied. Stations are shown by black diamonds at the top of the contour. (b) Classification of the water types that satisfy the SAMW criteria, based on the mean temperature and vertical temperature (bottom figure).

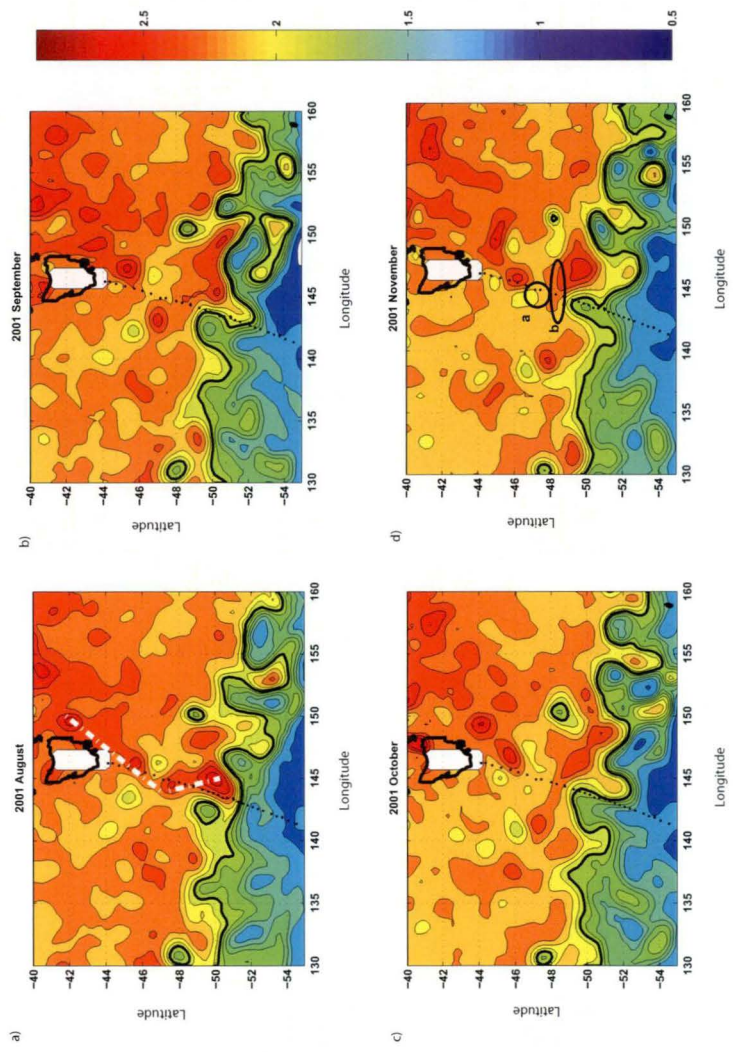

Figure 3.9: Sea Surface Height maps (m) south of Tasmania at the time of the World Ocean Circulation Experiment (WOCE) SR3 section held on November 2001. Black bold line correspond to the 1.9 m steric height as the position of the time–varying SAF (calculated from the Olbers 0/2500 m mean steric height plus the sea level anomalies from the Topex/Poseidon + ERS1–2 altimetry data defined by *Sokolov and Rintoul* (2002)).

interact with the meandering SAF. In September, it is located at 50°S, 144°E – 149°E (figure 3.9 b). It is surrounded by SAF waters to the south and to the east by a SAF–eddy. The core of the eddy seems to be stronger during October, maintaining part of its initial subtropical properties which imprinted the characteristics of cluster **B** water mass (figure 3.9 c). A warm temperature anomaly in the SST satellite images (not shown) supports the conclusion that the properties of **B** are influenced by advection of subtropical waters by eddies. Note that the eddies remain in the SAZ for several months during the winter, where they will be exposed to cooling by the atmosphere and deepening of the surface mixed layer, producing a volumetric mode. *Morrow et al.* (2007) showed how the November 2001 SR3 section had strong mesoscale eddy structures. They also noticed a sub–surface warming. They suggested the warming was forced by a poleward shift of the STF associated with a stronger Tasman Outflow. Following the time history of SSH, we arrive at a slightly different conclusion. The warm anomaly coincides with an eddy formed from the ridge of high SSH extending south from the subtropics, rather than a stronger Tasman Outflow. We showed a strong warm–core eddy (46°S, 145°E) is located at the STF position given by *Morrow et al.* (2007). By tracking eddies back in time, we explained how the advection of anomalous water by eddies or meanders, rather than a stronger Tasman Outflow, influenced the SAMW properties.

3.3.4 SAMW variability: Seasonality

The seasonal evolution of the homogeneity of the SAMW core was studied using the distribution of the first derivative of temperature with respect to depth from the XBT sections. The SURVOSTRAL program only occurs during the austral spring–summer period that is from October to March, due to ice conditions. The homogeneity of the core of the SAMW is reflected in figure 3.10 (a): the smaller the gradient, the stronger the thermostad. *Qiu et al.* (2006) showed the erosion of the North Pacific subtropical Mode Water thermostad by evaluating the vertical gradient of potential vorticity at the edges of

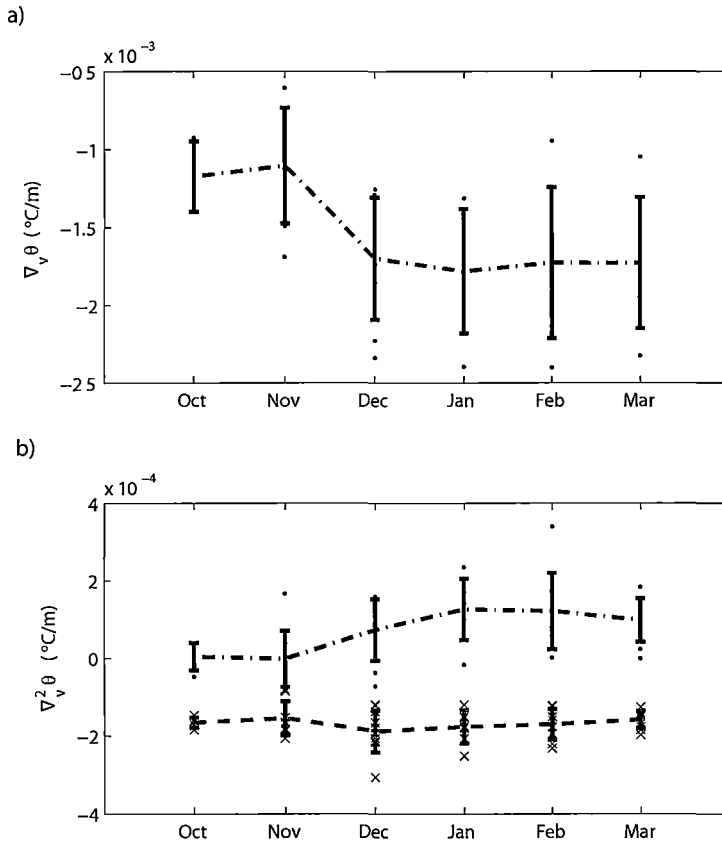

Figure 3.10: SAMW Intra–annual variability. (a) Seasonal evolution of the SAMW core homogeneity. (b) Seasonal evolution of the erosion of the thermostad, for the top (dashed–dotted line) and bottom (dashed line) of the SAMW pool.

the Subtropical Mode Water. Here, we show the erosion of the thermostad, at the top and bottom of the SAMW pool, by the second derivative of temperature with respect to depth (figure 3.10 b). The size of the error bars reflects the high intra–annual variability in the mode water. During October to November, the gradient is small (figure 3.10 a) and SAMW is found from the surface to depths as great as 700 m. The summer mixed layer generally starts to form in mid–November as the seasonal thermocline develops. Consequently, some of the SAMW formed that winter is capped by the summer mixed layer and some is advected away from the formation area. We can see this interaction in figure 3.10 (a) where mode water dT/dz increases with the formation of the seasonal thermocline. The most pronounced dT/dz increment occurs from November to December at the same time as the top of the SAMW core erodes (figure 3.10 b). The strength of the SAMW core remains constant from January to March. These results suggest that erosion of the SAMW core occurs mainly at the top of the SAMW pool, where it interacts with the seasonal mixed layer, with little further erosion of the thermostad during the summer.

3.4 Summary

The variability of SAMW south of Tasmania has been evaluated. We find evidence for significant year–to–year (and in some cases, month–to–month) variability of SAMW properties, but no trend over the 17 year–period of observations. SAMW physical and biogeochemical properties at Drake Passage also showed substantial intra– and inter–annual variability over the last four decades (*Naveira–Garabato et al.*, 2009). The large variability found south of Tasmania suggests caution is required when interpreting changes in SAMW properties from infrequently sampled sections. A clear mechanistic understanding of the source of SAMW variability is needed in order to interpret changes observed from sparse observations. In this study, we have focused on the contribution of mesoscale eddies to the variability of SAMW.

We have shown that rapid and large shifts in SAMW properties can be explained by

the advection of anomalous water by mesoscale features. It is often assumed there is a single mode or type of mode water at each location. Figure 3.3 showed strong "modes" with different temperature/salinity characteristics in SAMW. Sea surface height maps and water mass properties suggest these "modes" can be explained by the advection of anomalous water by mesoscale features into the SAZ, modifying SAMW properties in the formation area (sampling bias). Once the eddies have entered the SAZ, they can influence SAMW properties through isopycnal mixing. In addition, deep winter mixing will tend to mix the anomalous water vertically.

It is likely that cold/fresh modes occur frequently due to eddies spawned from the ACC. The Australian sector of the Southern Ocean is a region with a high eddy kinetic energy (*Phillips and Rintoul*, 2000). Baroclinic and barotropic instabilities of the SAF result in the formation of eddies and meanders. Eddy activity is enhanced in this region as a result of the interaction of the flow with the Southeast Indian Ridge as an attempt of the circulation to conserve its potential vorticity (*Wolff et al.*, 1991; *Morrow et al.*, 2004). The frequent formation of cold–core eddies or meanders from the SAF explains why cold anomalies of SAMW are more frequent than warm anomalies in this region.

Nevertheless, warm SAMW anomalies are occasionally observed. The SSH maps suggest these events can be linked to the input of warm and salty subtropical water by eddies of the East Australian Current (EAC). The EAC also regularly spawns eddies, and occasionally these warm–core features extend as far south as the SAZ and influence the properties of the SAMW. *Ridgway* (2007a) shows that the EAC extends further south in austral summer and so the input of subtropical water to the SAZ is more common during the summer season. During the following winter, air–sea interaction drives deep convection and removes some but not all of the anomalous properties in the remnant eddy, resulting in a relatively warm and salty variety of SAMW.

A key link in the Southern Ocean overturning circulation is the conversion of deep water

upwelling at high latitudes to less dense SAMW and AAIW. The SAMW and AAIW are relatively fresh, and their export to lower latitudes closes the hydrological cycle by returning the excess precipitation falling at high latitudes. The formation and export of SAMW and AAIW also carries anthropogenic carbon dioxide into the interior and returns nutrients from the deep ocean to the upper ocean to support biological productivity. The contribution of SAMW and AAIW to the overturning circulation, carbon storage, nutrient transport and the hydrological cycle make SAMW and AAIW critical components of the Earth's climate system. A change in the formation rate of SAMW would alter the capacity of the Southern Ocean to store heat and carbon and to export nutrients and influence the rate of climate change. Therefore it is important to understand what drives variability in SAMW properties in the present climate and how SAMW formation and export will be affected by climate change.

The Southern Annular Mode (SAM) is the primary mode of atmospheric variability in the Southern Hemisphere. A positive trend in the SAM toward higher index state has been observed over the past three decades (*Thompson and Solomon*, 2002) and is projected to continue in the future as a result of increasing greenhouse gas concentrations in the atmosphere (*Cai et al.*, 2003). A higher positive SAM implies a strengthening in circumpolar wind stress over the Southern Ocean, with two important consequences. First, changes in wind stress can induce changes in the intensity of the Southern Ocean eddy field (*Meredith and Hogg*, 2006). Second, changes in the Southern Hemisphere winds are also related to the intensification of the EAC southward penetration (*Cai et al.*, 2005; *Ridgway*, 2007b). As a result, the influence of mesoscale features over SAMW properties south of Tasmania is expected to increase.

Our results suggest that assessing SAMW variability from infrequently repeated sections may produce misleading results by aliasing large inter–annual variability. Mesoscale circulation plays an important role in the inter–annual SAMW variability south of Australia, and it is expected to increase in a global warming scenario. As the fronts

bounding the SAZ are hot spots for eddy kinetic energy along much of their circumpolar paths, we believe that mesoscale features will likely influence the properties of the SAMW at other locations in the Southern Ocean.

Chapter 4 Regional circulation and its impact on upper ocean variability south of Tasmania

4.1 Introduction

The Southern Ocean plays a major role in global climate and global biogeochemical cycling. It is a key component of the overturning circulation, where deep water upwells and is transformed into mode and intermediate waters that ventilate part of the global ocean. These transformed water masses also contribute to global heat, freshwater, carbon, and nutrient budgets. The Subantarctic Zone (SAZ), bounded by the Subtropical Front (STF) and the Subantarctic Front (SAF), is the region of the Southern Ocean with the largest zonally–integrated inventory of anthropogenic carbon dioxide (*McNeil, et al.*, 2001; *Sabine, et al.*, 2004). Biological production in the SAZ drives a strong seasonal cycle of dissolved nutrient and carbon dioxide concentrations on the surface and a large net uptake of carbon dioxide from the atmosphere (*Metzl, et al.*, 1999; *Lourey and Trull*, 2001; *Wang et al.*, 2001) which is accompanied by the export of organic carbon in sinking particles (*Trull, et al., 2001*).

The SAZ–Sense project[1] sought to characterize the key components of the Southern Ocean planktonic community, with a focus on the SAZ, and examine their role in transferring carbon dioxide from the surface to the deep ocean. The properties of the SAZ vary around the circumpolar belt (*Hanawa and Talley*, 2001, *McCartney*, 1977), particularly in the interaction with subtropical waters. However, the relative importance of air–sea fluxes, regional circulation, and exchanges across the STF and SAF on water mass

[1] www.cmar.csiro.au/datacentre/saz-sense/

properties in the SAZ is unclear. The region east of Tasmania (150 °E to 160 °E) generally has a relatively large phytoplankton surface biomass and productivity, in contrast with the lower surface biomass in the west (135 °E to 145 °E) (*Trull et al.*, 2001; *Griffiths et al.*, submitted to DSR). The contrast is clearly seen in ocean colour satellite images, which provides a natural context within which to identify, describe, and evaluate the response of subantarctic ecosystems to changes in the environment. The Tasman Sea, situated along the eastern coast of Australia, shows some of the highest rates of temperature change observed in the Southern Hemisphere (*Hill et al.*, 2008) and in global circulation model simulations of greenhouse–gas driven climate warming (*Cai et al.*, 2005). A southward shift of the westerlies might already have changed atmospheric and oceanic circulation, strengthening the influence of subtropical waters in the SAZ (*Poloczanska et al.*, 2007, *Ridgway*, 2007a; *Hill et al.*, 2008), especially to the east of Tasmania.

Two intermediate water masses are found in the upper ocean in the SAZ, Subantarctic Mode Water (SAMW) and Antarctic Intermediate Water (AAIW) (*Hanawa and Talley*, 2001). SAMW is a thick, homogeneous layer formed by deep convection in winter in the SAZ (*McCartney*, 1977). The interaction of the SAF with the South East Indian Ridge creates numerous eddies and meanders which can influence the properties of the SAMW formed just north of the SAF (see Chapter 2). AAIW is a low–salinity water mass that occupies most of the Southern Hemisphere and the tropical oceans at intermediate depths (800 to 1200 m). SAMW and AAIW ventilate the main oceanic thermocline and contribute to large–scale fluxes and budgets of heat, freshwater, carbon dioxide, and nutrients. For example, *Sarmiento et al.* (2004) suggested that the nutrients supplied by SAMW ultimately supported 75% of the export production north of 30 °S. Understanding the mechanisms involved in setting the properties of the SAZ is important for improving our knowledge of SAMW, and vice versa.

The main regional circulation features south of Tasmania are shown in figure 4.1. *Cresswell* (2000) described the major currents over the slope and continental shelf around

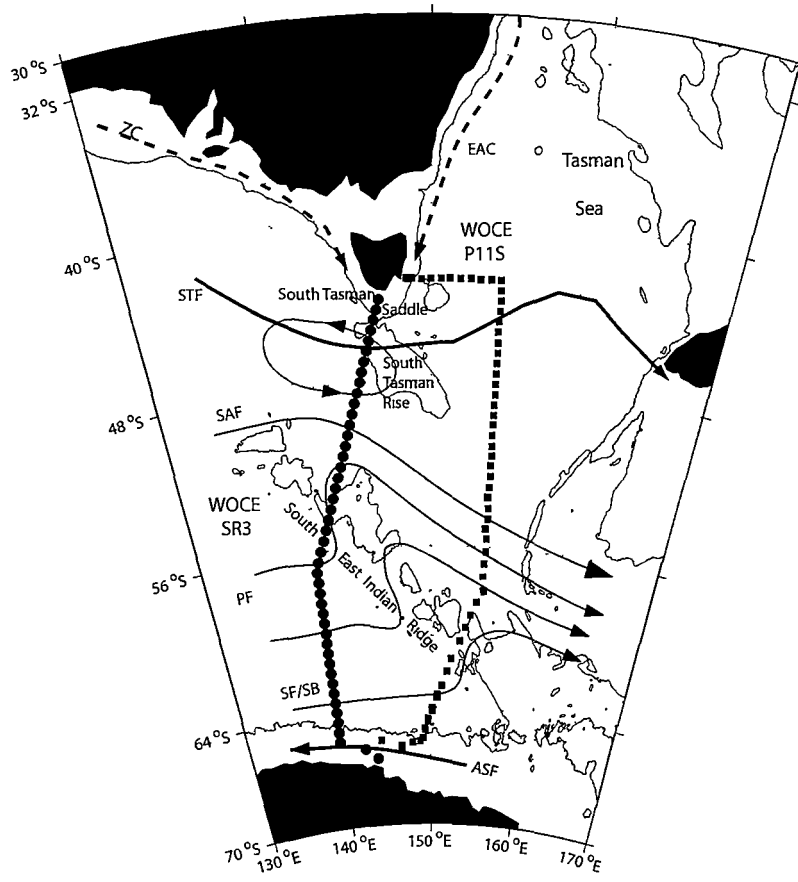

Figure 4.1: Summary of the main features for the regional circulation south of Tasmania. World Ocean Circulation Experiment sections, SR3 and P11S. EAC, extension of East Australian Current; ZC, Zeehan Current; STF, SubTropical Front; SAF, Subantarctic Front; PF, Polar Front; SF, southern ACC front; SB, southern boundary of the ACC; ASF, Antarctic Slope Front. Bathymetry higher than 2000 m appears as shaded contours.

Tasmania, namely the Zeehan Current and the East Australian Current (EAC). The Zeehan Current flow is restricted to waters over the western Tasmanian continental shelf and upper slope. The Zeehan Current is stronger during winter. It flows southward along western Tasmania to turn and run northward off eastern Tasmania where it deflects the EAC to the east creating many mesoscale features. Although most of the EAC separates from the coast and flows to the east around 32 °S, some flow (termed the EAC Extension) continues southward along the coast, reaching the east coast of Tasmania during summer. When it reaches the southeast point of Tasmania, it interacts with the Zeehan Current and the South Tasman Rise, limiting the southwest extent of the EAC waters. The seasonal circulation around Tasmania is described in detail in *Ridgway* (2007b).

Rintoul and Sokolov (2001) documented two major circulation features in the vicinity of the SAZ. (i) West of the South Tasman Rise, a deep–reaching anticyclonic recirculation is located between $\sim$ 47 °S and 49 °S. (ii) East of Tasmania, a weak northward flow enters the Tasman Sea, turns anti–clockwise to flow southward along the Tasmanian coast, and passes westward through the South Tasman Saddle (the relatively deep channel (3500 m) that separates the South Tasman Rise from the continental slope of Tasmania). Our results suggest a slightly different interpretation of the flow in this region, as discussed in Section 4.4.

The goal of the present study is to assess the influence of the regional circulation on the water properties and biomass differences observed east and west of Tasmania. This study has broad implications because these same processes may affect SAMW, AAIW, and SAZ variability elsewhere. The study also provides new information on the nature of the exchange between the Pacific Ocean and the Indian Ocean south of Australia (*Speich et al.*, 2002; *Ridgway and Dunn*, 2007; *Cai*, 2005). The paper is structured as follows. Sections 4.2 and 4.3 describe the data used and the temperature–salinity distributions in the water column, focusing on the main water masses, SAMW and AAIW. The regional circulation inferred from Argo float trajectories and its relationship with the distribution

of water mass properties is discussed in Section 4.4, and our findings are summarized in Section 4.5.

4.2 Data

World Ocean Circulation Experiment (WOCE) transects

Two late–summer CTD transects were collected during voyages of the research vessel R/V *Aurora Australis* in March–April 1993 (SR3 and P11S) (figure 4.1). Stations along the sections were generally about 55 km apart in the Subantarctic Zone, both southwest (SR3) and east (P11S) of Tasmania. They provide a good reference to locate the two main water masses in the SAZ: SAMW and AAIW, which are described in Section 4.3. Useful information on the SR3 sections can be found in *Rintoul and Bullister* (1999), *Sokolov and Rintoul* (2002), and *Rintoul et al.* (2002).

Profiling floats: Argo

The vertical structure of the water column in the South Tasman Sea and Subantarctic Zone (SAZ) south of Tasmania was obtained from the Argo data set, which provides data covering vast areas of the Southern Ocean for the first time. Data are made freely available by the International Argo Project and the national programs that contribute to it. In the SAZ, south of Tasmania, around 200 Argo floats have been deployed, providing more than seven thousand temperature and salinity profiles of the top 2000 metres. This study used delayed–mode profiles that passed the Argo quality control, with data on their position, date, temperature and salinity from 10 m to 1800 m.

4.3 Water mass properties

Vertical sections of potential temperature, salinity, and neutral density from SR3 and P11S show the main vertical structure of the water column in the SAZ (figure 4.2, SR3, left; P11S, middle and right).

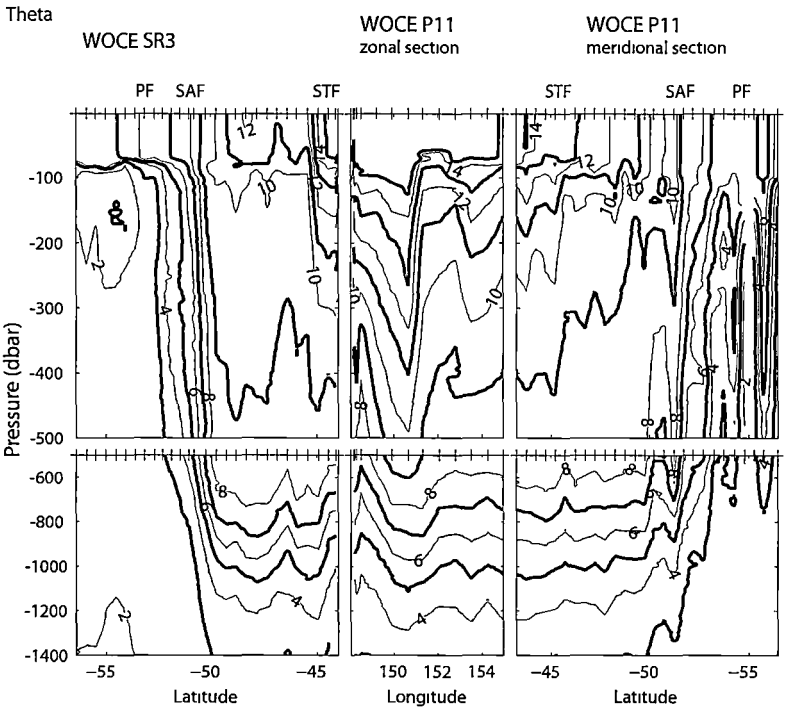

(a)

Figure 4.2: Property distributions along sections P11S (zonal and meridional legs) and SR3: (a) Potential temperature, θ; (b) Salinity, where shaded contours represent salinity values higher than 34.7 psu; (c) neutral density (γ^n) (kgm^{-3}). The locations of the major fronts are indicated above: STF, Subtropical Front; SAF, Subantarctic Front; PF, Polar Front. Upper ticks depict the sampled stations.

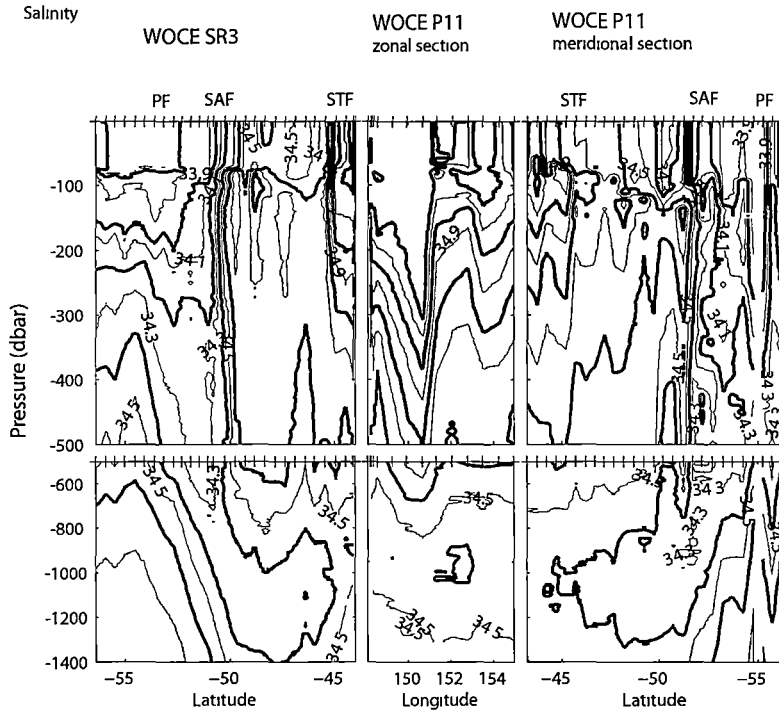

(b)

Figure 4.2: Continued: Salinity

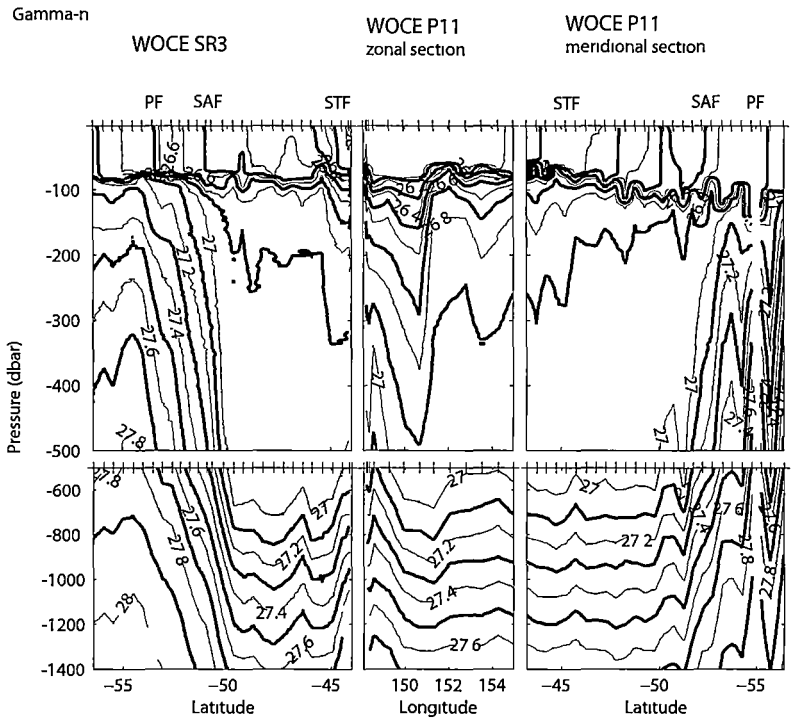

(c)

Figure 4.2: Continued: Neutral density (γ^n) (kgm^{-3})

The region of the SAZ–Sense project is affected by three fronts: the Subtropical Front (STF), the Subantarctic Front (SAF) and the Polar Front. The STF represents the boundary between warm, salty subtropical waters and cold, fresh subantarctic waters. The STF in this region coincides with the crossing of the 11 °C isotherm at 150 m depth and the southern limit of the water with salinity greater than 34.8 psu (*Nagata et al.*, 1988; *Sokolov and Rintoul*, 2002). The SAF, which is the strongest front of the Antarctic Circumpolar Current south of Australia (*Sokolov and Rintoul*, 2002), is marked by the presence of a thermostad (the SAMW) and a salinity–minimum layer (the AAIW) to the north. The Polar Front is commonly defined by the northernmost extent of the subsurface temperature–minimum cooler than 2 °C near 200 metres depth (*Belkin and Gordon*, 1996). It is marked by a transition to very cold, relatively fresh, Antarctic Surface Water at the surface. The locations of the fronts are indicated above the plots in Figure 4.2.

The eastern SAZ receives inputs of warm and salty waters through two mechanisms: the East Australian Current extension and the Tasman Outflow. The EAC extension is a southward flow along the eastern shore of Tasmania (*Cresswell*, 2000), seen in the steeply sloping temperature, salinity and neutral density contours at ~149 °E – 151 °E (figure 4.2 a, b, c, upper middle panel). The Tasman Outflow (a remnant of the EAC at intermediate depths) reaches the south Indian Ocean as a relatively warm and salty flow. It also provides an additional component of the thermohaline circulation and a southern connection between the Pacific and Indian Oceans (*Rintoul and Bullister*, 1999; *Speich et al.*, 2002; *Ridgway and Dunn*, 2007).

The western SAZ shows properties more typical of the circumpolar SAZ: relatively cold and fresh, and less influenced by warm, salty, subtropical waters than the eastern SAZ. The top 200 m of the water column on P11S is warmer and saltier than that on SR3. A subsurface salinity intrusion, found in both sections, is more prominent at P11S (figure 4.2 b).

SAMW and AAIW occupy most of the upper ocean in the SAZ. South of Tasmania, SAMW forms a thick pycnostad (thus, minimum in potential vorticity) with a core temperature of 8.5 °C – 9 °C and salinity of 34.55 – 34.70 psu, and a high oxygen concentration. In the western hydrographic section (SR3), the upper and lower bounds of the SAMW pycnostad reach mean depths between ~190 m and 600 m, while in the eastern section, the upper and lower bounds are between ~170 and 500 m. The oxygen concentration in the SAMW pool west of Tasmania is uniformly high; while in the east, oxygen concentrations decrease from south to north within the SAMW pool. AAIW has a much lower oxygen concentration than SAMW. It is identified as a salinity minimum at intermediate depths north of the SAF and below SAMW (figure 4.2 b). South of Tasmania, the salinity minimum is not uniform in its properties, corresponding to a range of temperature and density: water with salinity less than 34.4 psu spans a range of 27.25 – 27.6 kgm^{-3} in neutral density and 3.43 °C – 5.63 °C in temperature (*Rintoul and Bullister*, 1999).

A review of the water mass properties, their distribution, and the relationship with the regional circulation in the area is given below, starting with the properties east and west of Tasmania.

4.3.1 Temperature – Salinity properties east and west of Tasmania

The distribution of the physical properties in the water column in and around the SAZ were studied using Argo float potential temperature (θ) and salinity (S) profiles. To get an overview of the mean potential temperature and salinity properties and their origin, we divided the region into seven boxes (figure 4.3). We focus on the salinity minimum to describe the main differences.

The θ–S curves span a wide range of properties even in this relatively small region, with a salinity difference of 0.1 psu between the freshest and the saltiest salinity minimum

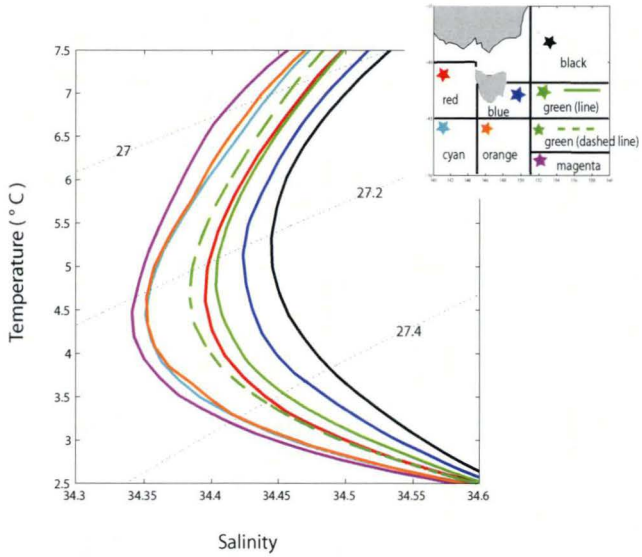

Figure 4.3: Mean Potential Temperature – Salinity (θ–S) at the salinity minimum from Argo profiles. Each colour represents a box in the map (top right).

values. The extreme θ–S curves represent the two main regions influencing the water–mass properties in the SAZ. The saltiest and lightest S–minimum is in the southern Tasman Sea, north of 43 °S (figure 4.3, black curve). The freshest and densest S–minimum is found along the SAF (figure 4.3, cyan, orange, magenta curves), reflecting the dominant influence of Southern Ocean waters on the physical properties of these three boxes. These southern waters change little from west to east. Intermediate S–minimum values from the middle boxes show stronger Tasman Sea input in the east, in particular near the southeast coast of Tasmania (blue curve), where the influence of the EAC is greatest.

4.3.2 Subantarctic Mode Water (SAMW)

The CTD profiles from the WOCE hydrographic sections and the profiling floats were used to study the SAMW distribution in detail. In order to use as many Argo profiles as

possible and avoid dealing with seasonality, the top 200 dbar were not used. SAMW was defined as water with potential vorticity (PV) less than $1 \times 10^{-9} m^{-1} s^{-1}$ and potential temperature (θ) between 8 °C and 9 °C (*Rintoul and England*, 2002) for depths greater than 200 dbar. The potential vorticity for a fixed depth interval of ~40 m was calculated as equation 2.1 in Chapter 2. The distribution and circulation of SAMW is illustrated by plotting the thickness of the SAMW layer and Modified Montgomery streamlines (Section 2.3) on the γ^n= 26.94 surface (figure 4.4, top). SAMW thickness was calculated as the difference in pressure between the top and bottom of the SAMW layer defined by our PV minimum range at each profile.

Mode water forms either side of Tasmania in the SAZ, but the SAMW properties are different in the east and the west. The SAMW layer is much thinner in the east than in the west (figure 4.4). The thermostad is also stronger (more vertically uniform) in the west (figure 4.4, bottom). Winter convection appears to less effectively homogenise the water column in the SAZ east of Tasmania. The extent and depth of the deep convection that forms mode water depends on the buoyancy loss to the atmosphere, the stratification, and regional circulation. The stratification, in turn, can be influenced by exchange with the subtropics (e.g. through interleaving, intrusions and eddies). The SAMW thickness in the area labeled in green in the inset of figure 4.3 (43 °S – 47 °S, 151 °E – 160 °E) is 250 – 300 dbar, about 100 dbar less than observed further south in the SAZ (figure 4.4, top).

The distribution of the pycnostads associated with SAMW is strongly influenced by the regional circulation, as revealed by the Montgomery streamfunction (figure 4.4). The South Tasman Rise seems to separate regions with different circulation patterns: on the eastern side, the circulation seems to be very slow, while on the western side, there is an anticyclonic circulation south of 43 °S. The thin SAMW pool in the east and thick pool in the west are separated by the South Tasman Rise. Thick SAMW is found in the northwestward anticyclonic flow, with the thickest SAMW pool embedded in the closed anticyclonic recirculation described by *Sokolov and Rintoul* (2002) (figure, 4.1, closed

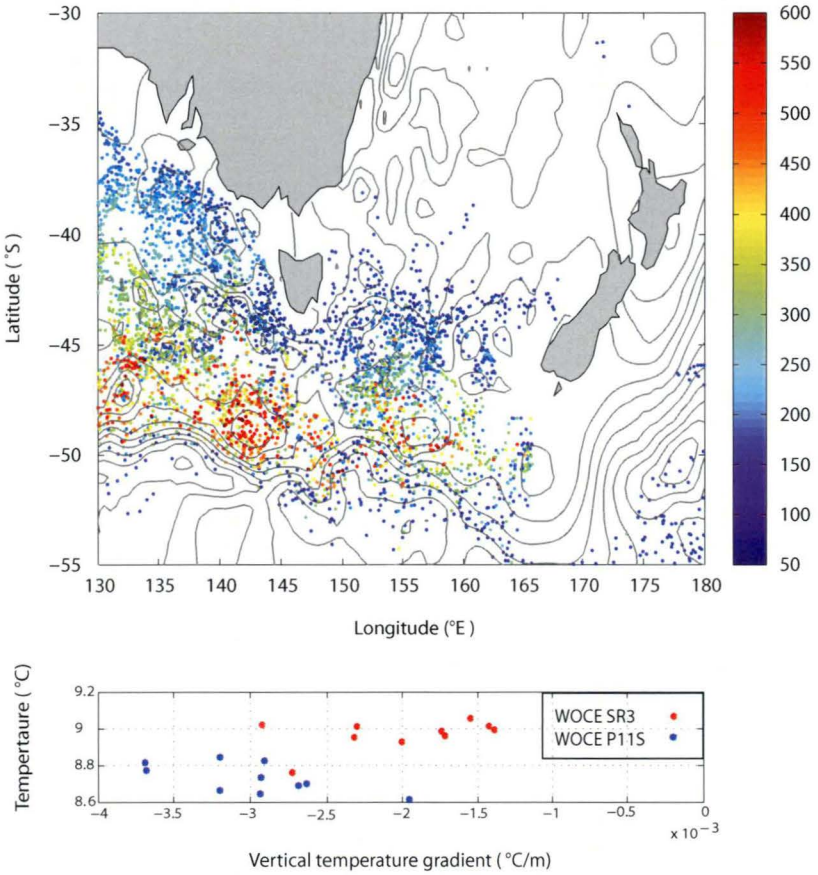

Figure 4.4: SAMW thickness (dbar) (top). Montgomery streamlines ($m^2 s^{-2}$) were calculated for γ^n= 26.94 kgm^{-3} corresponding to the mean density of SAMW south of Tasmania (as shown in Chapter 2 (dark grey lines). SAMW thermostads strength (dθ/dz) found at SR3 and P11S is shown at the bottom figure (red and blue, respectively).

contour centered at about 48 °S, 143 °W). Also, thick SAMW layers are found just north of the SAF.

4.3.3 Antarctic Intermediate Water (AAIW)

In Section 4.3.1, we showed that the properties of the salinity minimum defining AAIW varied strongly across the region, with low salinity AAIW (S $\leq$ 34.4) in the south and high–salinity AAIW (S $\geq$ 34.4 psu) in the north. The high–salinity AAIW is formed in the southeast Pacific and is carried around the subtropical gyre to enter the Tasman Sea between New Zealand and Fiji (*Wyrtki*, 1962; *Sokolov and Rintoul*, 2000). This variety of AAIW extends as far south as 40 °S, where the median properties are 34.44 psu and 5 °C (figure 4.3; black θ–S curve). South of $\sim$40 °S, this northern AAIW mixes with waters from the Subantarctic Zone, and decreases its salinity. The neutral density (γ^n) distribution for salinity minimum layers with S less than 34.4 psu peaks at γ^n= 27.4 kgm^{-3}. Figure 4.5 shows the temperature and salinity distribution at this density surface. Relatively warm, salty AAIW extends southwestward and through the South Tasman Saddle (figure 4.5, orange dots). A cooler, fresher variety of AAIW enters the SAZ from the south, with median properties of salinity $\approx$ 34.36 psu and temperature $\approx$ 4.44 °C (figure 4.5, green dots). AAIW with intermediate properties is produced by mixing between these two varieties in the SAZ (yellow dots). A homogeneous pool of AAIW with southern source characteristics (salinity $\approx$ 34.34 psu, temperature $\approx$ 4.4 °C) is found inside the anticyclonic feature west of the South Tasman Rise.

Interleaving is enhanced where the warm, salty northern and, cold, fresh southern varieties of AAIW meet, on the eastern side of Tasmania. This area is located between 43 °S – 48 °S and 151 °E – 160 °E. Figure 4.6 depicts the θ–S curves from the two hydrographic sections. At SR3, the θ–S profiles from the SAZ form a tight cluster (black curves, figure 4.6 left), with relatively little evidence of interleaving with profiles to the north

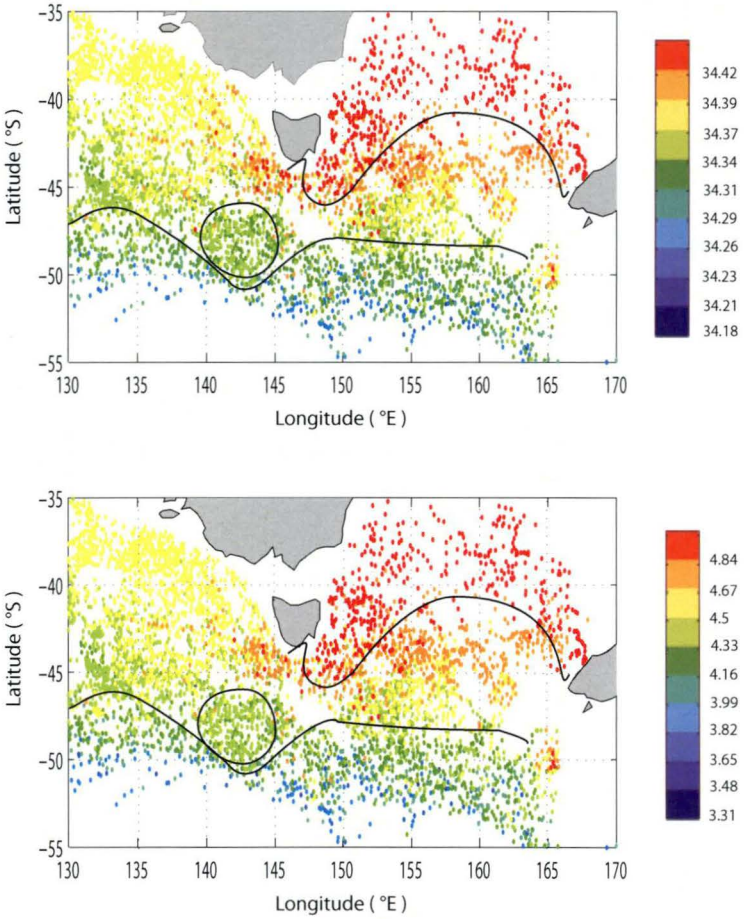

Figure 4.5: AAIW salinity (top) and temperature (bottom) at γ^n= 27.4 kgm^{-3}. Black lines mark the limit for the two AAIW sources. The position of the anticyclonic eddy on the west of the South Tasman Rise is indicated by an ellipse.

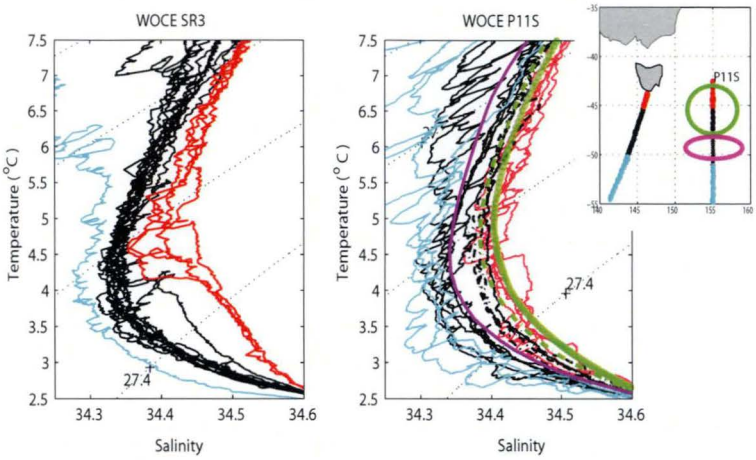

Figure 4.6: Potential temperature/Salinity (θ–S) curves for SR3 and P11S stations from 43° to 51°S. Stations belonging to the STF area of influence are in red, north of ~46°S. Stations within the SAZ are in black and waters in the SAF area are in blue, ~50°S. The mean θ–S properties on the east of Tasmania (green and magenta–purple) are compared to stations from P11S (right). Stations represented by black stars in the map correspond to black lines at P11S θ–S curves.

and south. This is explained by the presence of the permanent anticyclonic recirculation, which appears to inhibit exchange with surrounding waters. At P11S, θ–S curves from the SAZ fall in two clusters (figure 4.6, right; black solid and dash lines) resulting from interleaving with waters north and south of the SAZ.

4.3.4 Sub–surface salinity maximum

Vertical sections of salinity in the upper 500 dbar of the water column show stronger southward advection of warmer, saltier waters at subsurface depths in the east than in the west. As we mentioned at the start of Section 4.3, the EAC can be seen in the zonal leg of the P11S section, as a relatively warm, salty wedge between 149 °-- 151 °E (figure 4.2 a, b, c). For the meridional P11S section, water with salinity higher than 34.7 psu can be seen spreading as far south as 50 °S, with some isolated patches at 100 – 200 dbar below the surface (figure 4.2b, upper right panel, gray filled contours). The depth

of these warm, salty patches increases as they move southward. Isolated warm and salty sub–surface patches are also seen at the SR3 section, although there is no continuous connection with waters north of the STF as we see at P11S. Monthly mean salinity sections from the CSIRO climatological Atlas for Regional Seas (CARS2006a) (*Ridgway et al.*, 2002) at 140 °E and 150 °E show the seasonal evolution of this intrusion (figure 4.7 a, b, respectively). On the western side, at 140 °E (figure 4.7 a), the limit between the STF and the SAZ waters is more clearly defined during winter, with a very well developed winter mixed layer. In January, an intrusion of warm and salty water starts to develop south of the STF (~45 °S) at around 150 dbar. It gets stronger during February and weakens during March. On the eastern side, at 150 °E (figure 4.7 b), the influence of subtropical waters is remarkable. The subsurface intrusion advection of warm, salty waters into the SAZ is present all year round. During January, a plume of salinity higher than 34.7 psu (at ~ 100 dbar) starts to develop south of 45 °S. The core of the plume gets saltier during January and February reaching values higher than 35 psu that can detach from the main inflow and form similar patches or "eddies" between 100 – 200 dbar as seen at P11S (figure 4.2 b, upper right panel). From May to September, winter convection occurs, mixing these salty waters with the water below throughout the winter. The presence of the strong subsurface salinity maximum, hence stronger stratification, in the east could reduce the effectiveness of winter convection, resulting in a thinner and less homogeneous SAMW layer.

The larger contrast in temperature/salinity between north and south of the STF and the slower circulation in the eastern SAZ allows a stronger subsurface salinity–maximum to develop in the east. In summer, surface waters warm and become less dense on both sides of the STF (figure 4.2 a, c). With temperature and density being stratified as a result of the summer mixed layer formation, strong southward diffusion and advection of salinity along isopycnals are possible at the base of the mixed layer, forming a subsurface salinity maximum (figure 4.2 b).

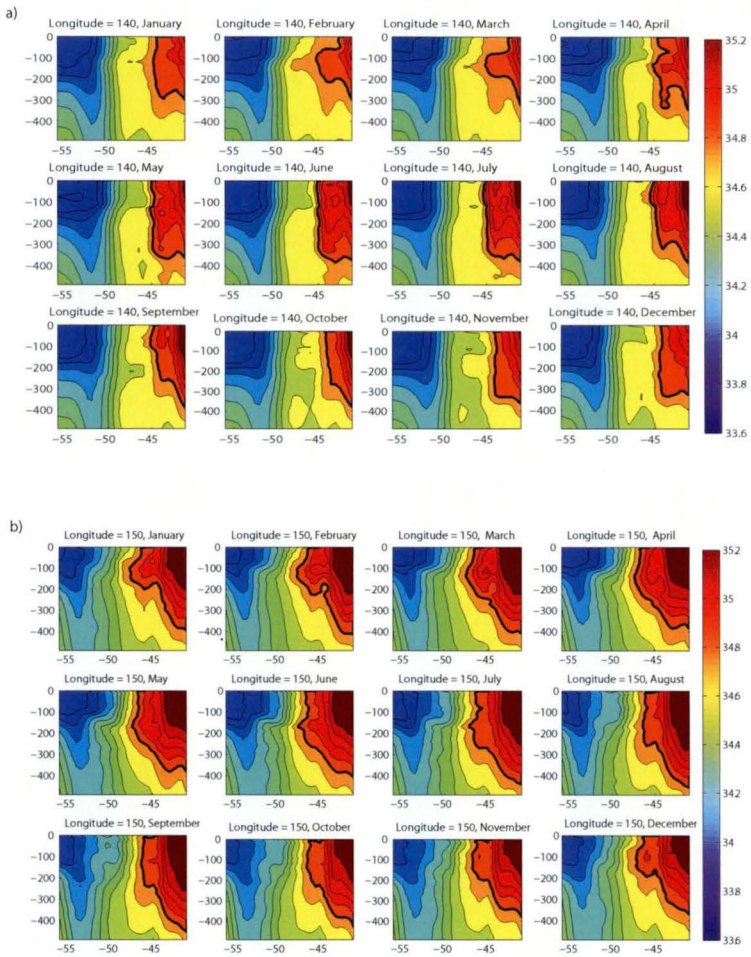

Figure 4.7: Monthly mean salinity section at 140°E (a) and 150°E (b) between 40°S to 56°S from January to December taken from CSIRO Climatological Atlas for Regional Seas (CARS2006a). The 34.7 psu isohaline is depicted by the black bold line.

The advection of subsurface salinity during summer is likely to supply micronutrients, especially iron, into the SAZ south of Tasmania. Subtropical waters in the region are generally replete with micronutrients and are mainly limited by major nutrient supply (N, P, Si) (*Ellwood et al.*, 2008). In the same area and depth range as the subsurface salinity maximum is found (approximately between 100 – 200 m), elevated dissolved and particulate iron concentrations have been documented (*Bowie et al.*, submitted to GBC). In winter, deep convection would transport this iron into the surface layer, perhaps contributing to higher biomass observed in the east. In addition, *Kahru et al.* (2007) reported how cross–frontal eddy activity in the Southern Antarctic Circumpolar Current Front enhanced conditions for phytoplankton biomass growth. Following the *Kahru et al.* (2007) interpretation, the mesoscale features associated with the EAC retroflection along ~45 °S could be a mechanism to bring those micronutrients from the subsurface "eddies" via upwelling back to the photic zone. The upwelled nutrients can be used by the phytoplankton and maintain the high biomass seen in this region.

4.4 Argo float trajectories

Water mass properties show a contrast between the eastern and western SAZ, south of Tasmania. The Montgomery streamfunction distribution and previous discussion suggest the E–W contrast is maintained by the regional circulation. We now use Argo float trajectories to reveal the regional circulation in greater detail and explore its connection to the distribution of water properties.

The trajectories of 48 Argo floats passing through the region tend to follow one of four distinct circulation pathways (figure 4.8). Route one and two represent 22% and 31%, respectively, of the total Argo float trajectories. Route one shows a westward flow south of Tasmania, between the continental shelf and the South Tasman Rise(STR) (figure 4.8, top left). It is followed by floats with very different origins: from the north, following the

path of the EAC; and from the eastern SAZ. Route two (figure 4.8, top right) represents a northwestward flow and a deep–reaching anticyclonic recirculation between 47 °S – 49 °S and 140 °E – 145 °E, described by *Rintoul and Sokolov* (2001), just west of the STR. The presence of this anticyclonic recirculation enhances the contrast between SAMW/AAIW properties to the east and west of Tasmania, as discussed in Sections 4.3.2 and 4.3.3. Bathymetry, in particular the STR, also exerts a strong influence on the characteristics of the main flows in the region. Route 1 passes through the gap between the Tasmanian continental slope and the STR. Floats approaching the STR from the west are blocked by the STR and turn back to the northwest toward the Great Australian Bight. No floats were observed to pass from the western SAZ to the eastern SAZ north of the southern limit of the STR.

East of Tasmania, Argo float trajectories are more variable in the SAZ. Routes three and four correspond to 18% and 15%, respectively, of the total float trajectories. Route three (figure 4.8, lower left) depicts a sluggish circulation mainly in the SAZ region between 150 °E and 160 °E and close to Tasmania. Route three also depicts trajectories moving back and forth across 44 °S, probably associated with mesoscale features as the EAC extension turns back to the northeast. A northward flow can be inferred from the slope of the isopycnals on the offshore end of the short zonal portion of P11S (figure 4.2 c). Route four (figure 4.8, lower right) is characterized by a slow northeastward flow in which the floats seem to be travelling in the same direction as the deflection to the east of the EAC between ~33 °S – 44 °S (east of 160 °E), and so these floats are more likely to be influenced by the EAC variability. *Rintoul and Sokolov* (2001) also described a recirculation in the east, extending northward to approximately 40 °S and then flowing westward. This recirculation shows characteristics of Routes one and three: waters from the eastern SAZ move northward and can get trapped in the flow southward along the Tasmanian coast to enter the west south of Tasmania. About 14% of the floats followed other trajectories not described here.

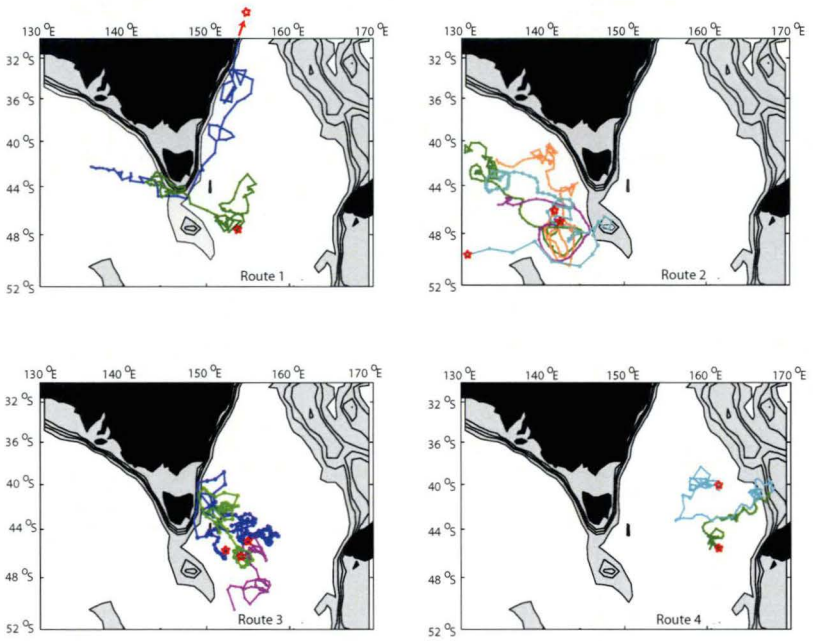

Figure 4.8: Routes of the main regional circulation described by the Argo float trajectories. Each colour represents a float. The start of each trajectory is signed by a red star. The Wmo number for each float is: R1: 5900873 (blue), 5900457 (green); R2: 7900117 (purple), 5900849 (orange), 5900841 (green), 5900689 (blue); R3: 5900452 (blue), 59001188 (green), 5901327 (purple); R4: 5900601 (light blue), 5901270 (green). Bathymetry higher than 2000 m is shown (shaded).

Properties of the February mixed layer and on the 27.2–γ^nsurface (mean depth of approximately 1100 metres) both reflect the large influence of the regional circulation in establishing the contrast between properties of the upper ocean between east and west of Tasmania (figure 4.9). In the east, the sluggish circulation in the SAZ and the strong input of warm, salty waters from the Tasman Sea at different depths promote a strong meridional temperature and salinity gradient (figure 4.9 b, c, d). A warm and salty wedge of subtropical water east of Tasmania is carried southward by the EAC (figure 4.9 b). The Tasman Outflow flows westward as a warm and salty filament just south of Tasmania (figure 4.9 c, d), following Route 1 (figure 4.8, top left). The temperature and salinity signature of the Tasman Outflow can be traced as far as 135 °E before it mixes with the surrounding waters.

The mixed layer depth shows a zonal contrast between the east and west of Tasmania. Mixed layer depths deeper than 50 m are found southwest of Tasmania, with a weak meridional gradient in mixed layer depth south of 44 °S. Southeast of Tasmania, mixed layer depths shallower than 50 m extend further south than in the west. A similar behaviour is found in the salinity distribution of the mixed layer (figure 4.9 b). West of Tasmania, salinity of the ML shows little contrast between the northern and southern SAZ boundaries. In contrast, the enhanced southward spreading of subtropical water in the east creates a strong meridional salinity gradient in the eastern SAZ. A similar pattern is found on the 27.2–γ^nsurface.

The Tasman Outflow carries older, lower oxygen SAMW and AAIW from the east to west through the South Tasman Saddle (*Rintoul and Bullister*, 1999; *Rintoul and Sokolov*, 2001). Oxygen concentrations of SAMW are lower between 43 °S – 47 °S on the zonal leg of P11S section compared to the SAMW found on the SR3 and the southernmost SAZ stations at P11 (not shown). As a result, the intermediate waters to the east of Tasmania include both older and poorly–ventilated, waters entering the region from the north, and younger waters entering fomr the south of (for SAMW) formed locally. The

weak circulation regime east of Tasmania is confined: in the east by the continental shelf west of New Zealand; in the north, by a strong contrast in T–S with subtropical waters moving southward from the Tasman Sea; and in the west, by the South Tasman Rise (figure 4.4). Water exits this region either eastward, with the SAF, or northwestward through the South Tasman Saddle (our Route 1, figure 4.8).

4.5 Summary

The water properties of the SAZ south of Tasmania show strong contrasts between east and west sectors. These property contrasts likely contribute to the biological and biogeochemical differences observed east and west of Tasmania, the main focus of the SAZ–Sense experiment.

Analysis of WOCE hydrography, Argo float profiles and trajectories, and high resolution climatology reveals the main features of the regional circulation. Warm, salty subtropical warters are carried into the eastern SAZ, south of Tasmania, by the EAC. At intermediate depths, the Tasman Outflow allows relatively warm and salty water from the east of Tasmania to enter the western region. This flow, connecting the Pacific and Indian subtropical gyres south of Australia, is part of a southern hemisphere "super–gyre" connecting the basins (*Ridgway and Dunn*, 2007). *Speich et al.* (2002) showed that this flow path contributes to the global overturning circulation. The STR divides the regional circulation into two regimes with strong contrasts in water properties. The circulation in the east shows a weak geostrophic flow and enhanced subtropical input by EAC warm core eddies, intrusions and a subsurface southward advection of salinity. Close to Tasmania, Argo float trajectories show that the STF is crossed back and forth, probably associated with strong mesoscale eddies of the EAC. Intrusions or interleaving are very important in this region because they promote strong isopycnal and diapycnal mixing between subtropical and subantarctic waters. The influence of the subsurface

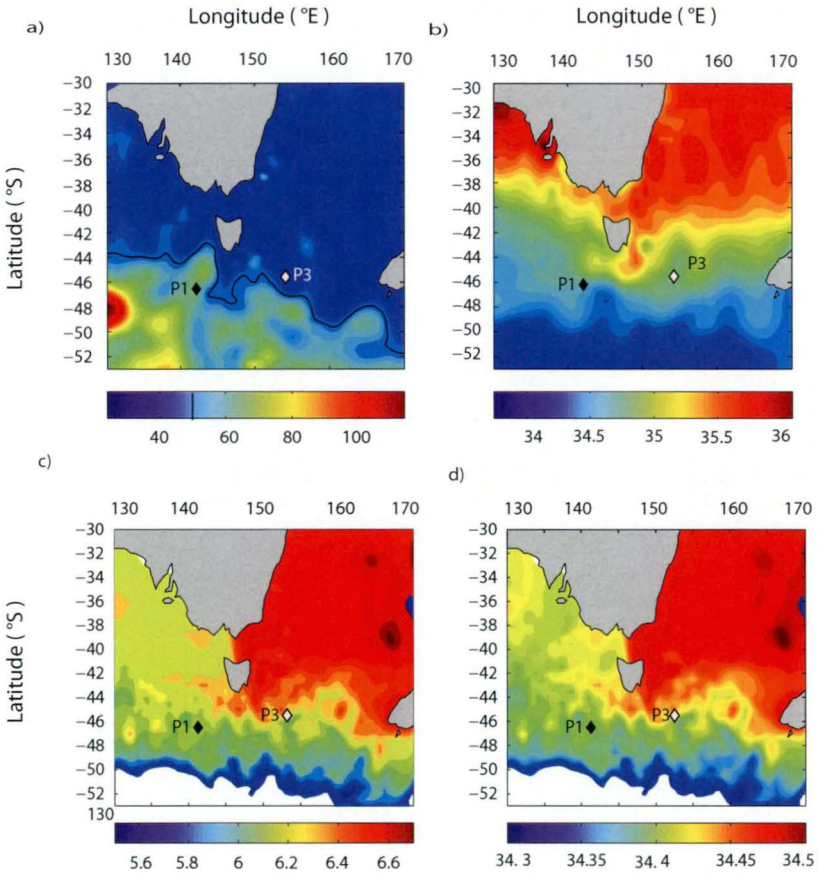

Figure 4.9: February mixed layer depth and salinity (a, b).The mixed layer depth has been calculated using a density difference criterion with a threshold of 0.03 kgm^{-3}. The 50 – 55 m mixed layer depth is depicted by the black contour line. Temperature and salinity at a neutral density surface of 27.2 kgm^{-3} (mean depth of 1100 metres) (c, d). Process stations 1 and 3 are also shown.

southward advection of salinity is higher in the east than in the west. While in the east it is a well–established event, in the west, it seems to depend on the seasonal strength of the EAC extension that reaches the western SAZ waters in the form of eddies. The regional circulation in the west is governed by a northwestward circulation with little apparent flow to the east across the STR. Immersed in the mean flow, a deep–reaching anticyclonic recirculation is located just west of the STR (47 °S – 49 °S, 140 °E – 145 °E).

These regional circulation and mixing processes therefore drive the strong contrasts in water properties in the eastern and western SAZ discussed here and by previous authors (e.g. *McCartney*, 1977; *Rintoul and Bullister*, 1999; *Sokolov and Rintoul*, 2002). Southern Ocean waters exert a strong influence over the western SAZ, resulting in relatively cold and fresh waters compared to the warm and salty waters in the east. Two local varieties of SAMW and AAIW have been found inside the permanent anticyclonic recirculation west of the STR. The thickest SAMW is found here, suggesting the deep isopycnal bowl, associated with the anticyclonic flow, preconditions the region for deep winter convection. θ–S relationships around Tasmania reveal the confluence of AAIW with two very distinct origins, a warmer and saltier AAIW formed in the eastern South Pacific Ocean and a colder, fresher and better ventilated AAIW formed in the western South Atlantic Ocean. The latter water mass is advected eastward by the ACC and is found prominently on the west, just north of the SAF. AAIW of intermediate θ–S properties are found in the east where interleaving is very strong and the circulation is very weak.

The enhanced input of subtropical water and shallower mixed layer depth in the east supports the higher biomass observed here. North of the STF, waters are replete with micronutrients, including iron, and are mainly limited by major nutrient supply (N, P, Si). The distribution of micronutrients in the SAZ varies from north to south (*Bowie et al.*, submitted to GBC; *Lannuzel et al.*, submitted to DSR): higher iron concentrations are found in the northern edge of the SAZ (compared to the south), particularly to the southeast of Tasmania. The SAF is low in Fe and in Si, and relatively high in P and N.

The high biomass region in the eastern SAZ is also affected by numerous EAC eddies that deliver higher dissolved iron concentrations from northern subtropical waters and enhance phytoplankton growth.

Tasmanian and SAZ marine ecosystem changes are expected to be larger in the eastern SAZ than on the western side of the SAZ south of Australia (*Hill et al.*, 2008). Our results suggest that intensification of the EAC extension would strongly affect the marine ecosystems of the eastern SAZ, as the region becomes more subtropical. As a result, the input of micronutrients, especially iron, to the macronutrient rich waters of the Southern Ocean could increase. Higher salinity intrusion is also likely to occur, intensifying the contrast between the northeast and the southeast SAZ. Such intrusions would also likely affect the depth of the mixed layer, intensifying the stratification and hence, forming shallower mixed layers. The southward expansion of subtropical waters has been linked to ecosystem changes near the coast of Tasmania, where kelp forest has declined and been replaced by sea urchin barrens, with impacts on the abalone and crayfish fisheries (*Ling*, 2008). Our results suggest a southward expansion of subtropical waters might also have had an impact on ecosystems in the eastern SAZ, where the influence of subtropical waters is larger. Strategies for the sustainable management of marine resources will need to take into account changes in regional circulation driven by climate change and natural variability (*Poloczanska et al.*, 2007).

Chapter 5 Conclusions

The primary aim of this study has been to clarify the variability of Subantarctic Mode Water. Water mass transformation in the Southern Ocean links the upper and lower limbs of the overturning circulation (*Sloyan and Rintoul*, 2001). Water masses exported from the Southern Ocean as part of the overturning circulation, such as Subantarctic Mode Water, are responsible for the ventilation of intermediate waters in other regions, and play an important role in the global transport and budgets of heat and freshwater, carbon and nutrients. Understanding SAMW variability is a step towards understanding the Southern Ocean's role in climate variability and change. Despite the importance of SAMW, very little was known about where SAMW subducts and its route into the subtropical gyres mainly due to the lack of data.

This study used a compilation of observational data from three different international programs: the World Ocean Circulation Experiment[1], Survostral[2], and Argo[3] Programs. The World Ocean Circulation Experiment (WOCE) was born in an effort to understand the circulation of the global oceans and its role in the climate system. Seven of the eight WOCE SR3 and the WOCE P11S hydrographic sections were used to test temporal variability and regional circulation influences over Subantarctic Mode Water (Chapter 3 and 4). The Survostral Program consists of the deployment of Expandable BathyThermograps (XBT) from Tasmania to the French Antarctic Base

[1]http://woce.nodc.noaa.gov/; and Ocean circulation and climate, International Geophysics Series, edited by Siedler G, J. Church, J. Gould, Academic Press, New York.

[2]www.legos.obs-mip.fr/en/projects/survostral/

[3]http://www.ifremer.fr/coriolis/cdc/argo.htm and http://www.argo.ucsd.edu

Dumont D'Urville (66°E, 140°E) and provided a unique 15-year-temperature record of the upper 800 metres of the water column where SAMW is found. The third of the programs is the Argo Program. Argo floats provide a unique spatial and temporal coverage of regions of the Southern Ocean, including areas where data were scarce or absent.

The main conclusions from our study are summarized as follows:

- Subantarctic Mode Water consists of multiple modes with distinct properties formed in each main oceanic basin rather than a continuous water mass with properties that gradually evolve towards the east as previously believed (Chapter 2).
- The distribution of the potential vorticity minimum revealed with great detail the structure of ventilation "windows". The injection of the SAMW into the ocean interior occurs at "hot spots" of subduction. Once subducted, the different SAMW modes follow narrow export pathways strongly influenced by bathymetry. Differences in the PV minimum distribution along streamlines between those in the Indian and in the Pacific Oceans are strongly related to the bathymetry. The Indian Ocean is characterized by a more complex topography than the Pacific Ocean, and so, PV minimum is conserved for longer distances in the south Pacific (Chapter 2).
- The densest south Pacific SAMW (γ^ncentered at 27.2 kgm^{-3}) that crossed Drake Passage suplies the salinity minimum layer of the South Atlantic Ocean. (Chapter 2).
- South of Australia, SAMW mean temperature shows no evidence of a warming trend over the 17-yr record analyzed. Temperature and salinity properties also show high intra- and inter-annual variability with abrupt changes within a short time scale of the order of several weeks to a few months (Chapter 3).
- Mesoscale features such as eddies and meanders strongly influence SAMW properties. These mesoscale features carry anomalous waters (cold and fresh waters

from the Subantarctic Front and, warm and salty waters originating from the East Australian Current) into the SAMW formation regions. Isopycnal mixing of SAMW with the anomalous advected waters explains the abrupt jumps observed in SAMW temperature and salinity records (Chapter 3).

- Vertical gradients of temperature in the SAMW core "pool" showed SAMW is formed by multiple "types" or "modes" of different vertical homogeneity rather than a single "pool". We showed that strong "modes" have distinct temperature and salinity characteristics and these are also explained by the advection of water by eddies and meanders, such as those found in November 1991 and July 1995 (Chapter 3).

- Enhanced input of subtropical water high in micronutrients (such as iron) in the Subantarctic Zone (SAZ) east of Tasmania likely supports the higher surface biomass observed in the SAZ southeast of Tasmania compared to the southwest SAZ. The physical processes responsible for maintaining the east-west contrast south of Tasmania (e.g. regional circulation, eddies and intrusions) are likely to drive variability in physical and biogeochemical properties of SAMW, Antarctic Intermediate Water and the SAZ elsewhere in the Southern Ocean (Chapter 4).

Our results lead us to the re-analysis of SAMW distribution, to the evaluation of SAMW temporal variability and, to the analysis of the influence of the regional circulation over the upper ocean variability in the Subantarctic Zone south of Tasmania. In earlier studies, SAMW was presented as a continuous water mass with gradual downstream evolution of its properties north of the Subantarctic Front. The export to the subtropics occurred more or less gradually across the basin. And the within–subtropical gyre circulation was thought of as a uniform broad (basin–wide) scale. Our results have revealed the spatial variability of SAMW in greater detail than was possible before the Argo data became available. SAMW consists of different modes formed in each oceanic basin. Changes

in their properties are related to circulation. Ventilation "windows" revealed by the PV minimum distribution showed "hot spots" where SAMW subducts following narrow pathways, influenced by topography. The export of relatively warmer, saltier SAMW in these "hot spots" contributes to the circumpolar evolution of mode water properties towards cooler, fresher and denser modes in the east. We also found that mesoscale features strongly influence SAMW variability south of Tasmania, and are likely to be important in setting SAMW properties in other regions with high eddy kinetic energy.

Future work

The Argo program has proven to play an enormous role in the understanding of the ocean. The continuation of the Argo program is of great importance as it provides an excellent operational tool that allows the forward study of the ocean, at spatial and temporal scales impossible to equal with ship observations. Yet, deep–reaching sampling of the water column from ships are needed as Argo only covers the first top 2000 metres of the water column and needs continuous calibration. Also, repeat sections such as those from the World Ocean Circulation Experiment are fundamental to the study of the climate variability and the evaluation of heat/freshwater transport within and outside the Southern Ocean through Subantarctic Mode Water (and Antarctic Intermediate Water). In this regard, new measurements, such as mooring and deep-reaching hydrographic sections at and around the "hot spots" described in this thesis are necessary to complement existing data and improve the quantification of the variability of heat/freshwater exchange as part of the overturning circulation.

Another significant outcome provided by this work is a methodology to evaluate how well ocean general circulation models and coupled models reproduce the formation, circulation and variability of SAMW. The comparison of our results with outputs from such models are required to assess and improve their performance and accurately assess the likelihood of future changes to Subantarctic Mode Water.

Within the Antarctic Circumpolar Current (ACC), the Southern Ocean upper ocean has warmed 0.17 °C centered on 25.5 kgm^{-3} (~1000 dbar) between 1950s and 1990s (*Gille*, 2002). However, the top 400 m has experienced larger averaged warming than long-term trends near 40 °S over the last 10 years (*Bindoff et al.*, 2007). This warming has been attributed to a southward shift and increased intensity of the Southern Hemisphere westerlies, possibly driving a poleward shift of the ACC position (e.g. *Cai*, 2006). The response of the ACC to stronger westerlies is still under debate. Circumpolar warming and freshening trends along isopycnals in the Southern Ocean has also been found in accordance with anthropogenic changes in the heat and freshwater cycles from climate models although no change in the ACC transport was found (*Böning et al.*, 2008). In this regard, a new statistical approach, an experimental design, has been developed and used to evaluate the role of the ACC southward shift in the changes of the Southern Ocean Water masses, in particular, in SAMW and AAIW. Results using this new statistical approach will be reported elsewhere and not given in this thesis.

Several physical mechanisms are known to play a major role in the formation of SAMW: namely, air-sea fluxes, northward Ekman transport, eddy heat fluxes and advection of anomalous water formed outside the SAMW formation region by mesoscale eddies. How these physical mechanisms interact to one another along the northern flank of the Antarctic Circumpolar Current is yet to be completely understood. To address this question, I have engaged in a collaboration with Dr. Matthew R. Mazloff from the Scripps Institution of Oceanography (San Diego, USA). Our aim will focus on the quantitative evaluation of the role of these physical mechanisms involved in the formation of SAMW using an eddy permitting Southern Ocean State Estimate (SOSE)[4] model. Understanding the processes involved in Subantarctic Mode Water spatial variability in the formation areas of the Southern Ocean will enable us to understand the consequences of recent warming detected in the SAMW formation regions of the Southern Ocean as a result of

[4]http://www.mit.edu/~mmazloff/current_research.html

climate change.

SAMW (and AAIW) ventilates the main oceanic thermocline and make an important contribution to large-scale fluxes and budgets of heat, freshwater, carbon dioxide, and nutrients. *Sarmiento et al.* (2004) suggested that the nutrients supplied by SAMW to the main thermocline ultimately supported 75% of the export production north of 30 °S. In chapter 3, we discussed the influence of mesoscale features advecting waters into the SAMW formation region (cold, fresh waters from the Subantarctic Front, and warm, salty waters originating from the East Australian Current (EAC)). These anomalous waters also carry with them nutrient characteristics from their source regions. The south Tasman Sea has shown the greatest warming rate in the Southern Hemisphere with an intensified East Australian Current (*Cai et al.*, 2005). The analysis of the nutrients variability within the SAMW is necessary to evaluate how the supply of nutrients to the thermocline is subject to change under a warmer climate scenario. In this context, the repeat hydrographic WOCE SR3 section is located at an excellent location and it provides the data to infer how nutrients variability within SAMW may change in response to a warmer climate.

Aoki, S, M. Yoritaka, and A. Masuyama, 2003. Multidecadal warming of subsurface–temperature in the Indian sector of the Southern Ocean, *J. Geophysis. Res., 108* (C4), 8081, doi: 10.1029/JC000307.

Banks, H. T. and N. L. Bindoff, 2003. Comparison of Observed temperature and salinity changes in the Indo–Pacific with results from the Coupled climate model HadCM3: processes and mechanisms, *J. Clim., 16*, 156–166.

Banks, H. T., R. A. Wood, J. M. Gregory, T. C. Johns, and G. S. Jones, 2000. Are observed decadal changes in intermediate water masses a signature of anthropogenic climate change?, *Geophys. Res. Lett., 27*, 2961–2964.

Belkin, I. M. and A. L. Gordon, 1996. Southern Ocean fronts from the Greenwich meridian to Tasmania, *J. Geophys. Res., 101* (C2), 3675–3696.

Bindoff, N. L., and J. A. Church, 1992. Warming of the water column in the southwest Pacific Ocean, *Nature, 357*, 59–61.

Bindoff, N. L., and T. J. McDougall, 2000. Decadal changes along an Indian Ocean section at 32°S and their interpretation, *J. Phys. Oceanogr., 30*, 1207–1222.

Bindoff, N. L., J. Willebrand, V. Artale, A, Cazenave, J. Gregory, S. Gulev, K. Hanawa, C. Le Quéré, S. Levitus, Y. Nojiri, C. K. Shum, L. D. Talley and A. Unnikrishnan, 2007: Observations: Oceanic Climate Change and Sea Level. In: *Climate Change 2007: The Physical Science Basis.* Contribution of Working Group I to the Fourth Assessment Report of the Intergovernmental Panel on Climate Change [Solomon, S., D. Qin, M. Manning, Z. Chen, M. Marquis, K. B. Averyt, M. Tignor and H.L. Miller (eds.)]. Cambridge University Press, Cambridge, United Kingdom and New York, NY, USA.

Böning, C. W., A. Dısper, M. Visbeck, S. R. Rintoul and F. U. Schwarzkopf, 2008. The response of the Antarctic Circumpolar Current to recent climate change, *Nature Geoscience, 1*, 864–869, doi:10.1038/ngeo362.

Bowie, A. R., D. Lannuzel, T. A. Remenyi, T. Wagener, P. J. Lam, P. W. Boyd, C. Guieu, A. T. Townsend, and T. Trull, 2009. Different processes structure biogeochemical iron budgets in the subantarctic and polar Southern Ocean south of Australia during summer, Submitted to *Global Biogeochemical Cycles.*

Bryden, H. L., and S. Imawaki. 2001. Ocean heat transport in *Ocean circulation and climate, International Geophysics Series*, edited by Siedler G, J. Church, J. Gould, 373–386, Academic Press, New York.

Bryden, H. L., E. L. McDonagh, and B. A. King, 2003. Changes in water mass properties: Oscillations or trends?, *Science, 300,* 2086–2088.

Cai, W., 2006: Antarctic ozone depletion causes an intensifi cation of the Southern Ocean super-gyre circulation. *Geophys. Res. Lett.*, 33, doi:1029/2005GL024911

Cai, W. J., G. Shi, T. Cowan, D. Bi, and J. Ribbe, 2005. The response of the Southern Annular Mode, the East Australian Current, and the Southern mid–latitude ocean circulation to global warming, *Geophys. Res. Lett., 32,* L23706, doi: 10.1029/2005GL024701.

Cai, W. J., P. H. Whetton, and D. J. Karoly, 2003. The response of the Antarctic Oscillation to increasing and stabilized atmospheric CO2, *J. Clim., 16,* 1525–1538.

Cresswell, G., 2000. Currents of the continental shelf and upper slope of Tasmania, *Papers and Proceedings of the Royal Society of Tasmania. 133, 3,* 21–30.

Curry, R., B. Dickson, and I. Yashayaev, 2003. A change in the freshwater balance of the Atlantic Ocean over the past four decades, *Nature, 426* (6968), 826–829.

De Miranda, A. P., B. Barnier, and W. K. Dewar, 1999. Mode waters and subduction rates in a high–resolution South Atlantic simulation, *J. Mar. Res., 57,* 213–244.

Deacon, G. E. R., 1937. The hydrology of the Southern Ocean. *Discovery Rep., 15,* 3–122.

Deacon, G. E. R., 1982. Physical and biological zonation in the Southern Ocean. *Deep–Sea Res., 29,* 1–15.

Domingues, C. M., Maltrud, M. E., Wijffels, S. E., Church, J. A., and Tomczak, M. (2007). Simulated Lagrangian pathways between the Leeuwin Current system and the upper–ocean circulation of the southeast Indian Ocean. *Deep–Sea Res. II* (Special Issue), *54* (8–10), 797–817, doi:10.1016/j.dsr2.2006.10.003.

Dunn, J. R., and K. R. Ridgway, 2002. Mapping ocean properties in regions of complex topography, *Deep–Sea Res. I, 49,* 591–604.

Ellwood, M.J., Boyd, P.W., and Sutton, P., 2008. Winter–time dissolved iron and nutrient distributions in the Subantarctic Zone from 40–52S; 155–160E, *Geophys. Res. Lett., 35*, L11604, doi:10.1029/2008GL033699.

Fine, R. A., 1993. Circulation aof Antarctic Intermediate Water in the South Indian Ocean. *Deep–Sea Res., 40*, 2021–2042.

Fine, R. A., K. A. Maillet, K. F. Sullivan, and D. Willey, 2001. Circulation and ventilation of the Pacific Ocean, *J. Geophys. Res., 106, C10*, 22159–22178.

Fine, R. A., W. M. Smethie Jr, J. L. Bullister, M. Rhein, D–H Min, M. J. Warner, A. Poisson, and R. F. Weiss, 2008. Decadal ventilation and mxing of Indian Ocean Waters, *Deep–Sea Res. I, 55*, 20–37.

Gille, S.T., 1994. Mean sea–surface height of the Antarctic Circumpolar Current Geosat data: Method and application, *J. Geophys. Res., 99, C9*, 18255–18274.

Gille, S. T., 2002. Warming of the Southern Ocean since 1950s, *Science, 295* (5558), 1275–1277.

Gille, S. T., and K. A. Kelly, 1996. Scales of spatial and temporal variability in the Southern Ocean, *J. of Geophys. Res., 101, C4*, 8759–8773.

Gordon, 2001, Interocean Exchange, in *Ocean circulation and climate, International Geophysics Series*, edited by Siedler G, J. Church, J. Gould, 303–314, Academic Press, New York.

Griffiths, F. B., Bowie, A. R., Dehairs, F., and T. Trull, 2009. The SAZ–Sense experiment: a biogeochemical comparison of Sub–Antarctic and Polar Frontal Zone waters south–west and south–east of Tasmania. *Deep–Sea Res. II*, submitted to *Antarctic Biochemistry special issue.*

Hanawa, K., and, L. D. Talley, 2001. Mode waters, in *Ocean circulation and climate, International Geophysics Series*, edited by Siedler G, J. Church, J. Gould, 373–386, Academic Press, New York.

Hill, K. L., S. R. Rintoul, R. Coleman and, K. R. Ridgway, 2008. Wind forced low frequency variability of the East Australian Current. *Geophys. Res. Lett., 35*, L08602, doi: 10.1029/2007GL032912.

Hughes, C. W. and E. R. Ash, 2001. Eddy forcing of the mean flow in the Southern Ocean, *J. Geophys. Res., 106, C02*, 2713–2722.

Iudicone, D., K. B. Rodgers, R. Schopp, and G. Madec, 2007. An exchange window for the injection of Antarctic Intermediate Water into the South Pacific, *J. Phys. Oceanogr.*, *37*, 31–49. doi: 10.1175/JPO2985.1

Jackett, D. R., and T. J. McDougall, 1997. A Neutral Density Variable for the World's Oceans, *J. Phys. Oceanogr.*, *27*, 237–263. doi: 10.1175/1520–0485(1997)027.

Johnson, G. C. and A. H. Orsi, 1997. Southwest Pacific Ocean water mass changes between 1968/69 and 1990/91, *J. Clim.*, *10*, 306–316.

Joyce, T. M., J. R. Luyten, A. Kubryakov, F. B. Bahr et al., 1998. Meso–to large–scale structure of subducting water in the subtropical gyre of the eastern North Atlantic Ocean, *J. phys. Oceanogr.*, *28*, 40–61.

Kahru, M., B. G. Mitchell, S. T. Gille, C. D. Hewes, and O. Holm–Hansen, 2007. Eddies enhance biological production in the Weddell–Scotia confluence of the Southern Ocean, *Geophys. Res. Lett.*, *34*, L14603. doi: 10.1029/2007GL030430.

Karstensen, J., and Quadfasel, D., 2002a. Formation of southern hemisphere thermocline waters: water mass conversion and subduction, *J. of Phys. Oceanogr.*, *32*, 3020–3038.

Karstensen, J., and Quadfasel, D., 2002b. Water subducted into the Indian Ocean subtropical gyre, *Deep–Sea Res. II*, *49*, 1441–1457.

Karstensen, J., and M. Tomczak, 1997. Ventilation processes and water mass ages in thermocline of the southeast Indian Ocean, *Geophys. Res. Lett.*, *24*, 2777–2780.

Lannuzel D., T. Remenyi, P. Lam, E. Townsend, Ibisanmi, E. Butler, T. Wagener, V. Schoemann, and A. R. Bowie, 2009. Distributions of dissolved and particulate iron in the sub–Antarctic and Polar Frontal Southern Ocean (Australian sector). *Deep–Sea Res. II*, submitted to *Antarctic Biogeochemistry special issue.*

Lass, H. U., and V. Mohrholz, 2007. On the interaction between the subtropical gyre and the Subtropical Cell on the shelf of the SE Atlantic, *J. of Mar. Res.*, *74*, 1–43.

Le Traon, P., F. Nadal, and N. Ducet, 1998. An improved mapping method of multisatellite altimeter data, *J. Atmos. Oceanic Tech.*, *15*, 522–534.

Ling, S. D., C. R. Johnson, S. Frusher, and C. K. King, 2008. Reproductive potential of marine ecosystem engineer at the edge of a newly expanded range, *Global Change Biology, 14*, 907–915.

Lourey, M. J., and T. W. Trull, 2001. Seasonal nutrient depletion and carbon export in the Subantarctic and Polar Frontal zones of the Southern Ocean south of Australia. *J. Geophys. Res., 106*, 31463–31488.

Maamaatuaiahutapu, K., C. Provost, C. Andrié, and Xavier Vigan, 1994. Origin and ages of mode waters in the Brazil–Malvinas Confluence region during austral winter 1994, *J. Geophys. Res., 104, C9*, 21051–21061.

McCarthy, M., and L. D. Talley, 1999. Three–dimensional isonetral potential vorticity structure in the Indian Ocean, *J. Geophys. Res., 104, C6*, 13251–13267.

McCartney, M. S., 1977. Subantarctic mode water, in *A voyage of discovery, Deep–Sea Research George Deacon 70th Anniversary volume*, edited by Angel, M., 103–119, Pergamon Press, New York.

McCartney, M. S., 1982. The subtropical recirculation of mode waters, *J. Mar. Res,. 40* (Suppl.), 427–464.

McCartney, M. S., and M. O. Baringer, 1993. Notes on the S. Pacific hydrographic section near 32°S – WHP P. WOCE Notes, 5.

McDougall, T. J., 1989. Streamfunctions for the lateral velocity vector in a compressible ocean, *J. Mar. Res., 47*, 267–284.

McDougal, T. J., and A. Klocker, 2009. An approximate geostrophic streamfunction for use in density surfaces. Submitted to *Ocean Modelling.*

McNeil, B. I., B. Tilbrook, and R. J. Matear, 2001. The accumulation and uptake of anthropogenic CO2 in the Southern Ocean south of Australia between 1968 and 1996. *J. Geophys. Res., 106*, 31432–31445.

Mémery, L., M. Arhan, X. A. Alvarez–Salgado, M.–J. Messias, H. Mercier, G. C. Castro, and A. F. Rios, 2000. The water masses along the western boundary of the south and equatorial Atlantic. *Prog. in Oceanog., 47*, 69–98.

Meredith, M. P., and A. M. Hogg, 2006. Circumpolar Response of Southern Ocean eddy activity to a change in the Southern Annular Mode, *Geophys. Res. Lett., 33*, L16608, doi: 10.1029/2006GL026499.

Metzl, N., B. Tillbrook, and A. Poisson, 1999. The annual fCO_2 cycle and the air–sea CO_2 in the sub–Antarctic Ocean, *Tellus, 51B*, 849–861.

Montgomery, R. B., 1937. A suggested method for representing gradient flow in isentropic surfaces, *Bull. Amer. Meteor. Soc., 18*, 210–212.

Morrow, R., A. Brut, A. Chaigneau, 2003. Seasonal and interannual variations of the upper ocean energetics between Tasmania and Antarctica, *Deep–Sea Res. I, 50*, 339–356.

Morrow, R., J. R. Donguy, A. Chaigneau, S. R. Rintoul, 2004. Cold–core anomalies at the Subantarctic Front, south of Tasmania, *Deep– Sea Res. I, 51*, 1417–1440.

Morrow, R., G. Valledean, J–B Sallée, 2007. Observed subsurface signature of Southern Ocean sea level rise, *Prog. Oceanog., 77, 4*, 351–366.

Nagata, Y., Y. Michida, Y. Umimura, 1988. Variations of positions and structures of the ocean fronts in the Indian Ocean Sector of the Southern Ocean. In: Sahrhage, D. (Ed.), Antarctic Ocean and Resources Variability. Springer–Verlag, Berlin, 92–98.

Naveira–Garabato, A. C, L. Jullion, D. P. Stevens, K. J. Heywood, and B. A. King, 2009. Variability of Subantarctic Mode Water and Antarctic Intermediate Water in Drake Passage during the Late 20th and Early 21 st. Centuries, *J. Clim., 22, 13*, 3361–3388 doi: 10.1175/2009JCLI2621.1.

Naviera–Garabato, A. C., D. P. Stevens, and K. J. Heywood, 2003. Water mass conversion, fluxes, and mixing in the Scotia Sea diagnosed by an inverse model, *J. Phys. Oceaongr., 33*, 2565–2568.

Olbers, D., V. Gouretski, G. Seiß, and J. Schröter, 1992. Hydrographic Atlas of the Southern Ocean, *Alfred Wegener Institute for Polar and Marine Research*, Bremerhaven, 17 pp. + 82 plates.

Onogi, K., J. Tsursui, H. Koide, M. Sakamoto, S. Kobayashi, H. Hatsushika, T. Matsumoto, N. Yamasaki, H. Kamahori, K. Takahashi, S. Kadokura, K. Wada, K. Kato, R. Oyama, T. Ose, N. Mannoji, and R. Taira, 2007. The JRA-25 reanalysis, *Journ. of Meteo. Soc. Jap., 85*, 369-432.

Orsi, A.H., T. III Withworth, W.D. Jr. Nowlin, 1995. On the meridional extent and fronts of the Antarctic Circumpolar Current. *Deep–Sea Res. I, 42, 5*, 641–673.

Phillips, H. E. and S. R. Rintoul, 2000. Eddy variability and energetics from direct current measurements in the Antarctic Circumpolar Current south of Australia, *J. Phys. Oceanog., 30, 12,* 3050–3076.

Poloczanska, E. S. , R. C. Babcock, A. Butler, A. J. Hobday, O. Hoegh–Guldberg, T. J. Kunz, R. Matear, D. A. Milton, T. A. Okey and A. J. Richardson, 2007. Climate change and australian marine life, *Oceanography and Marine Biology: An Annual Review, 45,* 407–478.

Provost, C., S. Gana, V. Garçon, K. Maamaatuaiahutapu, and M. England, 1995. Hydrographic conditions in the Brazil–Mainas Confluence during austral summer 1990. *J. Geophys. Res., 110, C6,* 10655–10678.

Provost. C., C. E. Scoffier, K. Maamaatuaıahutapu, A. Kartavtseff, and V. Garçon, 1999. Subtropical mode waters in the South Atlantic Ocean, *J. Geophys. Res., 104, C9,* 21,033–21,049.

Qiu, B., S. Chen, K. A. Donohue, Watts, D. R., H. Mitsudere, N. G. Hogg, S. R. Jayne, 2006. Observations of the subtropical Mode Water evolution from the Kuroshio Extension system study, *J. Phys. Oceanog., 36,* 3, 457–471.

Qu, T., S. Gao, I. Fukumori, R. A. Fine, and E. J. Lindstrom, 2008. Subduction of south Pacific Waters, *Geophys. Res. Lett., 35,* L02610, doi: 10.1029/2007GL032605.

Reid, J. L., 1997. On the total geostrophic circulation of the Pacific Ocean: flow patterns, tracers, and transports, *Prog. Oceanogr., 39,* 263–352.

Reid, J. L., 2003. On the geostrophic circulation of the Indian Ocean: flow patterns, tracers, and transports, *Prog. in Oceanogr., 56,* 137–186.

Ridgway, K. R., 2007a. Seasonal circulation around Tasmania: An interface between eastern and western boundary dynamics, *J. Geophys. Res., 112,* C10016, doi: 10.1029/2006JC003898.

Ridgway, K. R., 2007b. Long–term trend and decadal variability of the southward penetration of the East Australian Current, *Geophys. Res. Lett., 34,* L13613, doi:10.1029/2007GL030393.

Ridgway, K. R., and J. Dunn, 2007. Observational evidence for a Southern Hemisphere oceanic supergyre, *Geophys. Res. Lett.*, *34*, L13612, doi: 10.1029/2007GL030392.

Ridgway K. R., J. R. Dunn, and J. L. Wilkin, 2002. Ocean interpolation by four–dimensional least squares–Application to the waters around Australia, *J. Atmos. Ocean. Tech.*, *19*, *9*, 1357–1375.

Rintoul, S. R., 1991. South Atlantic Interbasin Exchange, *J. Geophys. Res.*, *96*, *C2*, 2675–2692.

Rintoul, S. R., and J. L. Bullister, 1999. A late winter hydrographic section from Tasmania to Antarctica, *Deep–Sea Res. I*, *46*, 1417–1454.

Rintoul, S. R., and M. H. England, 2002. Ekman transport dominates local air–sea fluxes in driving variability of Subantarctic Mode Water, *J. Phys. Oceanog.*, *32*, 1308–1321.

Rintoul, S. R., C. W. Hughes, and D. Olbers, 2001. The Antarctic Circumpolar Current System. in *Ocean circulation and climate, International Geophysics Series*, edited by Siedler G, J. Church, J. Gould, pp. 271–302, Academic Press, New York.

Rintoul, S. R., and S. Sokolov, 2001. Baroclinic transport variability of the Antarctic Circumpolar Current south of Australia (repeat section SR3), *J. Phys. Res.* (O), *106*, *C2*, 2815–2832.

Rintoul, S. R., S. Sokolov, and J. A. Church, 2002. A six year–record of baroclinic transport variability of the Antarctic Circumpolar Current at 140°E, derived from XBT and altimeter measurements, *J. Geophys. Res.–Oceans*, *107*, *C10*, art. no. 3155.

Roden, G., 1986. Thermohaline fronts and baroclinic flow in the Argentine basin during the austral spring of 1984, *J. Geophys. Res.*, *91*, 5075–5093.

Sabine, C. L., R. A. Feely, N. Gruber, R. M. Key, K. Lee, J. L. Bullister, R. Wanninkhof, C. S. Wong, D. W. R. Wallace, B. Tilbrook, F. J. Millero, T–S. Peng, A. Kozyr, T. Ono, A. F. Ríos, 2004. The oceanic sink for anthropogenic CO_2. *Science*, *305*, 367–371.

Sallée J. B., R. Morrow, K. Speer, 2008. Eddy heat diffusion and Subantarctic Mode Water formation, *Geophys. Res. Let., 35*, L05607.

Sallée, J. B., K. Speer, S. R. Rintoul, and S. Wijffels, 2009. Southern Ocean thermocline ventilation, *J. of Phys. Ocean.*, in press.

Sallée, J. B., N. Wienders, R. Morrow, and K. Speer, 2006. Formation of Subantarctic Mode Water in the Southeastern Indian Ocean, *Ocean Dynamics, 56*, 525–542.

Santoso, A. and M. H. England, 2004. Antarctic Mode Water circulation and variability in a coupled climate model, *J. Phys. Oceanogr., 34*, 2160–2179.

Sarmiento, J. L., C. G. H. Rooth and W. Roether, 1982. the Norh Atlantic tritium distribution in 1972, *J. Geophys. Res., 87*, 8047–8056.

Sarmiento, J. L., N. Gruber, M. A. Brzezinski and J. P. Dunne, 2004. High–latitude controls of thermocline nutrients and low latitude biological productivity, *Nature, 427*, 56–60.

Schmitz, W. J., 1996. On the World Ocean Circulation: Volume II. The Pacific and Indian Oceans/ A Global Update. Woods Hole Oceanographic Institution, Technical Report WHOI–96–08, 241 pp.

Schneider, N., A. J. Miller, M. A. Alexander and C. Deser, 1999. Subduction of decadal North pacific temperature anomalies: observations and dynamics, *J. Phys. Oceanogr., 29*, 1056–1070.

Schott, G., 1933. Die britische Tiefsee–Expedition auf 'Discovery II' 1932/3. Ann. Hydrog. *Mar. Meteorol.*, 342 – 344.

Sloyan, B., and, S. R. Rintoul 2001. Circulation, renewal and modification of Antarctic Mode and Intermediate Water, *J. Phys. Oceanog., 31*, 1005–1030.

Sokolov, S., and, S. R. Rintoul, 2000. Circulation and water masses along WOCE section P11: Papua New Guinea to Tasmania, *J. Mar. Res., 58*, 223–268.

Sokolov, S., and S. R. Rintoul, 2002. Structure of Southern Ocean fronts at 140°E, *J. Mar. Sys., 37*, 151–184.

Sokolov, S. and S. R Rintoul, 2007. Multiple jets of the Antarctic Circumpolar Current south of Australia, *J. Phys. Oceanog., 37, 5*, 1394–1412.

Speer, K., S. R. Rintoul and B. Sloyan, 2000. The diabatic Deacon Cell, *J. Phys. Res., 30*, 2313–3222.

Speich, S., Blanke, B., de Vries, P., Drijfhout, S., Döös, K., Ganachaud, S., and Marsh, R., 2002. Tasman leakage: A new route in the global ocean conveyor belt, *Geophys. Res. Lett., 29, 10*, 1416, doi: 10.1029/2001GL014586.

Stark, S., R. A. Wood, and, H. T. Banks, 2006. Re–evaluating the causes of observed changes in Indian Ocean water masses, *J. Clim., 19*, 4075–4086.

Stramma, L., and M. England, 1999. On the water masses and mean circulation of the South Atlantic Ocean, *J. Geophys. Res., 104, C9*, 20863–20883.

Stramma, L., and J. R. E. Lutjeharms, 1997. The flow field of the subtropical gyre of the South Indian Ocean, *J. Geophys. Res., 102, C3*, 5513–5530.

Talley, L. D., 1988. Potentail vorticity distribution in the North Pacific, *J. Phys. Oceangr., 18*, 89–106.

Talley, L. D., 1996. Antarctic Intermediate Water in the South Atlantic. In *The south Atlantic: Present and Past Circulation*, G. Wefer, W.H. Berger, G. Siedler and D. J. Webb (eds), Springer–Verlag., 219–238.

Talley, L. D., 1999. Some aspects of ocean heat transport by the shallow, intermediate and deep overturning circulations. Mechanisms of Global Climate Change at Millennial Time Scales; *Geophysical Monograph, 112*, 1–22.

Thompson, D.W. J., and S. Solomon, 2002. Interpretation of recent Southern Hemisphere climate change, *Science, 296*, 895– 899.

Trull, T., S. Bray, S. Honjo, and R. Francois, 2001. Moored sediment trap measurements of carbon export in the Sub–Antarctic and Polar Frontal zones of the Southern Ocean, *J. Geophys. Res., 106*, 31489–31510.

Tsuchiya, M., L. D. Talley, and M. S. McCartney, 1994. Water–mass distributions in the western South Atlantic; A section from the South Georgia Island (54S) northward across the equator, *J. Mar. Res., 52*, 55–81.

Wang, X., R. J. Matear, T. W. Trull, 2001. Modeling seasonal phosphate export and resupply in the Subantarctic and Polar Frontal Zones in the Australian sector of the Southern Ocean, *J. Geophys. Res., 106, C12*, 31525–31542.

Wijffels, S. E., J. M. Toole, and R. Davis, 2001. Revisiting the South Pacific subtropical circulation: a synthesis of the World Ocean Ciculation Experiment observations along 32 °S, *J. Geophys. Res., 106*, C9, 19481–19513.

Wolff, J. O., E. Maier–Reimer, and D. Olbers, 1991. Wind–Driven Flow over Topography in a Zonal β–Plane Channel: A Quasi–geostrophic Model of the Antarctic Circumpolar Current, *J. Phys. Oceanogr., 21*, 236–264.

Wong, A. P. S., N. L. Bindoff, and J. A. Church, 1999. Large–scale freshening of intermediate waters in the Pacific and Indian Oceans, *Nature, 400*, 440–443.

Wong, A. P. S., N. L., and J. A. Church, 2001. Freshwater and heat changes in the North and South Pacific Oceans between the 1960s and 1985–94, *J. Clim., 14, 7*, 1613–1633.

Wyrtki, K., 1962. The subsurface water masses in the western South Pacific Ocean. *Australian Journal of Marine and Freshwater Research, 13*, 18–47.

Wyrtki, K., 1971. Oceanographic Atlas of the International Indian Ocean Expedition. National Science Foundation, Washington DC, 531pp.

You, Y., 1998. Intermediate water circulation and ventilation in the Indian Ocean derived from water–mass contributions, *J. Mar. Res., 56*, 1029–1067.

You, Y., and M. Tomczak, 1993. Thermocline circulation and ventilation in the Indian Ocean derived from water mass analysis, *Deep–Sea Res., 40*, 13–56.

Zhang, H–M., and N. G. Hogg, 1992. Circulation and water mass balance in the Brazil Basin, *J. Mar. Res., 50*, 385–420.